Dissertation
submitted to the
Combined Faculties for the Natural Sciences and for Mathematics
of the Ruperto-Carola University of Heidelberg, Germany
for the degree of
Doctor of Natural Sciences

presented by

Dipl. Phys.:	Ulrich v. Pape
born in:	Hamburg
Oral examination:	30th January, 2002

Wavefront Sensing in the Human Eye

Referees: Prof. Dr. Josef Bille
Prof. Dr. Karl-Heinz Brenner

Zusammenfassung: Wellenfrontmessungen am menschlichen Auge

Fortschritte in der chirurgischen Technik zur Korrektur von refraktionsbedingten Sehfehlern haben es ermöglicht, dass heute die Form der Hornhautvorderfläche auch ortsaufgelöst geändert werden kann. Die Refraktionsmessungen am menschlichen Auge beschränkten sich allerdings auf die Messung von Sphäre und Astigmatismus, und zwar bei einer einzigen Pupillengrösse. Im Zuge dieser Arbeit wurde - basierend auf einem Hartmann-Shack Sensor - ein Wellenfrontmessgerät zur ortsaufgelösten Refraktionsmessung des Auges entwickelt, das den diagnostischen Anforderungen gerecht wird, die sich aus den neuen Möglichkeiten der Augenchirurgie ergeben.

Der Aufbau des Gerätes wird beschrieben. Die Ergebnisse von Messungen an Test-Optiken werden dargestellt und mit den theoretischen Möglichkeiten verglichen. Die Ergebnisse von Messungen an menschlichen Augen führen zu Einschätzungen über die tatsächliche und die erforderliche notwendige Auflösung des Geräts. Die Reproduzierbarkeit der Ergebnisse wird geprüft. Weitergehend wurde noch ein aktiver Senk-Matrix-Spiegel in das Gerät implementiert, der die Wellenfront korrigieren und dem Patienten seine aberrationsfreie Sehfähigkeit demonstrieren kann.

Es zeigt sich: Das Gerät ist in der Lage, die Refraktionsmessungen einfach, schnell und reproduzierbar durchzuführen, und zwar mit einer Genauigkeit, die die Erfordernisse noch übertrifft.

abstract: Wavefront Sensing in the Human Eye

Most recent technical advancements in the refractive surgery for correcting refraction errors of the eye allow a spatial-resolved reshaping of the cornea. The diagnostics up to now have been restricted to sphere and cylinder giving a mean value for one pupil size only.

For this study a wavefront sensor for spatial-resolved measurement of the refraction of the eye - using the Hartmann-Shack principle - was developed. To meet the diagnostic requirements of present day ophthalmology was the main goal.

The setup of the device is described. Measurements at test-optics are detailed and compared to theory. Measurements on human eyes give evidence for the actual resolution of the device and the requirements as well. In addition an active mirror was implemented. The use of this mirror lies in correcting the wavefront error and presenting the patient with wavefront corrected images to test the non-optical-limited capability of his vision.

The results show: The device is well suited for measuring the refraction of the eye - working fast, with results reproducible, and a precision, that even surpasses the needs of ophthalmology.

Contents

Chapter 1

Introduction

In the last few years new techniques in refractive laser surgery have been developed and the field has progressed rapidly. Prior to these developments we had excimer lasers with a potential to remove cornea tissue in a symmetric way only, correcting sphere and - with limitations - cylinder.
Nowadays flying spot laser or laser scanning systems are capable to reshape the cornea spatially resolved by sizes smaller than 1 mm.
This development has created new challenges for diagnostics. So far there were subjective and objective methods like manifest refraction and autorefractometer, useful for measuring sphere and cylinder only. For the new refractive surgery methods they were no support.
New efforts have been made - or older ones intensified - to avoid a gap between the techniques of surgery and the tools for diagnostics. A combination of corneal topography and manifest refraction was a first approach. On the assumption that most of the higher order aberrations originate in the cornea, it was thought that dealing with the cornea should be sufficient. However it turned out that the whole optical system has to be taken into account. At this point wavefront sensors came in consideration (e.g. see [Kl98]).
These sensors are based on a number of principles, the main ones being Tscherning, Ray-Tracing and Hartmann-Shack or - as it is called in America - Shack-Hartmann.
The wavefront sensor used in our study is based on the Hartmann-Shack principle. The idea behind this approach was developed in astronomy in the

seventies with the objective of determining the quality of telescope optics. Liang in 1991, in our group in Heidelberg, was the first to make a case for using this method for measurements on the human eye [Li91]. In his dissertation he layed out the theory and described how the first experimental setup was built.
Another main part of the waveform device originates in astronomy as well: This is the adaptive optic, which is a combination of wavefront devices, one for measuring (the HSS) and the other one for correction (active mirror, ASKM). In astronomy it is used for correcting the aberrations caused by the atmosphere in order to sharpen the images of objects in space. In our device it is used to correct the higher order aberrations of the eye. This gives a chance to demonstrate a patient the quality of vision he will achieve by correction the higher order aberrations.

Compared to man made optics the optic of the eye is very poor. So the standard for the measurement at eyes is low too, especially compared to astronomy. The problem here lies in the fact that the eye is alive and gets damaged very easily. These circumstances set the frame for the development.

The setup for the measurements is detailed. In testing the device several steps were taken. A first set of tests was designed to determine the precision of our measurements. Sphere, cylinder and higher order aberrations were measured for a well known rigid test optic.
Following this, tests were performed for human eyes. The results were compared to those obtained from classical methods for determining refraction. The reproducibility of the values is established.
Higher order aberrations vary on their own in short or long time periods and in processing accommodation as well. The range of these aberrations gives a suggestion of the bound of precision still making sense. The results also give an idea of the minimum amount of aberration a laser surgery may be helpful for.

Two applications of our device bring the study to a close.
“Perfect Vision“ and its optical prerequisite is object of the first study. The

Visual Acuity of about 70 eyes was measured and the result was compared to their higher order aberrations.
What results can be expected from excimer refractive surgery? This is the question a second study centers around. 42 patients were treated both ways, with wavefront guided laser surgery on one eye and the traditional way on the other. A glimpse at the potential of the new method is given.

Chapter 2

The Human Eye

In dealing with the anatomy of the human eye we have to consider two main parts: The optical unit and the retina.
The optical unit depicts the world around us upside down onto the retina. The retina records the image, converts it into an electrical signal, does a first step of image-processing, and transmits the signal to other parts of the brain. (The retina is a part of the brain itself). Compared to man-made optical apparatus the optical properties of the eye are quite inadequate - even in a normal emmetropic eye. If the vision is still of a high quality, this is mainly due to the excellent performance of the brain in analyzing the received image. However: The job of reconstructing a picture can't be done without a minimum of information. The causes for loss in the quality of vision vary over a wide range: Age-related loss of accommodation, Myopia, Hyperopia, accidental damages of the cornea, opacity of the lens or retinal damage. The deficiencies can be grouped as below:

1. the optical imaging quality of the eye
2. the light scattering in cornea and lens
3. the light scattering at the retina
4. the neuronal use of the retina

The Hartmann-Shack Sensor is designed primarily as a tool for determining the quality of the optical image. Moreover it is - via the brightness of the

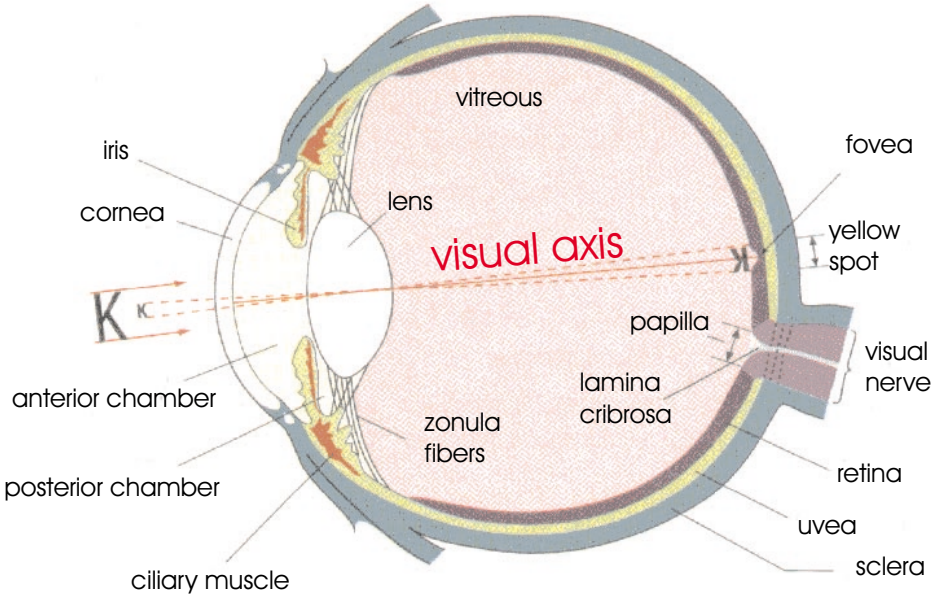

Figure 2.1: Cross section of the eye

HSS spots - suitable to give information about effects of group 2 and 3. To the neuronal use there is no access by Hartmann-Shack Sensors. Most of the problems related to the optical unit can dealt with by an intervention at the cornea - even if the problem does not originate in this very place.

2.1 Anatomy of the Eye

This section gives a description of the elements of the eye with special emphasis on their optical properties. The interaction between these elements is the main subject of the next section.
The normal adult eye is approximately spherical with an anterior-posterior diameter averaging 24.5 mm.
The outer protective coating of the eye is the sclera. It is dense, white and continues with the cornea anteriorly and the dural sheath of the optic nerve posteriorly. The cornea is a transparent tissue inserted in the sclera at the limbus.
The uveal tract is composed of the iris, the ciliary body and the choroid. It

is the middle vascular layer of the eye and contributes blood supply to the retina. The lens is a biconvex structure suspended behind the iris by the zonules which connects it with the ciliary body. The retina is a thin multilayered semitransparent sheet of neural tissue that lines the inner aspect of the posterior two-thirds of the wall of the globe.

2.1.1 Tear Film

A very thin film - measuring about 10 μm - covers the cornea. For the optic it is quite important: It is responsible for a smooth surface by compensating rough parts of the cornea.
The film consists of three layers. The outer lipid layer (0.02 μm-0.4 μm) - mainly different fats - prevents evaporation. The middle aqueous layer - mainly water (98 %) and anorganic salts (1 %) - is the thickest part. The internal mucin - an extremely thin mucous layer of 0.2 μm - ensures the adherence to the cornea. Abnormalities of the tear film cause fluctuations and impair the optical properties of the eye. A tear in the tear film leads to strong reflections and aberrations to the eye.

2.1.2 Cornea

The cornea is the most important optical part of the eye. The front may be thought of as a section of a sphere with diameter 16 mm, the base-circle being 12 mm in diameter, the curvature slightly diminishing towards the periphery. The width of the layer increases from about 0.5 mm in the center to about 0.8 mm at the periphery.
The cornea is built in several layers: The epithelium in front, the Bowman Membrane, the stroma, the Descemets Membrane and the endothelium. Making up 90 % in thickness, the stroma is the dominating part. The importance of the cornea lies in the fact that with about 43 D ($\approx$75 %) the impact on the total refraction of the eye is the largest. The refraction at the front (49 D) goes along with a much smaller refraction with a reverse sign at the back (-6 D).
The effect of the front is due to the extent of the difference between the refraction index n of air (n=1.0) and cornea tissue (n=1.376), the difference

of n at the back being much smaller (δn=0.04).
The front of the cornea has the shape of a ball, which is flattened to the periphery and mostly combined with some cylinder. A mathematical description of the shape may be:

$$z = \frac{c_x x^2 + c_y y^2}{1 + \sqrt{(1 - (1 + k)(c_x x^2 + c_y y^2)}} \tag{2.1}$$

with z=height c_x=curvature in x-direction, c_y=curvature in y-direction, k=conic constant. This model does not regard rotation around the z-axis and tilt.
In general the rear of the cornea has the same shape with a slightly smaller curvature. The curvature of the cornea can vary by 0.06 mm in the course of each day. This causes a shift in the refraction of about 0.3 D. It may also have an effect on the cylinder.

2.1.3 Anterior Chamber

The space between the endothelium of the cornea and anterior surface of the lens is called the Anterior Chamber.
It measures 12 mm in diameter and about 3.6 mm in depth. By grows of the lens during life the depth decreases continually.
The aqueous humor - as medium very clear - is responsible for the intraocular pressure. It is produced in the ciliary body and is diverted through the trabecula and the Schlemms canal into the venous system.

2.1.4 Iris

The iris consists of an elastic diaphragm with a central expandable circular opening, the pupil. The iris has a diameter of 12 mm and a thickness of about 0.6 mm. The pupil is the aperture stop of the eye and limits the passage of light into the eye. Its diameter is shifted by two muscles. The musculus sphincter pupillae contracts the pupil and the musculus dilatator pupillae widens it. The diameter can be changed between 2 mm and 8 mm, corresponding to approximately 16 times variation in area. The aperture of an optical system has always great influence on the optical properties. A stricture of the pupil has some effects on vision:

- reducing the brightness
- reducing the higher order aberration
- increasing the diffraction effects
- increasing the depths of focus

The higher order aberration and the diffraction effects oppose each other with the change of the pupil size. The optimal vision quality will be achieved at 2 mm-3 mm depending on the eyes aberration.
The center of the pupil also defines - together with the fovea centralis - the visual axis of the eye.

2.1.5 Crystalline Lens

The lens of the eye is much more complex than the cornea. It can be seen as an asymmetric deformable biconvex gradient index lens. It has a diameter of about 8 mm, a thickness of about 4 mm and a curvature radius of 10 mm at the front, and 8 mm at the back. The refractive index of about n=1.4 decreases from the center to the periphery.
The lens keeps growing during lifetime. Starting with a small core at birth, new layers of fibres keep growing around this core continually. So the lens can grow up to double of its original size. As a consequence the inner parts have a reduced metabolism and harden. This leads to a higher refractive index and a smaller accommodation range. The accommodation of children can be up to 14 D and goes down to about 2 D at the age of 50 and less than 0.5 D at the age of 70. This causes a shift of the near point, from 7 cm for a child to more than 2 m for a seventy year old person in an emmetropic eye.
The accommodation is regulated by the ciliary muscles and by the zonulafibres. The zonulafibres pull the lens in radial direction. If the ciliary muscles are relaxed the refraction of the eye is at a minimum. By straining these muscles the refraction rises.

2.1.6 Vitreous

The vitreous forms the largest part of the eye. It is the transparent colorless and gelatinous mass - consisting to 99 % of water and 1 % of collagen and hyaluronic acid - between the lens and the retina. The refraction index is very close to the refraction index of water.
The main importance of the vitreous lies in its high refractive index.

2.1.7 Retina

The retina is the light sensitive part of the eye. It converts the light stimulus into a signal which can be processed by the brain.
The photosensitive cells can be classified in two groups, the rods and the cones. These cells are arranged like a mosaic on the retina. The cones support photopic (day, color) vision. The usually smaller rods support scotopic (twilight) vision, which is in black and white only. In the fovea - the area receiving the sharpest image - there are no rods at all. Relative the number of rods increases to the periphery, as the number of cones decreases. The total number of rods is about 100 million, compared to just 7 million cones. The size of the cones depends on the position in the eye. Their minimum lies - with 2.5 μm to 4 μm - in the fovea.
Looking at the retina from the front two spots attract attention. On the nasal side there is the optic papilla, the area where the nerves pass out of the eye into the brain. In this area the retina has no light active cells and the eye is blind.
The other spot is the macula. It contains the area with the sharpest vision called the "fovea centralis". This part of the retina is built in a way that minimizes distortion of the image. There are no rods in the macula and no blood vessels either. The cones dominating the vision in this area are very small. The field of view of the fovea centralis is very small (about 1 degree or 0.1 % of the retina).
Still this area is the only target of the standard visual acuity tests. This area is night blind due to the absence of rods.
The retina consists of ten layers of cells. The most important are:

- pigment epithelium.
  this layer is responsible for the supply of the retina
- light sensitive layer.
  It consists of rods and cones. If light hits these cells a chemical reaction starts.
- Layer of neurons called bipolar cells.
  These cells transform the chemical signal into an electrical signal.
- The ganglion cells.
  The innermost layer of neurons.
- Layer of nerve fiber.

Apart from these layers there are others which establish a horizontal connection between the different areas of the retina.
In the retina some first image processing is taking place. The number of cells decrease with every layer. So the information of more than 100 million receptors can be transmitted with about 1 million nerve fibres.
The effective place of reflection and the place of absorption - corresponding to the maximum - varies with the wavelength of the light.

2.2 The Dioptric System

From the optical point of view the eye must be seen as a system with four almost spherical surfaces - the anterior and the posterior surfaces of the cornea and the crystalline lens. The effect grows, as the difference of the refraction index between the two materials increases, and the radius of curvature of the surfaces decreases.
The total refraction of the eye is about 59 D, dominated by the refraction of the front of the cornea.
In contrast to most human made optical systems, the optical axis of the eye is not identical with the functional axis of the eye. The visual axis is tilted by about 5 degrees against the optical axis (=symmetry axis) which causes

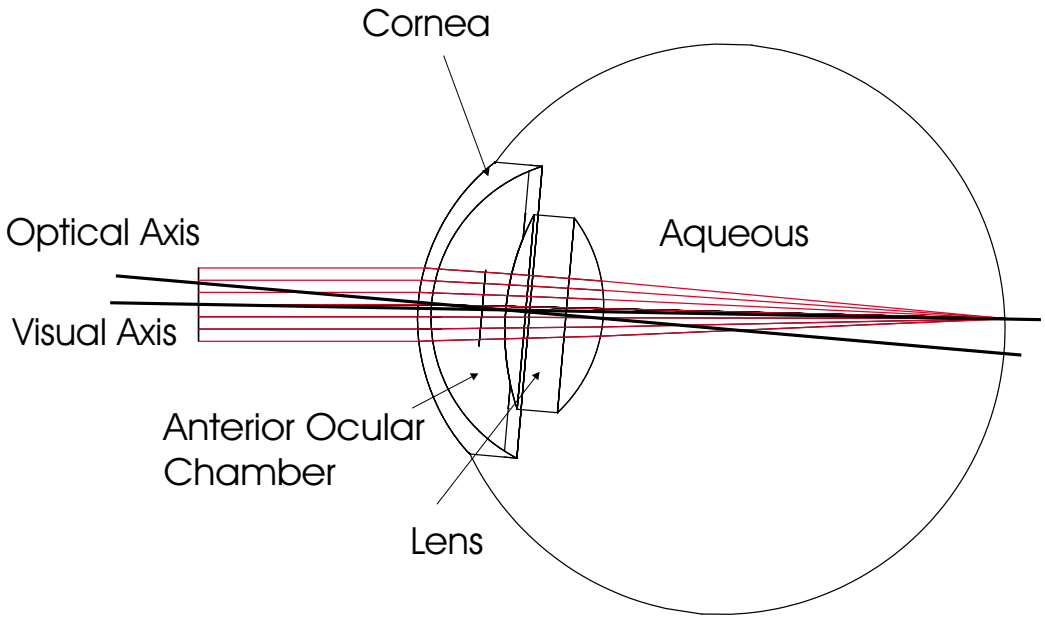

Figure 2.2: Optical setup of the human eye

coma. The most important eye model was developed by Gullstrand at the beginning of the 20th century. It is still in use for many applications, even the most modern eye models are based on the Gullstrand eye.
The Gullstrand eye has just one lens. The basic values stem from measuring a very large number of emmetropic eyes, and taking mean values. In this way he obtained a model for a non accommodating eye with a thin lens with 58.64 D 1.48 mm behind the cornea and a distance of 17.05 mm between lens and retina.
Apart from the refractive properties of the eye the transparency has another decisive role for our application. The transparency of the optical components depends to a great deal on the wavelength. This is shown in Fig.2.3. In the visible range (550 nm to 750 nm) as well as in the neighboured near infrared range (750 nm to 900 nm) the transparency for the total optical path, from cornea to retina, is about 75 %. The transparency for a wavelength is not constant throughout life. It decreases with age as shown in fig.2.4.

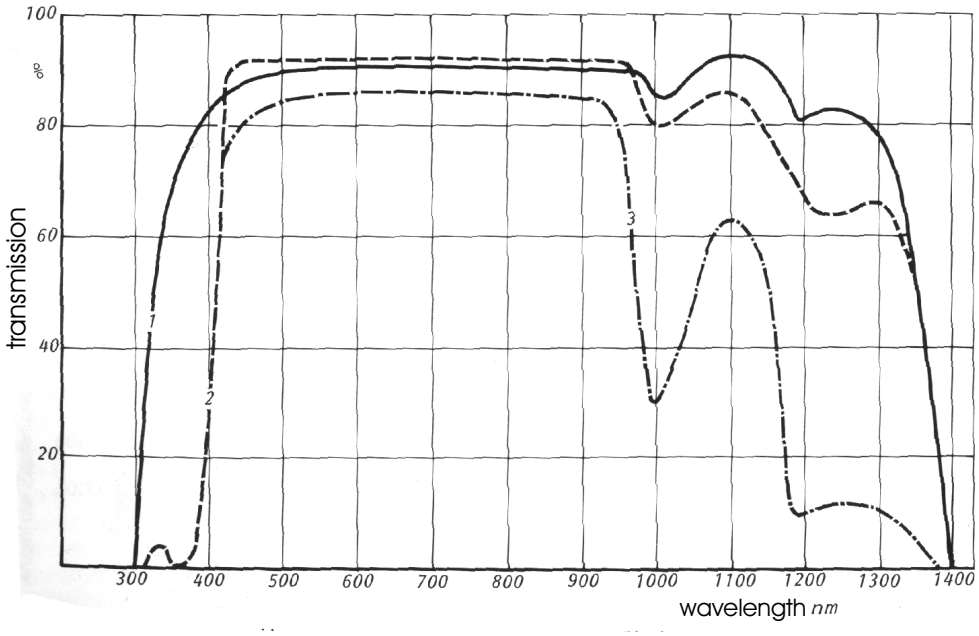

Figure 2.3: The transparency of the human eye [Me96]
1) transmission of cornea
2) transmission of lens
3) transmission of the vitreous body

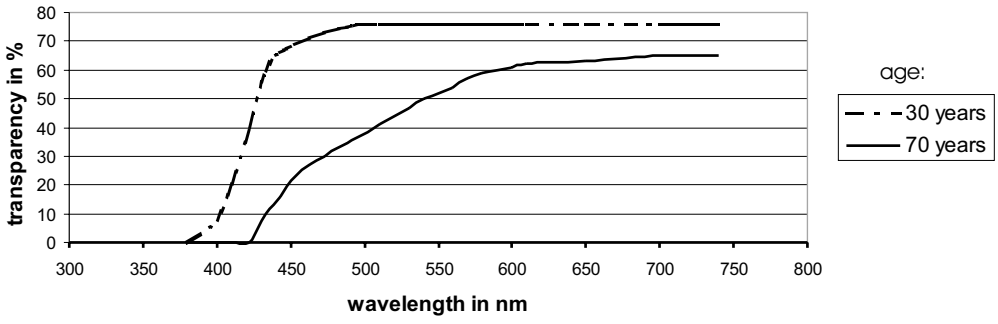

Figure 2.4: Change of transparency with age

	unit	no accommodation	max accommodation
refractive index			
cornea		1.376	1.376
aqueous		1.336	1.336
lens		1.386	1.386
core lens		1.406	1.406
place			
cornea front	mm	0	0
cornea back	mm	0.5	0.5
lens front	mm	3.6	3.2
lens back	mm	7.2	7.2
radius of curvature			
cornea front	mm	7.7 - 7.8	7.7 - 7.8
cornea back	mm	6.8	6.8
lens front	mm	10	5.33
lens back	mm	6	5.33
total optical system			
refractive power	D	58.64	70.57
place first cardinal point	mm	1.348	1.722
place second cardinal point	mm	1.602	2.086
place first focus point	mm	-15.707	-12.397
place second focus point	mm	24.387	21.016
front focal length	mm	-17.055	-14.169
back focal length	mm	22.785	18.030
place of fovea	mm	24.0	24
axial refraction	D	1.0	-9.6
place of near point	mm	—	-102

Table 2.1: The optical properties of the eye ([Me96])

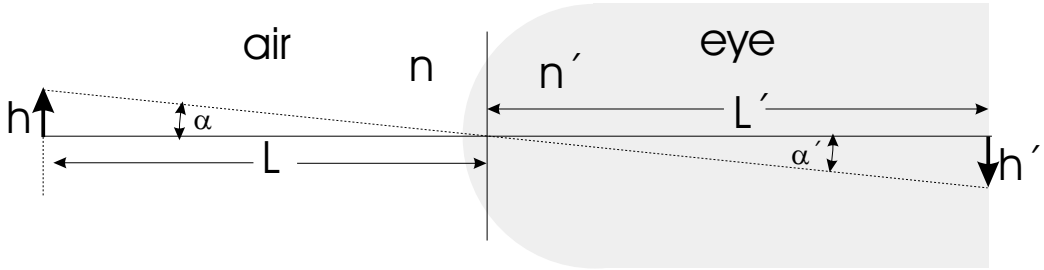

Figure 2.5: The magnification depends from the length of the eye.

2.3 Styles-Crawford Effect

The Styles-Crawford effect lies in an angular dependence of retinal sensitivity. Rays parallel to retinal receptors, entering the pupil near its center, are more effective (appear brighter) than oblique rays, entering the pupil near its margins. This fact reduces the effective pupil size. This phenomenon was discovered by Styles and Crawford in 1933. In a model this effect goes as a filter, in which transmission decreases with diameter.

2.4 Magnification

In visual science the linear distance on the retina corresponding to 1 degree of visual angle is called the retinal magnification factor.
The magnification of the optics can be easily computed by applying Snells law on a simple eye model (fig. 2.5):

$$n \sin(\alpha) = n' \sin(\alpha') \tag{2.2}$$

which gives us - with the small angle approximation and taking the angles trigonometrical equivalent:

$$\frac{h}{L} = \frac{h'}{L'} \tag{2.3}$$

So we finally get for the magnification m

$$m = \frac{h'}{h} = \frac{L'}{L} \tag{2.4}$$

Since the length L' grows from a hyperopic to a myopic eye the magnification also gets larger. For example the magnification factor for a 10 D myopic eye

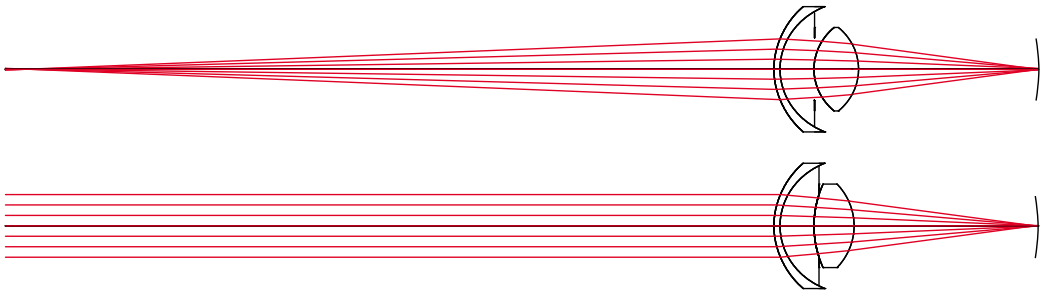

Figure 2.6: Accommodation of an emmetropic eye
a) the eye is maximally accommodated
b) the eye is not accommodated

is 20 % larger than for an emmetropic eye - objects in the same distance seem to be larger and Vision Charts can be read better.

2.5 Eye Movements

Each eye is moved by six muscles, arranged in couples. Two of the pairs are responsible for moving the eye up/down and right/left and the third pair induces a rotation of the eye around the visual axis. The rotation guarantees that the eye is always horizontal. This is most important for orientation.
Usually all six muscles work together. Only horizontal views, with the head also being horizontal, can be achieved by using just one pair of muscles. Horizontal movements - e.g. used for reading - can be realized very fast and precise.

2.6 Accommodation

Accommodation is the ability of the eye to change the focus to different distances. The accommodation is realized by the ability of the eye to change the shape of the lens (fig. 2.6). In the normal relaxed state the lens is relatively flat. By tensing a muscle the lens gets rounder in shape and the refraction of the eye increases. Thus objects closer to the eye will be imaged on the retina.

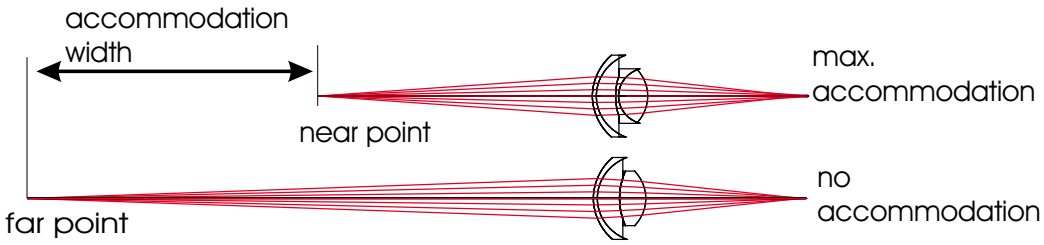

Figure 2.7: Accommodation of a myopic eye

The "near point" (fig. 2.7) is the nearest point for which the sight is sharp. Likewise the furthermost point is called the "far point". The difference in D is called "accommodation width". In a normal young emmetropic eye the far point is in infinity and the near point about 20 cm in front of the eye. This gives an accommodation width of 5 D. Due to the hardening of the lens the accommodation width decreases with age as described above.

2.7 Monochromatic Aberrations

Deviations from the normal abilities of vision are called ametropia. The standard case of ametropia occurs when the image of an infinite object - with the eye relaxed - is not on the retina. The main kinds of ametropia are myopia, hyperopia and astigmatism. These classical refraction errors are superimposed by higher order aberrations like coma and spherical aberrations.

2.7.1 Myopia and Hyperopia

The cause of ametropia normally lies in a deviation in the length of the eye, the distance between lens and retina. If this distance is too large the eye is myopic, if the distance is to small the eye is hyperopic, like can be seen in figure 2.8. A deviation in the curvature of the cornea or in the grade of refraction may also cause ametropia, being minor in effect.
In a relaxed hyperopic eye the focus point of an object positioned in infinity lies behind the retina.
The focal length can be shortened by accommodating so that the image lies

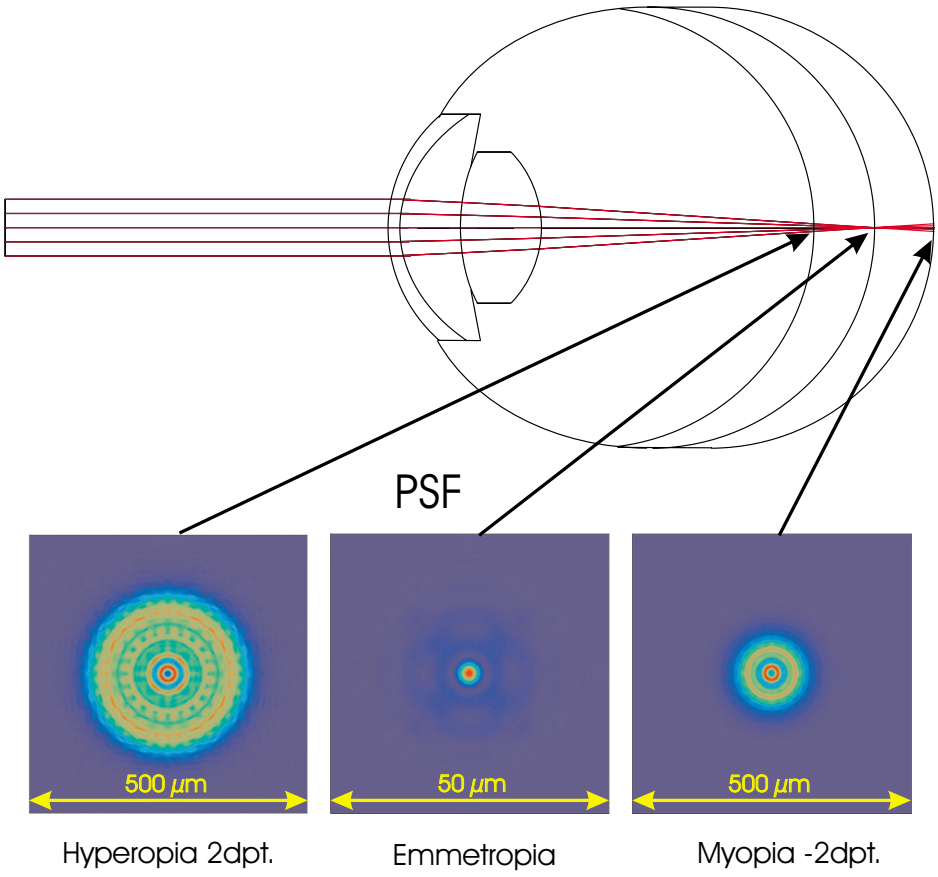

Figure 2.8: Top: Refractive errors of the eye
Bottom: Formation of the PSF

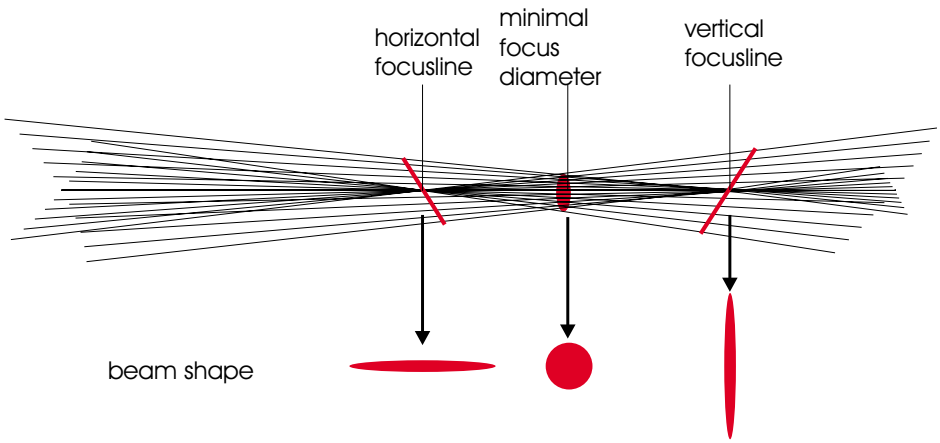

Figure 2.9: Development of astigmatism

on the retina. The nearest point of sharp vision is further away. In an emmetropic eye with rising age and falling accommodation range, the near point will rise to some meters.
If the focus point is in front of the retina, the eye is myopic. Even with a relaxed eye the far point is finite.
By accommodation the area closer than this far point can be seen sharply. The near point is closer than in a normal eye.
In myopia and hyperopia the image of a point spreads to a blur as can be seen in figure 2.8.

2.7.2 Astigmatism

The third kind of classic refraction failure is astigmatism. Astigmatism lies in the fact that different axes have different focal lengths.
The main cause is a kind of barrel shape of the cornea or - in a minor dimension - of the lens. An average eye has 0.5 D of horizontal cylinder called "regular cylinder". A difference in the curvature of 0.1 mm gives a cylinder of 0.5 D. With cylinder a point-lightsource gives - instead of one focus point - two focus lines, with a very large focus spot in between, as can be seen in figure 2.9. If the cylinder is uncorrected, the eye focuses to the spot with the minimal diameter.

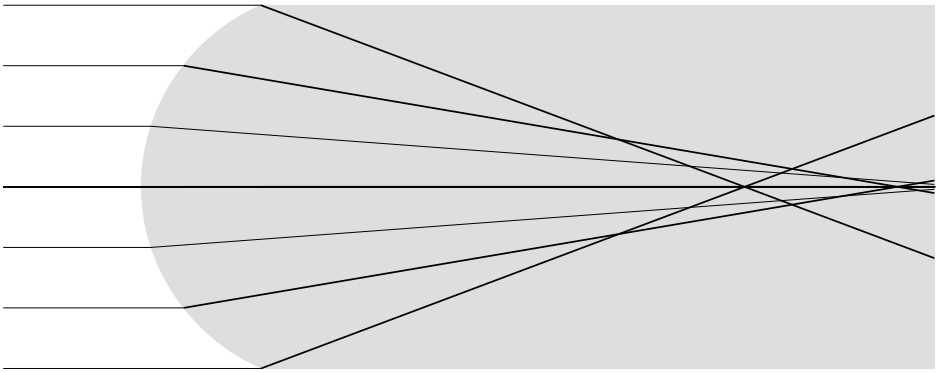

Figure 2.10: Development of spherical aberration

2.7.3 Higher Order Aberrations

Apart from these deficiencies there are higher order aberrations of a wide range. For their classification and characterization Zernike-polynomials are in use. The most important kinds of higher order aberrations in the human eye are spherical aberrations and coma.
Spherical aberrations occur if paraxial beams cross a spherical lens off-axis. As shown in fig. 2.10 with a larger distance to the axis the focal length becomes shorter and the focus spot smears.
Coma occurs if a beam crosses a lens off-axis or tilted. If coma exist, the focal point has a shape like the tail of a comet.
The higher order aberrations mainly occur at the cornea and at the lens.
The close to spherical shape in the center of the front of the cornea will make up most of the spherical abberation. If a beam tilted by 5 degrees enters the eye on the visual axis, it will also cause coma, which is even added by a displacement of the center of the cornea to the visual axis. This can be assumed the most important aberrations caused by the cornea.
The effect of the lens on the higher order aberrations is not quite easy to see. It causes spherical aberration depending on the state of accommodation, coma and also triangular astigmatism, probably induced by the 3 pairs of muscles.
If the size of the pupil is large, the aberrations obtain relevance.

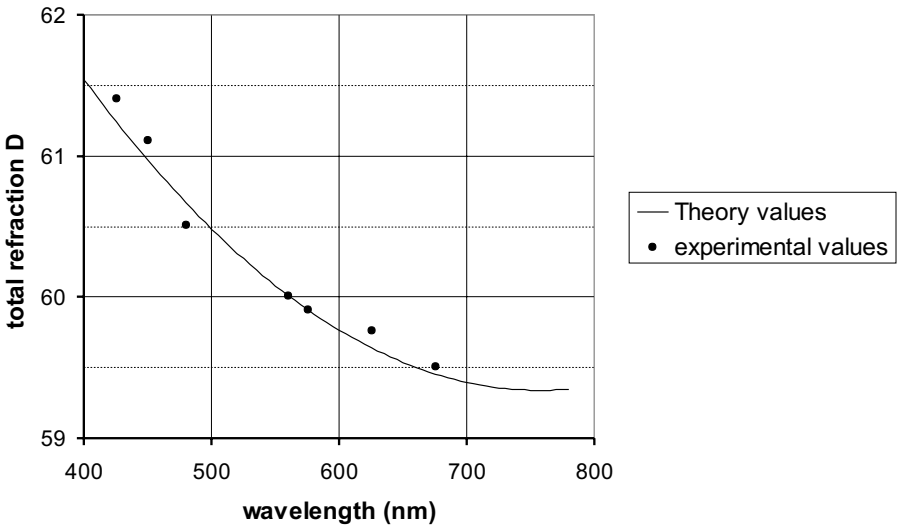

Figure 2.11: Dependence of the total refraction of the eye from the wavelength

2.8 Chromatic Aberrations

In addition to the monochromatic aberrations the eye also suffers from wavelength dependent aberrations. The chromatic aberrations occur in two ways. The first one relies on the fact that the refractive index of a material is dependent on the wavelength. The refractive index of the eye compares to that of water. The second way is generated by the fact that light of different wavelength is absorbed (and reflected) in different layers of the retina.
Chromatic aberrations can be divided into two kinds:

- Longitudinal Chromatic Aberration (LCA)
- Transversal Chromatic Aberration (TCA)

2.8.1 LCA

The shift of focal length with wavelength is called LCA. The effect is well known in the visible range. The difference in total refraction in an emmetropic eye between 400 nm and 600 nm goes beyond 1.5 D. The dependence

is shown in fig. 2.11. The theoretical values are based on Tucker [Tu74] . The experimental means are based on the values of 20 measured eyes [Li97].
The theoretical model-eye Tucker applied is quite simple. It has just one refractive surface. The refraction index changes in the same way, as the index of water does. In the visible range the theoretical results come very close to the experimental values. For the near infrared there are no experimental results for the LCA. So the assumption is that the models for visible light are valid also in this range.

2.8.2 TCA

TCA appears if polychromatic light enters the eye at an angle. The difference in the refraction index makes differences for the refraction of beams dependent on their color. So the position of the image is shifted transversally for oblique beams of different wavelength. This affects the magnification of the eye as well as the position of the image. The influence of the shift in the reflection depth on the TCA is negligible.
The influence of the TCA on our HSS measurement may be neglected as the measurements are on-axis.

Chapter 3

Basics of Wavefront Sensing

This chapter gives an introduction into Wavefront Sensing. It describes the basic properties of wavefronts and informs about different ways of measuring and describing them. Furthermore the connections of wavefronts to ophthalmological parameters are pointed out.
Beams from a pointsource are all in phase in the pointsource itself. If you have different beams originating from one pointsource at the same time their endpoints at any later time will generate a sphere (fig. 3.1). All points on the surface of this sphere are in phase again. A surface like this is called a wavefront: Wavefronts are phasefronts of light.
The direction of the propagation of light inside a medium is always orthogonal to the local surface of the wavefront.
The quality of an optical system (for our use) can be measured by its ability to keep beams, originating from a pointsource, spherical. This is essential for focussing them back to one point by another perfect optical system.
The difference in the optical path between a wavefront surface and the best fitted sphero-cylindrical surface is called the higher order wavefront error. The sphero-cylindrical surface is always used as reference here.
Detectors only respond to brightness levels and not to the phase of light. So wavefront sensors register wavefronts in a more indirect way. They transform optical path differences (OPD) to differences in light levels.
Wavefront Sensors differ in kind: Direct wavefront sensors measure the wavefront itself (as in Radial Shear Interferometry). Indirect wavefront sensors

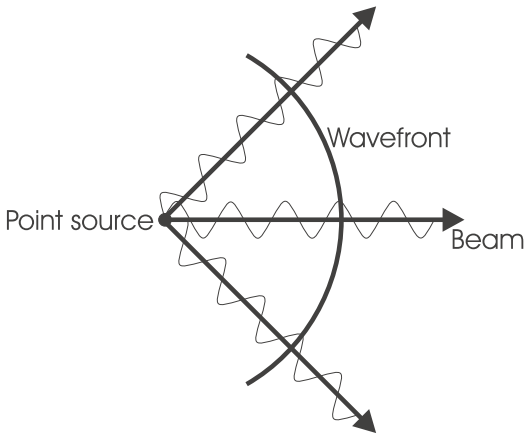

Figure 3.1: Definition of a Wavefront

measure the differential wavefront either in the pupil plane (e.g. knife edge test) or in the image plane (e.g. Hartmann-Shack Sensor).

3.1 Wavefront Sensors in Ophthalmology

As to applications for wavefront sensor systems, several uses can be thought of, especially for measuring cornea topography or the space-resolved refraction of the eye. In this section will be described different setups for the measurement of the space-resolved refraction.
Three types of this kind are in development: the Thinbeam Raytracing Aberrometer (fig. 3.2), the Tscherning Aberrometer (fig. 3.3) and the Hartmann-Shack Method (fig. 3.4).
The Raytracing Aberrometer uses the thin-beam principle of optical ray tracing. It rapidly fires a sequence of very small light beams into the eye. Through a beamsplitter a very fast PSD (Positioning Sensing Detector) measures for every beam the position where it hits the retina. This is a great advantage of this kind of sensor. Each measurement gives the values for one single beam. Even in case of strong aberration it is guaranteed that the beams can be discriminated by time. About 64 beams are distributed over the pupil size at random in a very short time (about 2 ms). On the basis of this the total refractive power and higher order aberrations can be deter-

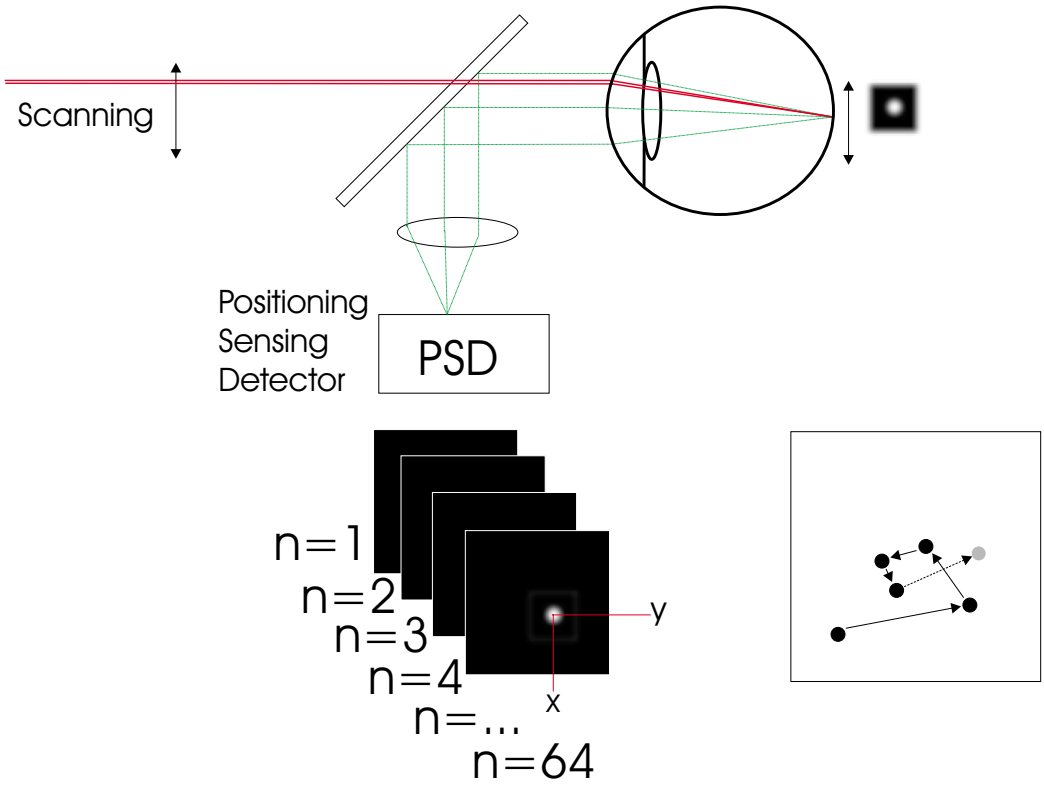

Figure 3.2: Thinbeam Ray-Tracing Aberrometer

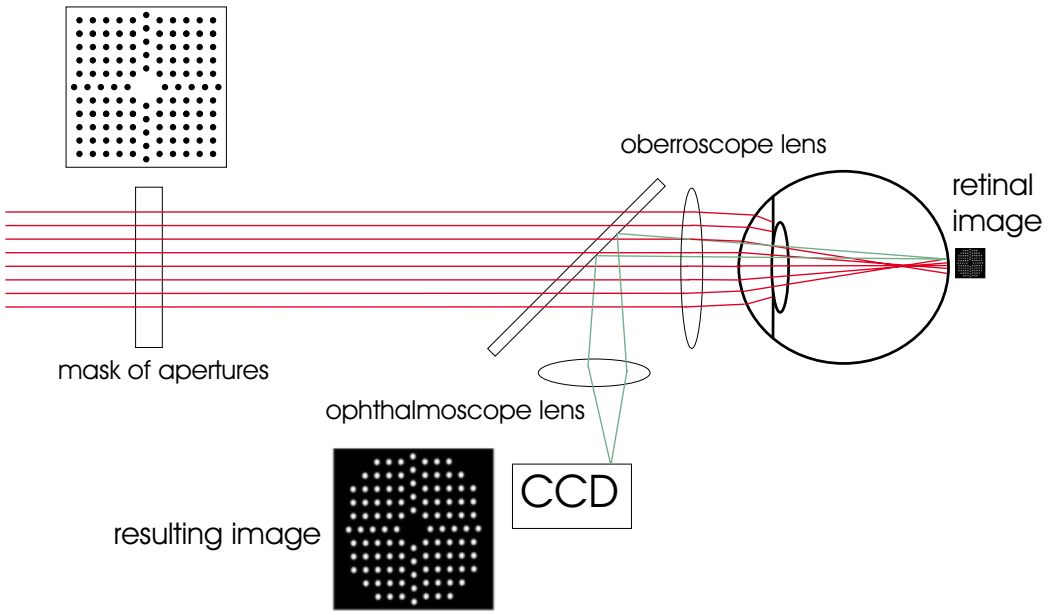

Figure 3.3: Tscherning Aberrometer

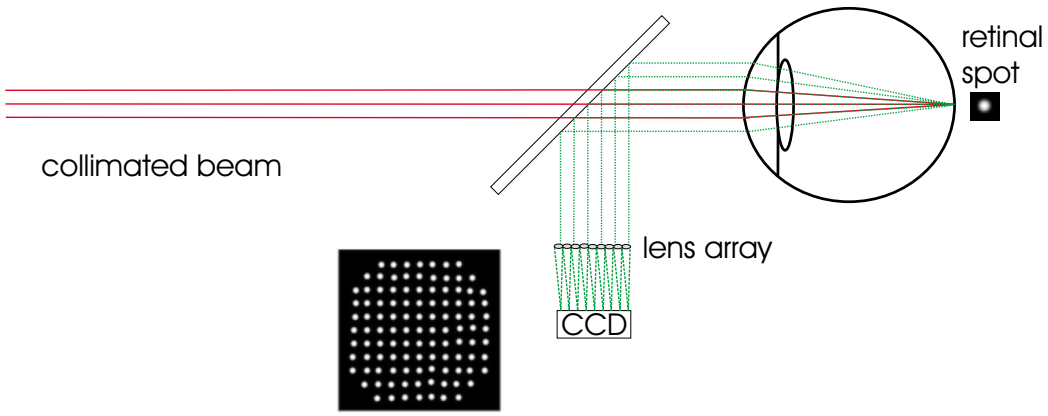

Figure 3.4: Hartmann-Shack Method

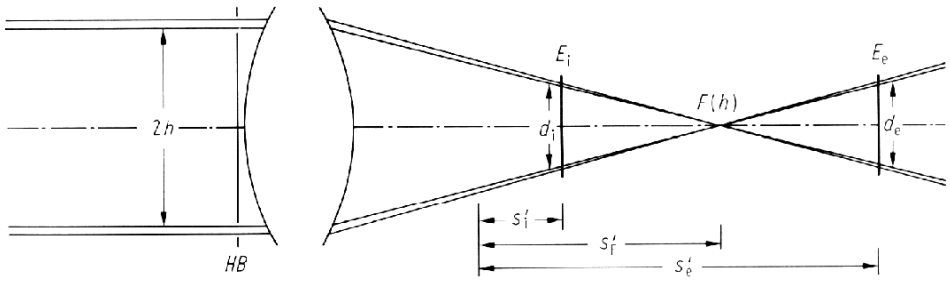

Figure 3.5: Hartmann test for testing the quality of lenses. With a Hartmann aperture in front of the lens pictures will be taken at points s_i and s_e (in front and behind the focus point) and the results will be compared.

mined. The possibility to vary the pattern of the entrance points enables the operator to concentrate on special areas of the pupil.
The Tscherning Aberrometer bases directly on the Hartmann-Test described in the next chapter. A collimated laser beam irradiates a mask of about 160 holes. The beams formed by the pattern will be imaged on the retina. A lens in front of the eye focuses each point 1 mm to 3 mm in front of the retina, so a grid with a diameter of 1 mm forms on the retina. A ccd camera takes pictures of this grid from the outside of the eye. By the distortion of the grid the wavefront can be calculated. In contrast to the Hartmann-Test, only one image outside the focal plane is used. That amount of aberration that can be measured in this way depends on the distance between the apertures and that of the focal plane from the retina.
The Hartmann-Shack Sensor will be described in detail in the next chapter.

3.2 Principle of a Hartmann-Shack Sensor

The conception of the Hartmann-Shack wavefront sensor comes from astronomy. In 1900 Johannes Hartmann introduced a new method for specifying the quality of large telescopes, called Hartmann test (fig. 3.5): An array of apertures (HB=Hartmann Blende) are placed in front of a lens. Light of a collimated beam passes through the lens. It is focussed with some aberra-

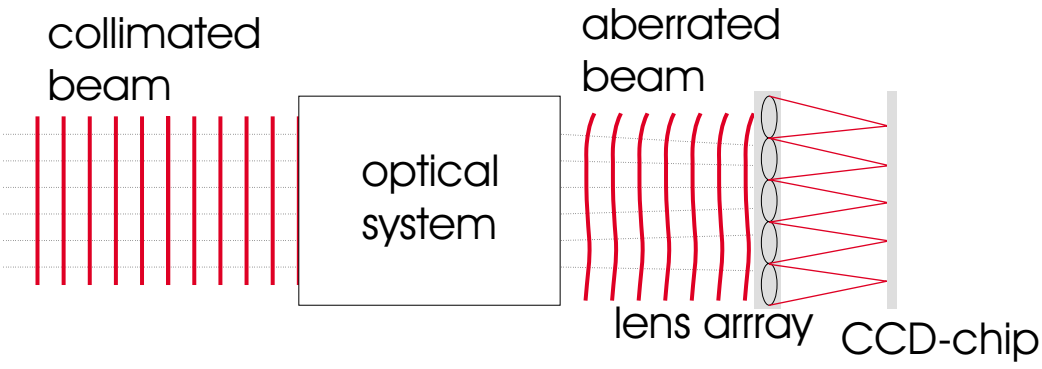

Figure 3.6: Idea of a Hartmann-Shack Sensor

tion. Photographic plates are positioned in front and behind the focus. Every aperture gives an image on each of the plates. By the total pattern taken on the plates, every image-point can be associated with one aperture. The focus position and the total aberration of the lens is calculated by taking the distance of the images from the optical axis and the positions of the plates. 70 years later Shack and Platt introduced an advanced kind of Hartmann sensor called Hartmann-Shack Sensor ([Pl71]). They proposed to use a lens array in the image plane followed by a photographic plate in the focal plane of the lens array (fig. 3.6). Later the photo-plate was replaced by a ccd-chip. The improvement of this setup is remarkable. The number of planes for measurement is reduced to one. This fact makes real-time measurements possible, using a ccd-chip. The optical path of the system is not involved. So it is possible to do measurements while the instrument is being used. The new setup makes measurement of the wavefront more precise and much faster.

Figure 3.7 shows the main idea of the Hartmann-Shack sensor on a single lens. A collimated beam hits a single lens. The beam is focussed by the lens in the focal plane. If the beam hits the lens parallel to axis, the focus point is on-axis. If the beam is tilted by an angle α, the focus lies off-axis by

$$d = f \tan(\alpha) \tag{3.1}$$

with $f = focal\ length\ of\ the\ lens$. The tilt of the focus is the clue to the mean slope of the wavefront on the area of the lens. The extent, to which

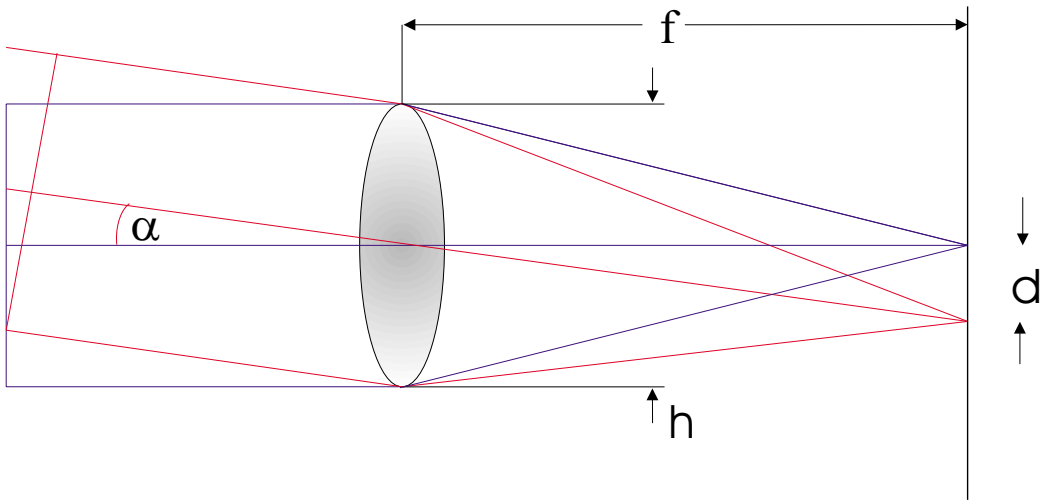

Figure 3.7: Functionality of a Hartmann-Shack Sensor demonstrated on a single lens

the slope varies on the diameter of the lens, should not be too large.
A Hartmann-Shack sensor uses a whole array of lenses instead of a single lens. The lenses divide the beam into sub-beams. Each sub-beam is focussed by a single lens on the ccd-chip. The position of the focus depends on the mean slope of the wavefront on every microlens (fig. 3.8).
The result is the mean derivation in x- and y-axis for every lens position:

$$P(x_n, y_m) = \frac{\delta W(x_n, y_m)}{\delta x} = \frac{\Delta x_{n,m}}{f} \tag{3.2}$$

$$Q(x_n, y_m) = \frac{\delta W(x_n, y_m)}{\delta y} = \frac{\Delta y_{n,m}}{f} \tag{3.3}$$

with $W(x_n, y_m) = mean\ wavefront\ at\ the\ microlens\ (n, m)$, and Δx, Δy the horizontal tilt of the axis.
This kind of measurement is limited to more or less continuous and differentiable wavefronts as seen in figure 3.9. Limitations of the HSS are shown in the diagram on the right. At the top the variation of the tilt between two microlenses is so strong that the focus points change places. Below, a leap in the wavefront between microlenses is shown. This leap has no influence on the result, so it cannot be measured. At the bottom lens the curvature

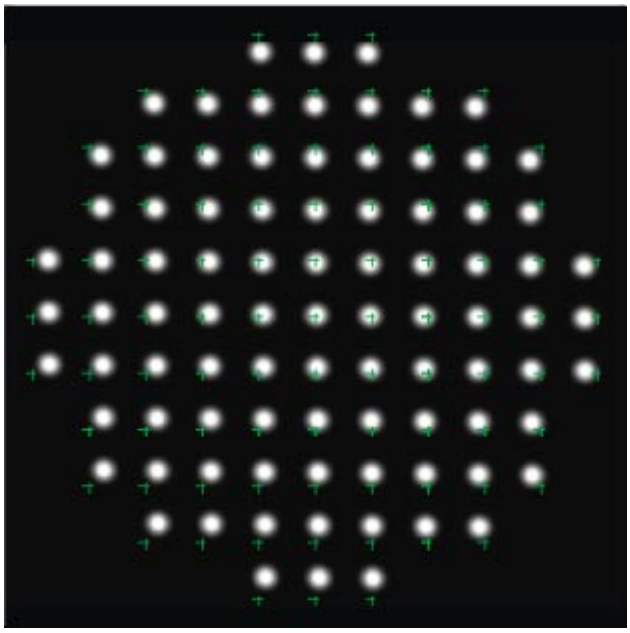

Figure 3.8: Image on the ccd-chip. The green crosses show the optical axes of the microlenses, the white points are the focus points of an uneven wavefront

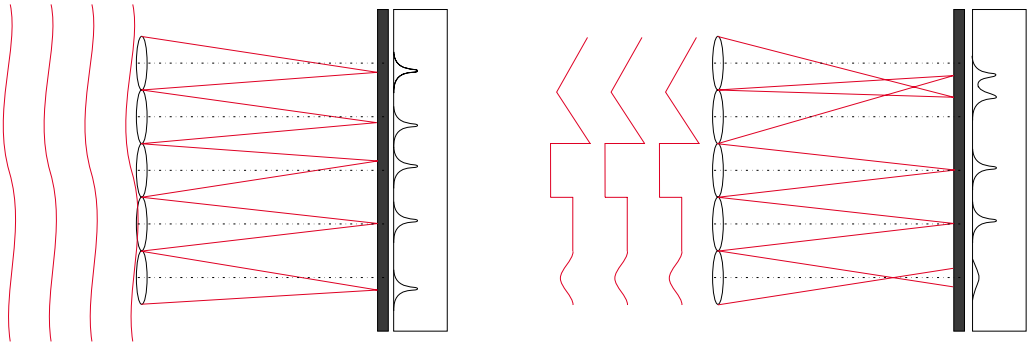

Figure 3.9: Limitations of the HSS
Left: A smooth wavefront reaches a HSS.
Right: A strongly aberrated wavefront reaches the HSS.

of the wavefront is too large for having a focus point at all.
Not only the position of the spots varies, their shape does so as well. The curvature of the wavefront surface on the area of each single lens has to be small. There are three properties of the HSS, which account for the dynamic range and the resolution: the pitch of the microlenses, the focal length of the microlenses (actually the distance between lens and ccd-chip) and the resolution of the ccd-chip. Their effects will be described in the next three subsections.

3.2.1 Shape of the Microspots

If the wavefront is not disturbed too much, each point can be seen as diffraction limited. So we get an Airy Disc. The diameter depends on the size of the aperture and the focal length of every microlens and the wavelength of light:

$$s = f\frac{\lambda}{h} = 30mm\frac{780nm}{400\mu m} \approx 60\mu m \tag{3.4}$$

with $s = spotdiameter$, $\lambda = wavelength$ and $h = pitch\ of\ the\ lens\ array$.
With 60 μm the size of the spot is less than a sixth of the distance to the next spot.
The shape of the spot gains relevance when stronger aberrations occur. For the determination of the focus-position the software uses a center of gravity algorithm. So a non-symmetric change in the shape of the spot could influence the result of the spotfinding and hereby the shape of the wavefront.
If stronger aberrations occur two effects have to be taken into account for calculating the spot shape.
Each HS spot is the image of the spot on the retina, imaged through the optical path through the individual micro lens. So for simulating the shape of the spots we need two PSF‘s:
Firstly the PSF we get from the beam coming into the eye including the precompensation of sphere and cylinder.
Secondly the PSF of the optical path out of the eye and through the machine to the HSS.
The final shape of the spot is now the convolution of both PSF‘s.
The first PSF is identical for all microspots, since the same lightsource on

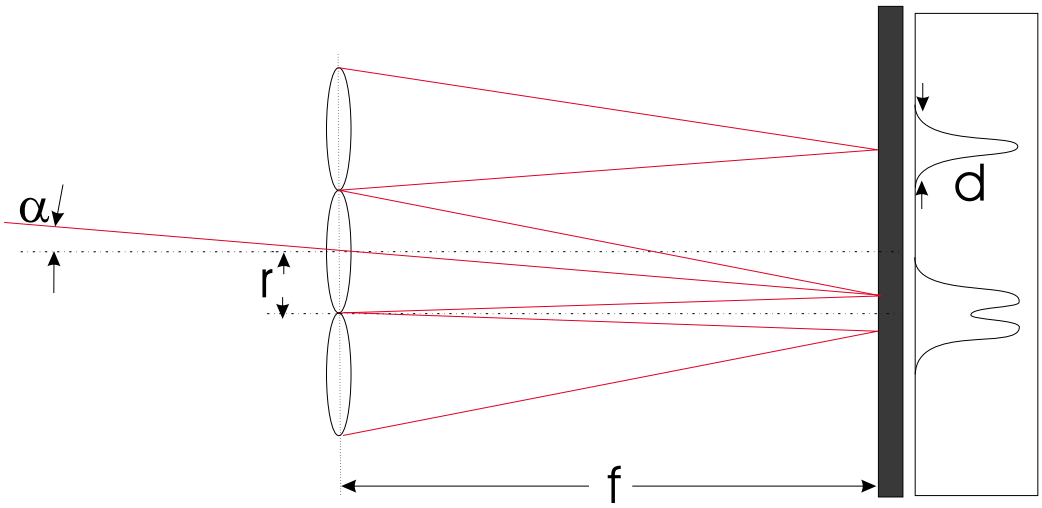

Figure 3.10: Dynamic range of a Hartmann-Shack Sensor.

the retina is used. The second PSF is different for every microlens, as every single lens is part of a different optical path through the pupil. The quality of the first PSF will normally be inferior as the beam diameter is larger here. The second PSF will be close to diffraction limited. If there is no strong local perturbation, the shape of all microspots will be very similar to the shape of the focal point on the retina.
A strong aberration of this spot will cause a shift in finding the center of gravity. This deviation is not that serious, because it affects all points in the same way. So it just changes the total tilt of the wavefront - which is not used anyway.

3.2.2 Dynamic Range

The dynamic range of a HSS specifies the range of aberrations that can be measured. As shown in fig. 3.9 the change in wavefront tilt may get so large that two focal points may overlap or even change places. To distinguish the focal points of different lenses we have to make sure that every focal point lies within the area of its own lens. This can be done by a fourier filter in the optical path.
Fig. 3.10 shows, in which way the dynamic range is limited. The displacement

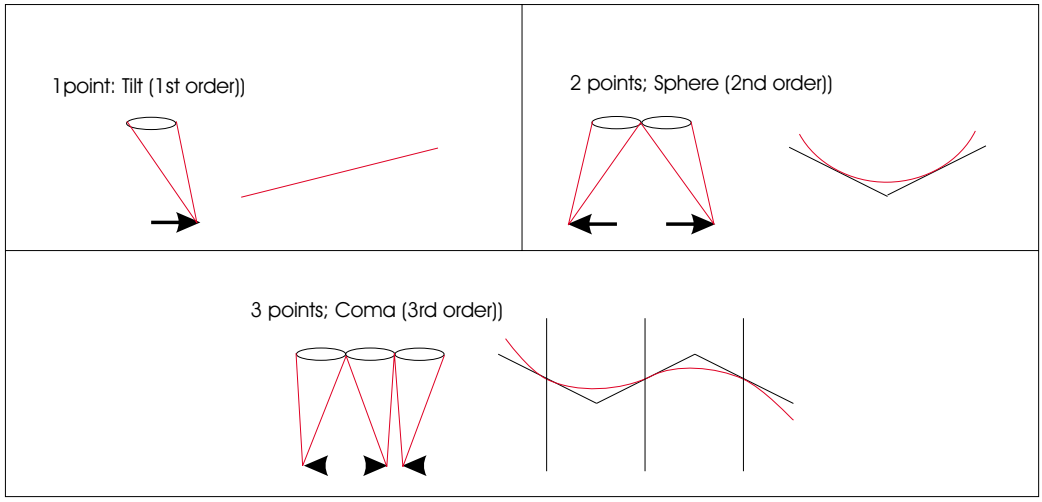

Figure 3.11: The maximum detectable wavefront complexity depends on the number of measured points.

of the focus point plus the spot size has to be smaller than the radius of the lens array. This leads to a maximum angle of:

$$\alpha_{max} \approx \tan\alpha \leq \frac{r - d/2}{f} \tag{3.5}$$

This gives us a maximum wavefront tilt of about 0.3°. So the maximum measurable sphere would be 1.8 D at a 6 mm pupil.

3.2.3 Resolution

There are two kinds of resolution: there is a minimum for the detectable wavefront slope and a maximum for the complexity of the wavefront.
Like the dynamic range the minimum wavefront slope depends on the focal length and the radius of the microlenses. The resolution of the ccd-chip matters at this point too.
For the minimum detectable wavefront slope the accuracy of the focus position is crucial. If the spot quality is high the position can be determined by fit routines by about a hundredth of the pixel-size of the ccd-chip. This

gives a minimum detectable tilt of

$$\alpha_{min} = \frac{ccd_{res}}{f} \approx \frac{0.12\mu m}{30000\mu m} \approx 4 \cdot 10^{-6} \tag{3.6}$$

So the minimum detectable angle is about $2.3 \cdot 10^{(-4)\circ}$. This corresponds to a change of the phase of $0.002\,\mu$m over a microlens and a minimum detectable defocus of 0.002 D.
The maximum detectable complexity depends on the number of detected points over the pupil-radius. As figure 3.11 shows the number of radial detected points equals the maximum of radial Zernike-orders that can be used. We get 15 Hartmann-Shack points over a 6 mm pupil, so we could calculate Zernike coefficients up to the 15th order. In fact we limit our calculations to the 6th order, due to computation time and necessary resolution.
For a two-dimensional pupil the maximum order of Zernike polynomials is fixed by the degree of freedom of the Hartmann-Shack points. Every point has two degrees of freedom, every Zernike polynomial one. For describing 6 orders of Zernike polynomials (=28 polynomials) we need at least 14 focus points. That corresponds to a pupil size of about 2.8 mm.

3.3 Zernike Polynomials

The wavefront error is described as a surface over the exit pupil. To describe the surface we use a function $W(x, y)$, which attributes a wavefront height for every position in the pupil $P(x, y)$. This height is the optical path difference between the reference sphere and the wavefront.
In ophthalmological optics the use of Zernike polynomials is dominating in the description of optical aberrations. Zernike polynomials were introduced in 1934 by F. Zernike as a convenient tool for representing wavefront aberrations over a circular pupil. A great advantage of these polynomials is the fact, that their relations to the classical aberrations are very simple. The polynomials have (among other things) the following properties:

- They are orthogonal over the circle with unit radius
- They are complete

	n				
$\|l\|$	0	1	2	3	4
0	1		$2\rho^2 - 1$		$6\rho^4 - 6\rho^2 + 1$
1		ρ		$3\rho^3 - 2\rho$	
2			ρ^2		$4\rho^4 - 3\rho^2$
3				ρ^3	
4					ρ^4

Table 3.1: Radial Polynomials $R_n^{|l|}(\rho)$, for $|l| \leq 4$, $n \leq 4$

The precision, an aberration can be described with by Zernike polynomials, depends on the order of the polynomials being used, and has no minor bound. The extension to higher order terms does not affect the coefficients of the lower order ones - at least in theory, on the assumption that the base of the fit is an infinite set of points distributed uniformly. In case a wavefront is represented as a linear combination of Zernike polynomials, the variance of the whole term is equal to the sum of the variances of the single terms.
The polynomial can be expressed as a product of two functions, one depending on the radial coordinate only, the other representing the dependence on the angular coordinate. The total polynomial can be described as follows:

$$Z_n^l = R_n^l(\rho)e^{il\theta} \tag{3.7}$$

with $n = \textit{degree of the polynomial}$, $l = \textit{angular dependence parameter}$, $\rho = \textit{normalized radial distance}$ and $\theta = \textit{angle with the axis } x$. The numbers n ($>$l) and l are either both even or both odd.
Tabular 3.1 gives the radial polynomials up to 4th order. Tabular 3.2 shows the full Zernike polynomials with their classical equivalent in non-complex presentation. Most classical aberrations can be represented by just one component, only nonrotationally symmetric aberrations like coma and astigmatism are decomposed into two components.

n	l	no.	Zernike Polynomial	Monomial Representation	aberration name
0	0	0	1	1	Piston
1	1	1	$\rho \sin\theta$	x	Tilt about y axis
	-1	2	$\rho \cos\theta$	y	Tilt about x axis
2	2	3	$\rho^2 \sin 2\theta$	$2xy$	Cylinder with axis at ±45 degree
	0	4	$2\rho^2 - 1$	$-1 + 2y^2 + 2x^2$	Defocus
	-2	5	$\rho^2 \cos 2\theta$	$y^2 - x^2$	Cylinder with axis at 0/90 degree
3	3	6	$\rho^3 \sin 3\theta$	$3xy^2 - x^3$	Triangular astigmatism on x axis
	1	7	$(3\rho^3 - 2\rho)\sin\theta)$	$-2x + 3xy^2 + 3x^3$	Third order Coma along x axis
	-1	8	$(3\rho^3 - 2\rho)\cos\theta)$	$-2y + 3y^3 + 3x^2y$	Third order Coma along y axis
	3	9	$\rho^3 \cos 3\theta$	$y^3 - 3x^2y$	Triangular astigmatism on y axis
4	4	10	$\rho^4 \sin 4\theta$	$4y^3x - 4x^3y$	
	2	11	$(4\rho^4 - 3\rho^2)\sin 2\theta$	$-6xy + 8y^3x + 8x^3y$	
	0	12	$6\rho^4 - 6\rho^2 + 1$	$1 - 6y^2 - 6x^2 + 6y^4 +$ $+12x^2y^2 + 6x^4$	Third order spherical aberration
	-2	13	$(4\rho^4 - 3\rho^2)\cos 2\theta$	$-3y^2 + 3x^2 + 4y^4 - 4x^4$	
	-4	14	$\rho^4 \cos 4\theta$	$y^4 - 6x^2y^2 + x^4$	
5	5	15	$\rho^5 \sin 5\theta$	$5xy^4 - 10x^3y^2 + x^5$	
	3	16	$(5\rho^5 - 4\rho^3)\sin 3\theta$	$-12xy^2 + 4x^3 + 15xy^4$ $+10x^3y^2 - 5x^5$	
	1	17	$(10\rho^5 - 12\rho^3 + 3\rho)\sin\theta$	$3x - 12xy^2 - 12x^3$ $+10xy^4 + 20x^3y^2 + 10x^5$	
	1	18	$(10\rho^5 - 12\rho^3 + 3\rho)\cos\theta$	$3y - 12y^3 - 12x^2y + 10y^5$ $+20x^2y^3 + 10x^4y$	
	-3	19	$(5\rho^5 - 4\rho^3)\sin 3\theta$	$-4y^3 + 12x^2y + 5y^5$ $-10x^2y^3 + 15x^4y$	
	-5	20	$\rho^5 \cos 5\theta$	$y^5 - 10x^2y^3 + 5x^4y$	

Table 3.2: First 5 orders of Zernike polynomials with classical description

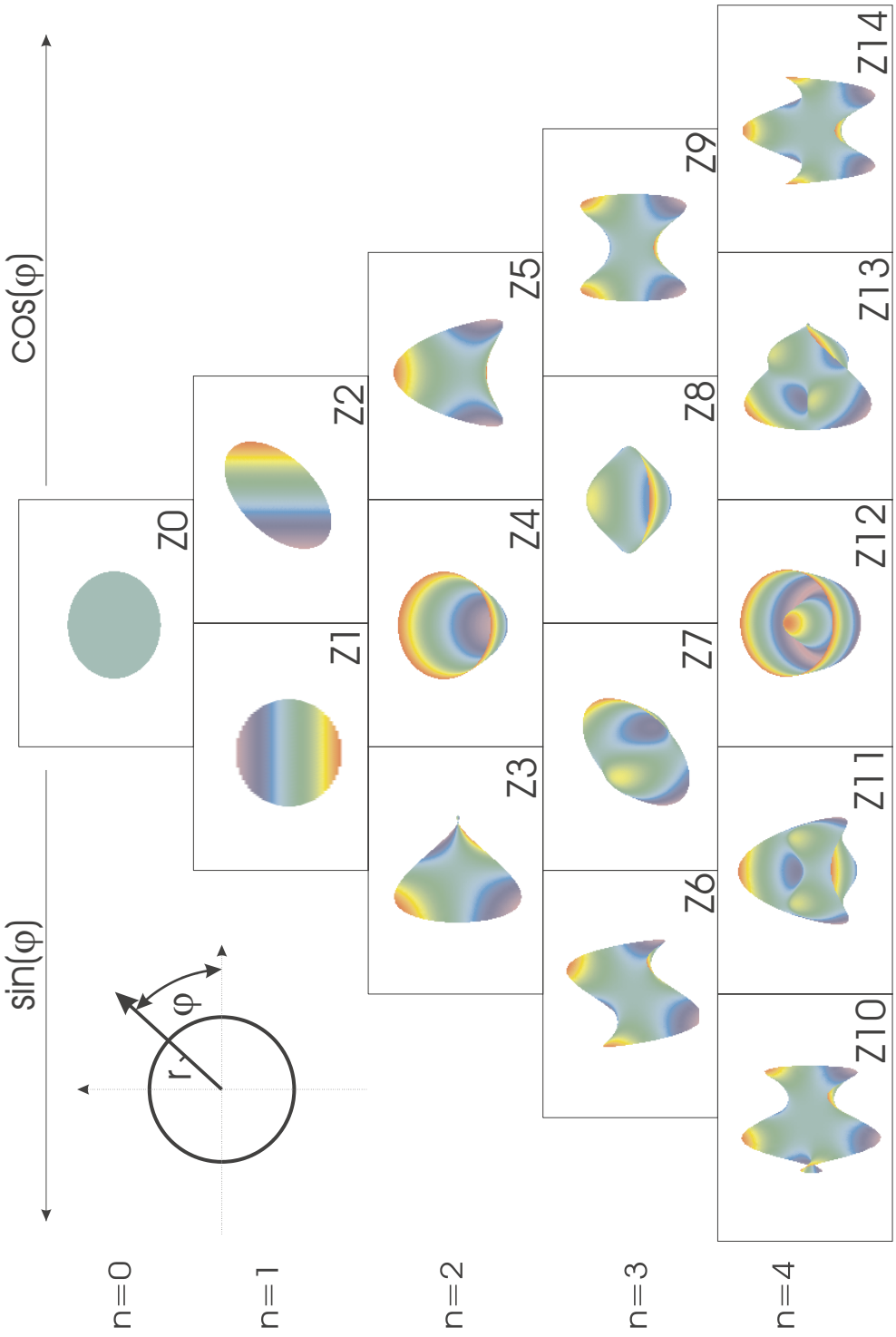

Figure 3.12: Chart of Zernike polynomials up to 4th order

3.4 Fourier Optics

This chapter gives a short overview of the use of Fourier methods in describing optics.
The Fourier transformation makes it possible to change over from space domain into frequency domain. Many optical processes - especially imaging with limited pupil size - can be handled much easier if the considerations and the calculations are done in the frequency domain. This counts especially for diffraction effects, which cannot be described with ray-tracing anymore.

3.4.1 Fourier Transformation

In the space domain an object is described by an intensity function $f(x, y)$. In the frequency domain the same object can be represented by use of the 2-dimensional Fourier Transformation as $F(\xi, \eta)$ with ξ and η representing the frequencies in x- and y-direction.
For the 2-dimensional case the transformation will be performed by

$$F(\xi,\eta) = \int_{-\infty}^{\infty}\int_{-\infty}^{\infty} f(x,y)e^{-i2\pi(\xi x+\eta y)}dxdy \tag{3.8}$$

The way back will be performed by:

$$f(x,y) = \int_{-\infty}^{\infty}\int_{-\infty}^{\infty} F(\xi,\eta)e^{i2\pi(x\xi+y\eta)}d\xi d\eta \tag{3.9}$$

3.4.2 Optical Imaging in Fourier Representation

$f(x, y)$ and $g(X, Y)$ are the complex entrance and exit functions of a linear system. The optical impact can be described by a linear operator $\mathcal{L}$:

$$g(X,Y) = \mathcal{L}[f(x,y)] \tag{3.10}$$

with the use of the principle of superposition we get:

$$g(X,Y) = \mathcal{L}\left[\int_{-\infty}^{\infty}\int_{-\infty}^{\infty} f(x',y')\delta(x-x')\delta(y-y')dx'dy'\right] \tag{3.11}$$

$$= \int_{-\infty}^{\infty}\int_{-\infty}^{\infty} f(x',y')\mathcal{L}[\delta(x-x')\delta(y-y')]dx'dy' \tag{3.12}$$

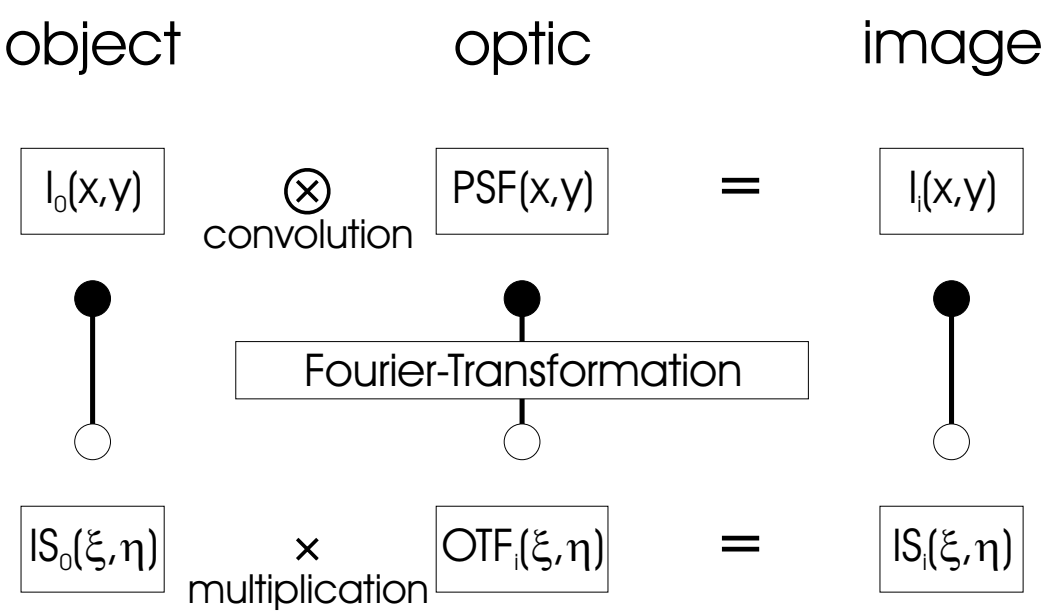

Figure 3.13: Fourier Optic in incoherent imaging

The application of the linear operator $\mathcal{L}$ on the δ-function gives us the so called "impulse answer".
The further application of the linear operator depends on the kind of illumination used. If the object is illuminated by coherent light, the optical system is linear in phase, otherwise it is linear in intensity. In the following we suppose the light to be incoherent.
Equation 3.12 shows a convolution in the space domain. A convolution on one side of a fourier-transformation is equal to a multiplication on the other side. This gives a multiplication in the frequency domain.

$$G(\xi, \eta) = OTF(\xi, \eta)F(\xi, \eta) \tag{3.13}$$

$G(\xi, \eta)$ and $F(\xi, \eta)$ are the fourier transformed of f(x,y) and g(x,y). Optical imaging can be seen as a filtering in the frequency domain.
Figure 3.13 illustrates this with $I = Intensity$, $OTF_i = incoherent\ optical\ transfer\ function$ and $PSF = point\ spread\ function$. The amplitude ratio is called modulation-transfer function (MTF).
The relation between the pupil function and the optical transfer function is of further interest. The incoherent optical transfer function is the autocorre-

lation of the pupil function:

$$PSF = |FT\{P(x,y)\}|^2 \tag{3.14}$$

This correlation makes it possible to obtain the PSF directly from the pupil function and therewith from the Zernike polynomials.

3.5 Propagating Wavefronts

Every wavefront changes its shape while propagating in space. Only an infinite widespread flat wavefront would keep unchanged. So the shape of a wavefront will be different in any two places.
A wavefront originating from a pointsource stays spherical in shape, but the curvature varies with the reciprocal distance from the source. In a sufficient distance, however, the wavefront can be seen as flat. The differences between a real wavefront surface and a theoretical flat surface make the total wavefront error.
In most cases it is not possible to have the wavefront sensor at exactly that place, we want the information about. So the wavefront has to be imaged in a definite way from the plane, we want to have values for, to a plane we can actually take values in by our sensor. The easiest way to realize this, is by using conjugate planes of a lens system.
A Badal system - consisting of two lenses - modifies the wavefront in just that accurately defined way. Defocus and cylinder can be eliminated, so the remaining higher order wavefront error will be recorded. The elimination of the lower order aberrations is a suitable means of optimizing the Hartmann-Shack sensor in different respects, aiming at either a large active range or a high accuracy. The active range the higher order aberrations need is far lower. So we optimize the HSS for a high accuracy and correct the sphere and cylinder ahead of the wavefront measurement.
A wavefront on one side of the optical system is - apart from small errors introduced by the system itself - similar to the wavefront in the conjugate plane.
An alteration in the shape may result from lens-failures or diffraction, the finite size of the object or the surfaces being of further influence. In particular

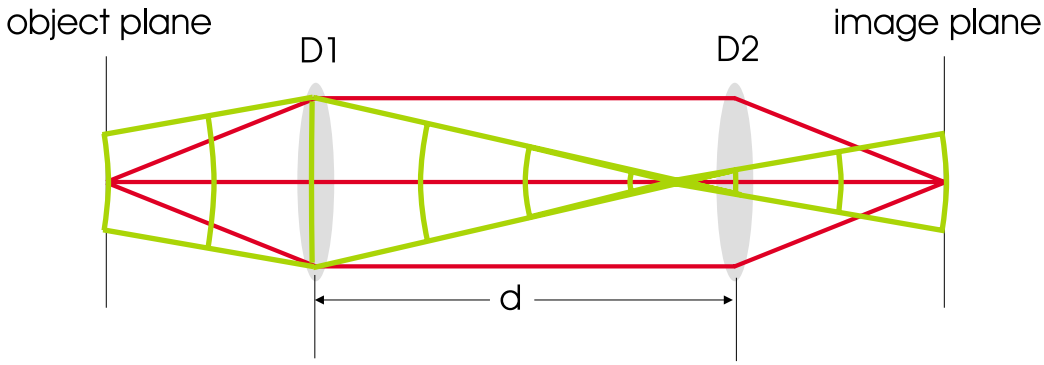

Figure 3.14: Wavefront propagating from a plane to its conjugate plane

a small aperture in the optical path will cause a flattening of the wavefront as it works as a Fourier filter.
For the pre-compensation there are three kinds of correction in use: Shifting the telescope for correcting the sphere, introducing cylinder lenses for correcting the cylinder and variations of the OPD in a conjugate plane by using an active mirror for correcting higher order aberrations.

3.5.1 Correcting Aberrations in the Conjugate Plane

Correcting aberrations works by a step-by-step-principle, using a series of conjugate planes, the first one being the object plane and the last one the measurement plane of the sensor. In the conjugate planes in-between the optical path can be varied for every longitudinal position in a controlled way. This can be done by an active mirror, a liquid crystal device, or simply by taking influence on the optical path-length by inserting a non uniform glass.

3.5.2 Using a Telescope for Correcting Sphere

The Sphere Correction will be realized by shifting the distance of the lenses in a Badal system. This shift has no influence on the position of the conjugate planes in respect to the lenses as you can see in fig. 3.14. Shifting the length of the telescope has influence on the curvature of the wavefront only, all other deviations staying unchanged. The total sphere is given by $D = D_1 + D_2 -$

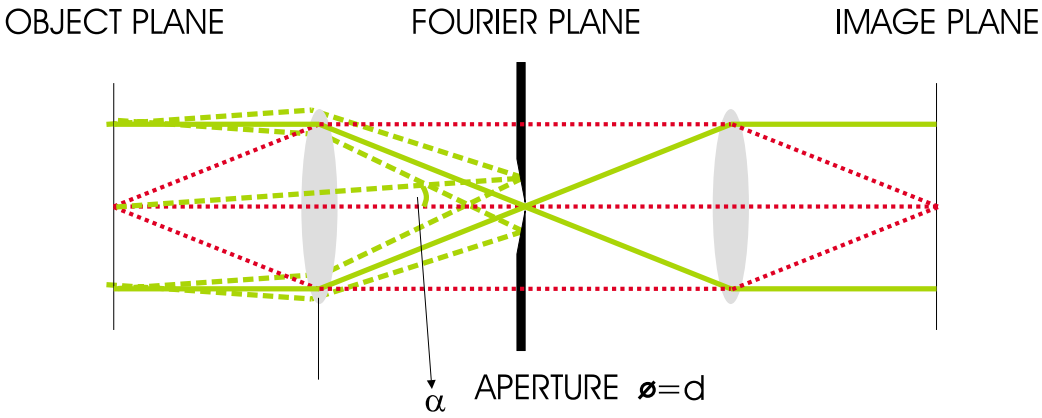

Figure 3.15: A Fourier Transform Lens

dD_1D_2. With the zero position of $d = \frac{1}{D_1} + \frac{1}{D_2}$ this leads to a change of sphere of

$$D = -\Delta d D_1 D_2 \tag{3.15}$$

with $D = effective\ sphere\ in\ D$, $D_1 = sphere\ of\ first\ lens\ in\ D$, $D_2 = sphere\ of\ second\ lens\ in\ D$ and $\Delta d = shift\ between\ the\ lenses\ in\ m$. The change of corrected sphere is thus proportional to the shift between the lenses with a paraxial system.

3.5.3 Correcting Cylinder

The cylinder pre-correction is realized by a pair of cylindrical lenses, positioned in the optical path of the system. The ideal position would be in a conjugate plane of the pupil.

3.5.4 Spatial Filtering

The wavefront system has to eliminate the reflections from surfaces other than the retina, especially those from the cornea. For this reason an aperture is introduced into the last telescope. The size of the aperture is crucial. If it is too large, unwanted light comes through, if it is too small, spatial frequencies of the wavefront will be cut off.
The first lens of the telescope works as a fourier transformer, the aperture in the Fourier plane as a filter for high frequencies.

In a perfect optic the crossing of the aperture will be limited to that part of the beam, of which the tilt satisfies the following conditions:

$$\tan\alpha \leq \frac{r}{f} \tag{3.16}$$

The spatial information for smaller frequencies gets lost. With f=80 mm and r=0,5 mm α should be smaller than 0.00625 which corresponds to a sphere of 2.1 D (PTV=18,7 μm) at a 6 mm beam.
Higher order wavefront distortions have a stronger maximal tilt with the same amplitude. So they get cut off with an even smaller amplitude. For third order spherical aberration the cut-off amplitude goes down - compared to a ideal sphere - by the factor 1/3, for fourth order terms the factor is about 1/4. In fact it is the total local tilt in a wavefront that matters, not the tilt per polynomial.

3.6 Single Pass Measurement

The Hartmann-Shack method works on the assumption that the focus-point on the retina is a point-lightsource. This is correct, if the reflection from the retina is diffuse and the light loses all its phase information of the way into the eye. Several retina models (e.g [Ar95], [Di00]) attribute the fact that the retina is diffuse to the roughness of the surface made up by the individual cones.
The single-pass or the double-pass property (corresponding to diffuse or specular reflex) may prevail. This can be tested by a simple setup. A measurement of a strongly aberrated eye - with a non symmetrical kind of aberration - is performed. If the double-pass property dominates the wavefront should be symmetric. In case of specular reflex and if incoming and outgoing beams have the same diameter the result should be an autocorrelation of the Single Pass. The described setup was simulated with ZEMAX, an optical design program. The result was compared to a real measurement on an artificial eye with diffuse and specular kind of reflection, and to the measurement on a real eye. For the diffuse reflector SPECTRALON was used, as specular reflector a mirror. The results are shown in figure 3.16.

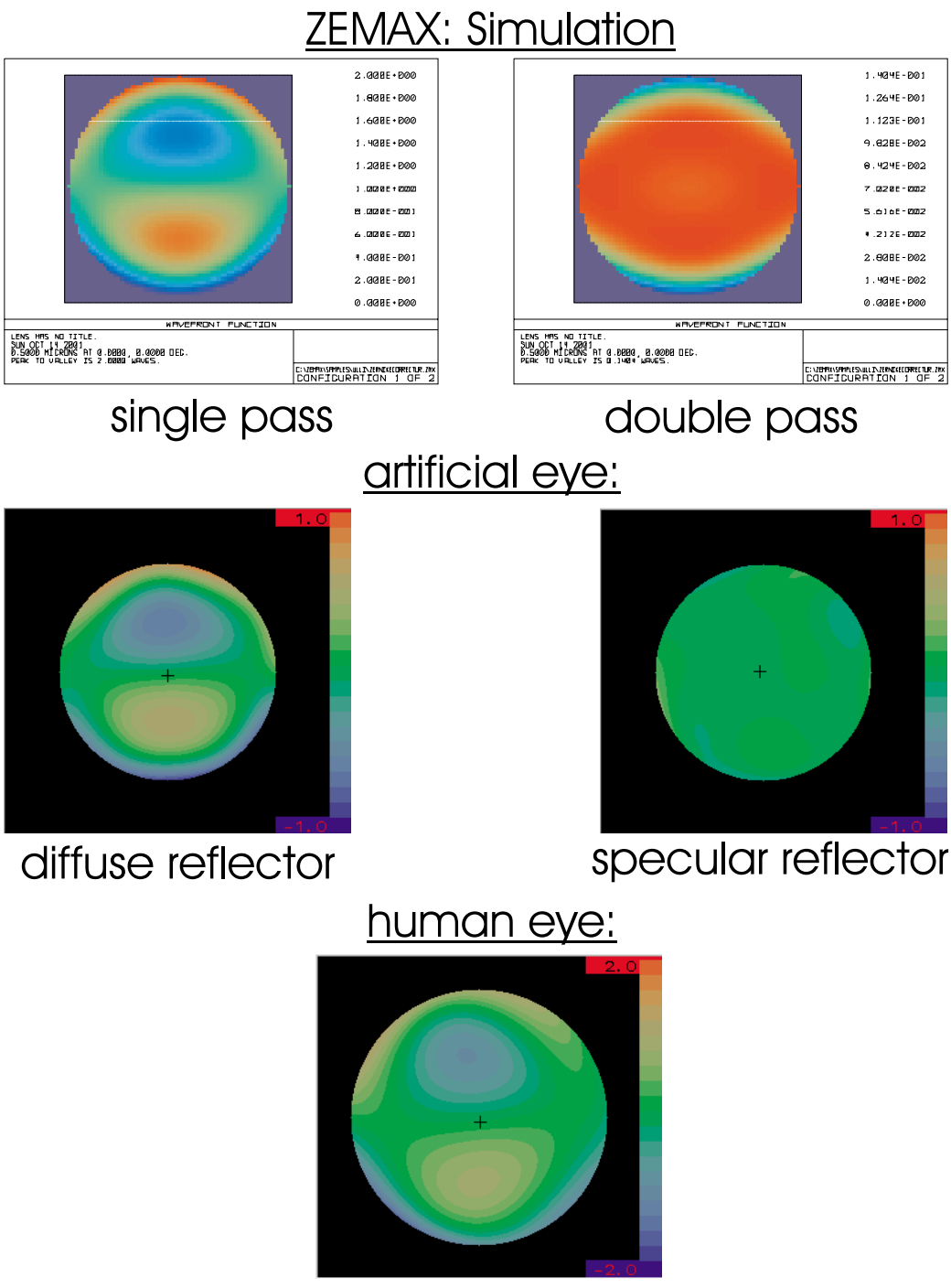

Figure 3.16: Simulation (by ZEMAX) and Measurement: Double-Pass vs. Single-Pass

The results of the single pass setup are seen on the left, those for the double-pass on the right. The ZEMAX-simulation is given at the top. The results for the artificial eye are shown below. Those for a real eye with a well known coma in front of the eye are given at the bottom.
Diaz-Santana points out the independence of phase information and intensity information. While the phase information of the first pass gets lost, the intensity information remains unchanged. This can be seen in the shape of the microspots, which vary with the size of the incoming beam.

3.7 Describing Optical Imaging Quality

For the description of the performance of an optical system there are several parameters in use. Some of them are applied to the human eye as well. A short overview of some scales used in ophthalmology will be given in this section.

3.7.1 Root Mean Square

The RMS of the wavefront is a very simple criterion. It is nothing but the integrated root mean square of the differences between the wavefront surface and the mean value of the surface. The complex phenomenon of aberration is packed into a single number. This makes it so convenient in ophthalmology. The RMS can be calculated directly from the Zernike polynomials.
For the calculation of the RMS we refer to Zernike polynomials of second order minimum. The zero order is not measured at all. The first order gives information about the tilt only, which is connected to the position of the eye. It does not supply any information about the characteristics of the eye itself. The Zernike polynomials are orthogonal and the zero order term is set to zero. So the mean value of the wavefront surface is zero, too. The RMS is thus simply the mean squared value of the wavefront over the pupil.

$$RMS = \sqrt{\frac{\int_0^r \int_0^{2\pi} W(\rho,\theta)^2 \rho d\rho d\theta}{\int_0^1 \int_0^{2\pi} \rho d\rho d\theta}} = \sqrt{\frac{1}{\pi}\int_0^1 \int_0^{2\pi} W(\rho,\theta)^2 \rho d\rho d\theta} \qquad (3.17)$$

In taking mean values of the Zernike polynomials the integral can be replaced by a sum of the weighted coefficients. For a real pupil size the integration will be from 0 to r.

$$RMS = \sqrt{\frac{\int_0^r \int_0^{2\pi} W(\rho,\theta)^2 \rho \, d\rho \, d\theta}{\int_0^r \int_0^{2\pi} \rho \, d\rho \, d\theta}} \tag{3.18}$$

$$= \sqrt{\frac{1}{\pi r^2} \int_0^r \int_0^{2\pi} \left(\sum_{i=0}^{order} c_i Z_i(\rho,\theta) \right)^2 \rho \, d\rho \, d\theta} \tag{3.19}$$

$$= \sqrt{\frac{1}{\pi r^2} \sum_{i=0}^{order} c_i^2 \int_0^{2\pi} \int_0^1 Z_i^2(\rho,\theta) \rho \, d\rho \, d\theta} \tag{3.20}$$

$$= \sqrt{\frac{1}{\pi r^2} \sum_{i=0}^{order} c_i^2 Z'^2_i} \tag{3.21}$$

with $Z'_i = weighting\ coefficient$ for each Zernike. It depends from the radial and angular order.

$$Z'_i = \frac{1}{(2-\delta_l) * (n+1)} \quad \text{with} \quad i = \frac{n(n+1)}{2} + \frac{n-l}{2} + 1 \tag{3.22}$$

With 3.21 the RMS can be calculated simply as a root of the sum of coefficients. This makes calculations with the RMS very easy.
The Peak To Valley (PTV) is closely connected to the RMS. While the PTV depends - heavily - on just two extreme values, the RMS is a kind of mean value received from the complete set of data points. This makes the RMS much more stable against deviations.

3.7.2 Optical Aberration Index

The Optical Aberration Index (OAI) is defined as

$$OAI = 1 - e^{(-RMS)} \tag{3.23}$$

The OAI has values between zero and one. Zero stands for an optical system that is perfect and 1 for infinite aberrations. The OAI is very sensitive in the typical range for higher order aberrations. It was introduced as an even simpler scale for the optical quality of an eye.

3.7.3 Modulation Transfer Function

A typical target for testing the quality of an optical system consists of a series of alternating black and white bars of equal width with a contrast of 1. These targets are connected to a vision chart with Snellen E's, as used in ophthalmology. The Modulation Transfer Function (MTF) gives the contrast of the image (as percentage of the contrast of the object) in dependence of the frequency. The contrast is defined by: $Contrast = \frac{I_{max}-I_{min}}{I_{max}+I_{min}}$. The MTF may be compared to the Aerial Image Modulation (AIM) curve. This curve shows the smallest amount of modulation a sensor like a ccd-camera or the retina is able to detect. The AIM is a function of the frequency used as well. As the MTF normally goes down with frequency increasing, the AIM increases with frequency. The point of intersection gives the resolution.
For a diffraction limited optic the MTF can be calculated by

$$MTF(\nu) = \frac{M_i}{M_o} = \frac{2}{\pi}(\Phi - \cos\Phi \sin\Phi) \tag{3.24}$$

with

$$\Phi = \arccos\frac{\lambda\nu}{2NA} \tag{3.25}$$

$\nu = frequency\ in \frac{cycles}{mm}$, NA=numerical aperture and $\lambda = wavelength$

3.7.4 Point Spread Function

The point response of an optic should still be a point. Even if the optic is perfect the response is a pattern - due to the diffraction. In a real system the aberrations widen the image up to a spot. The spot is represented by a 2-dimensional distribution. This is described by the Point Spread Function (PSF).
If the aberrations are smaller than $0.25\,\lambda$ (Rayleigh criterion) the diffraction pattern provides a good description of the PSF.
Up to about $2\,\lambda$ it is appropriate to consider the manner in which the aberration affects the diffraction pattern. For larger wavefront aberrations illumination described by raytracing is sufficient for description.
The aberrations of eyes are in this transition zone in most cases.

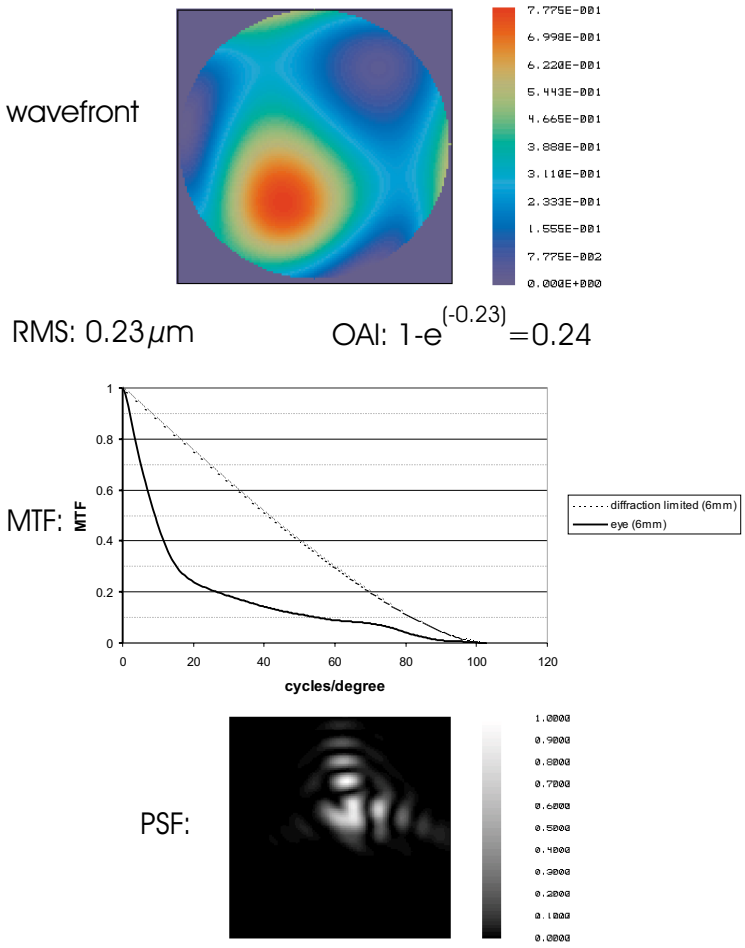

Figure 3.17: Different representations of the image quality of one eye

Chapter 4

Setup

This chapter gives a description of the device as a whole. First the purpose and the general idea of the optical setup are dealt with. The elements and their roles in the system make up the main part. Finally measurements at test optics are presented.

4.1 Specification of the System

Specifications originate in the scheduled application in ophthalmology: The measurement of higher order aberrations in a strongly aberrated human eye as tool for targeting refractive surgery in the cornea.
The most important specifications are the effective and the active range, the pupil size and the accuracy of the system:

- effective range:
  The sphere must be measured in a range from +8 D to -12 D
  The astigmatism must be measured in a range from 0 D to -5 D

- pupil size:
  An eye must be evaluable in a pupil size up to 6 mm.

- Accuracy:
  The amount of sphere and cylinder must be measured with an accuracy

of ± 0.1 D, the axis with an accuracy of ± 2 degrees.
The reconstructed wavefront must have an accuracy of $\pm 0.1\,\mu$m

The range is accustomed to the typical range of ametropia. The maximum pupil size is set by the typical size of a large pupil. A minimal evaluable pupil size of 3 mm derives from the minimum number of data points.
The accuracy should be in the order of the short-time fluctuations of the aberrations of the eye.

4.2 The Optical Setup

First an overview of the setup will be given then the details will be described in the subsections.
Fig. 4.1 gives the setup of the device. There are four main parts, two for the measurement itself and two for the accurate positioning of the eye. To prevent interferences between the parts each part uses a beam with a special wavelength or polarization optimized for the particular use.
The first part (blue) is used for the operators surveillance of the patient's eye position. The eye is illuminated by two LEDs at 900 nm. The anterior near-infrared ccd-camera gets a direct image of the illuminated eye through a dichroic beamsplitter. This picture enables the operator to align the device to the pupil in lateral and axial position.
The second part is a target provided for the patient (green dots). The green target ($\lambda \approx 550$ nm) leads the patient's line of sight to the right angle. A further task of the target is to relax the accommodation. The target is a very small picture in the focal plane of a lens. The beam originating from this lens is coupled into the optical axis of the device by a dichroic beamsplitter. Then the beam crosses both precompensation units. So the image arriving at the retina is already sphero-cylindrically corrected.
Using both parts in combination - the surveillance unit and the target - makes sure that the real line of sight of the eye will be measured.
The third part (red) is the illumination beam (red-dashed, 780 nm). At the top you see the laser diode. The collimated polarized beam originating from the diode is coupled into the optical axis by a polarizing beamsplitter-cube.

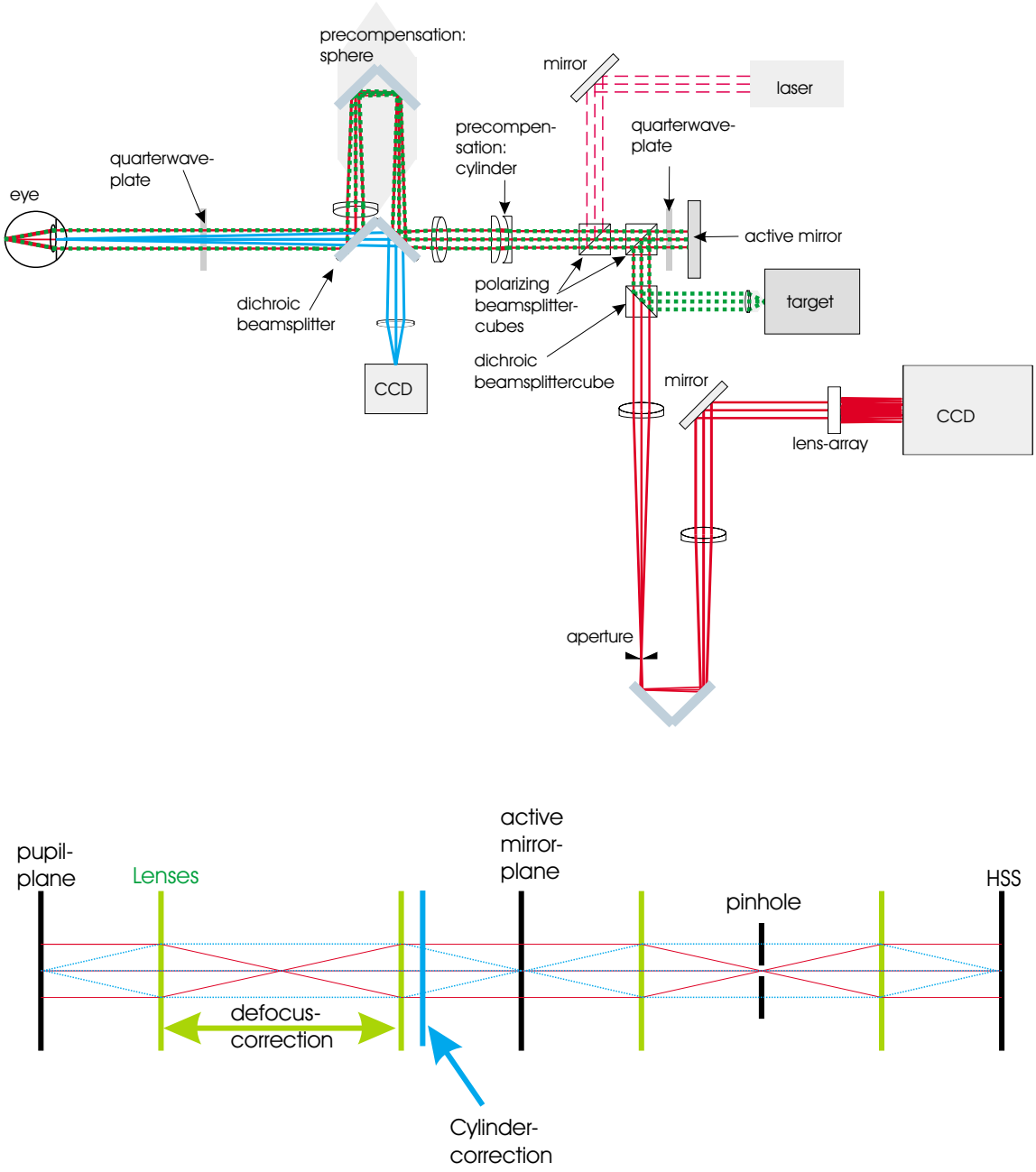

Figure 4.1: Setup of the measurement device

After the precompensation of the sphero-cylindrical aberrations of the eye the beam crosses a quarterwave-plate before entering the eye. The eye collimates the beam onto the retina. The spot we get here is - depending on the higher order aberrations - close to being diffraction limited. The diffuse reflection of this spot is used as lightsource for the measurement.
The fourth part is the sensor beam itself (also 780 nm). The intensity of the entering beam exceeds the intensity of the beam coming back from the retina by the factor 1000. So reflections from optical surfaces have to be kept small.
The quarterwave-plate changes the polarization of the light from linear to circular polarization. Crossing the quarterwave plate once again on the way back the polarization rotates by 90 degrees compared to the illumination beam. So the way back can be distinguished from the way into the eye.
For directing the beam there are two telescopes (fig. 4.1, bottom). The first one images the wavefront at the pupil plane onto the plane of the active mirror, the second one takes the image over to the HSS plane. For the first telescope the length - and thereby the optical power - can be shifted by moving the retro mirror. So it is used for compensating the beam for defocus. After the second lens of the anterior telescope there is a cylinder compensation unit consisting of two rotatable cylinder lenses with focal lengths identical in amount and diverse in sign. The beam reaching the mirror behind these elements has only higher order aberrations and some residual cylinder and sphere.
The second telescope is fixed. In the focal point of the first lens there is an aperture used to filter out the reflections from the lenses and the cornea. It also limits the dynamic range of the wavefront sensor. In the focal plane of the second telescope there is the HSS measuring the residual aberrations. This plane is once more conjugate to the pupil plane again. The outgoing and the incoming beam are discriminated by different linear polarization and by their direction.

4.3 The Observation Unit

The observation unit provides a life image of the eye and permits the operator to adjust the device precisely.
It consists of a camera with one lens imaging the retina to the ccd-chip. The camera is directed onto the eye through a dichroic mirror directly on the optical axis of the machine. The aperture is very large in order to have the depth of focus very small. The operator watches the image on the monitor. He gets information about any transversal or axial displacement of the eye. A transversal displacement makes the image of the eye move off center, thus it can be recognized on the screen directly. The interest in this kind of displacement is minor, as it can also be measured by the HSS, and a shift can be considered in the results. The influence of a lateral shift on the measurement wouldn't be large anyway. An axial displacement results in the image on the observation camera being blurred. This displacement cannot be reconstructed, therefore the effect must be kept small.

4.3.1 Determination of the Axial Position of the Eye

Fig. 4.2 shows the importance of a precise adjustment of the the z-position of the eye. The transversal position is not that important as it can be reconstructed with the HSS-picture.
A wrong estimation in the z-position of z mm in an eye with sphere S causes a failure in the determination of the sphere of

$$\Delta S = S - \frac{1}{\frac{1}{S} + z} \tag{4.1}$$

If the eye is 1 mm off, at a 10 D eye the result will be wrong by 0.1 D. So the depths of focus should be smaller than 2 mm to meet the specifications.
It is not possible to reconstruct the z-position of the eye, so it has to be set precisely with the monitoring camera.
The monitoring camera is designed with a very low depth of focus. This causes a blur of the image if the eye is out of the perfect position. An image can be considered as blurred if the image of a point-source gets so large that it will be imaged on two pixels. A single pixel of our camera has a size of

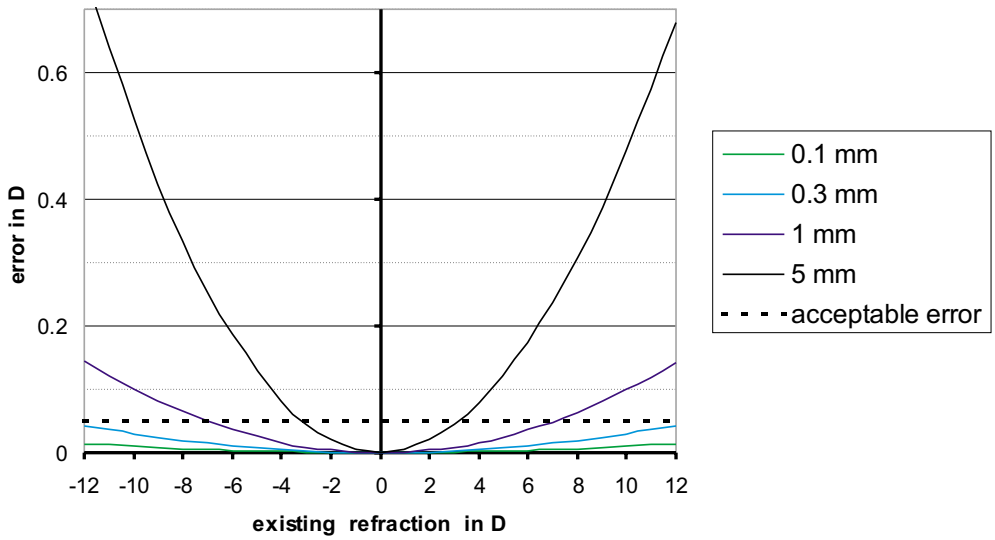

Figure 4.2: Correlation between the precision in z-position and the following error in sphere. In the y-axis is shown the error in D with the existing sphere on the x-axis. The different curves show the different facilities in the determination of the eye position.

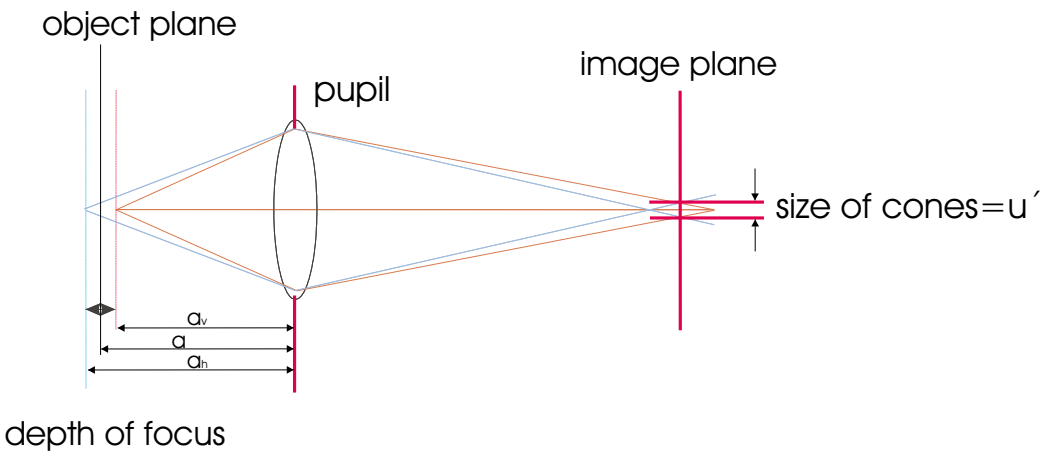

Figure 4.3: Definition of the depth of focus

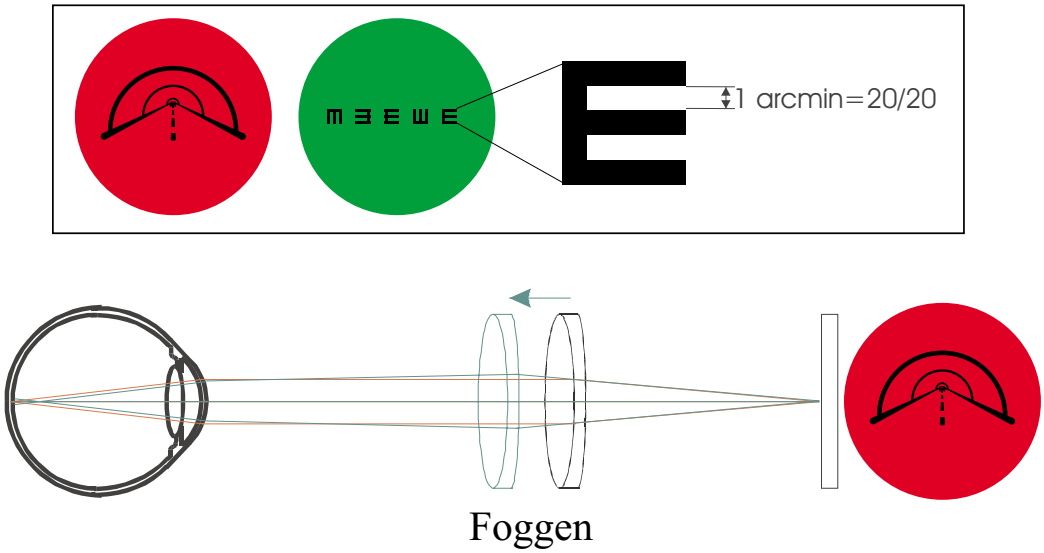

Figure 4.4: Target and Vision Chart Unit:
Left: Target
Right: Vision Chart

about 11 μm. As seen in fig. 4.3 the depth of focus can be calculated by

$$a_f = a_h - a_v \frac{af'^2 2u'k(a+f')}{f'^4 - (u'k(a+f))^2} \tag{4.2}$$

with $a_f = depth\ of\ focus$, $a = optimal\ object\ distance$, $f' = image\ focal\ distance$, $k = numerical\ aperture$, $u' = blur\ size$. If the blur size is set to a more realistic 0.1 mm (=5 pixel) the depth of focus in this setup is about ± 0.3 mm.

4.4 The Target and Vision-Chart Unit

The Target Unit presents a stimulus to the proband. This has two main functions:

- Providing a relaxed accommodation status of the eye.
- Doing Vision Tests in the machine.

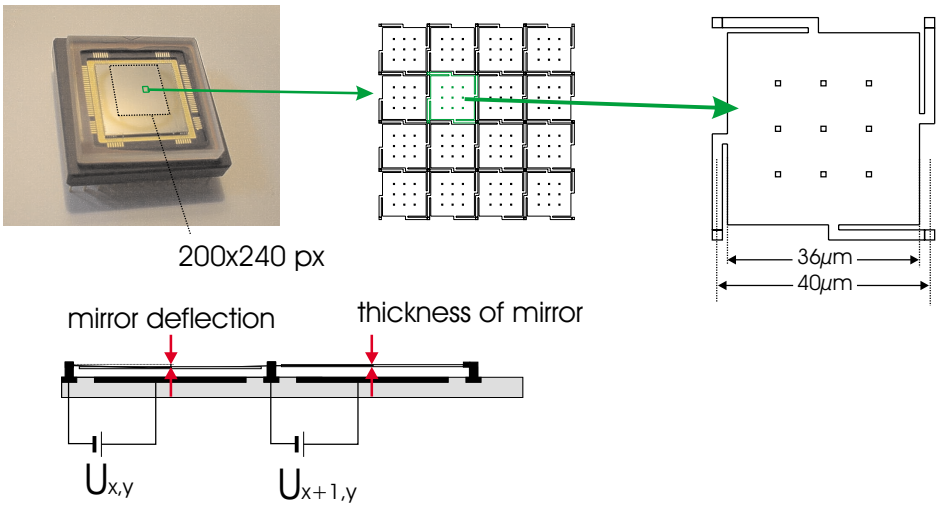

Figure 4.5: Setup of the micromirror

The optic of the vision chart is limited to a lens with a photolithographic monochrome drawing in its focal plane. The drawings can be swapped by a revolving mechanism. It is back-lighted with an alternatively green or red LED.

The lens works like a simple magnifying glass. The object is projected to infinity, so that the proband relaxes his accommodation to obtain a sharp image. To make sure that the eye is relaxed the distance between lens and object can be increased. So the patient gets a blurred image that is shifted 1.5 D to the hyperope even in a relaxed eye. This shifting is called fogging, since the object cannot be seen clearly anymore.

The target is fogged during the measurement. It shows a schematic of a tunnel leading the eye to the far point.

After the measurement the lens moves back to its original position. Now Snellen lines of different sizes can be presented. The structure size on the target reaches from 8 μm to 25 μm. These sizes correspond to a vision range from 20/10 to 20/32 (0.5 arcmin to 1.6 arcmin).

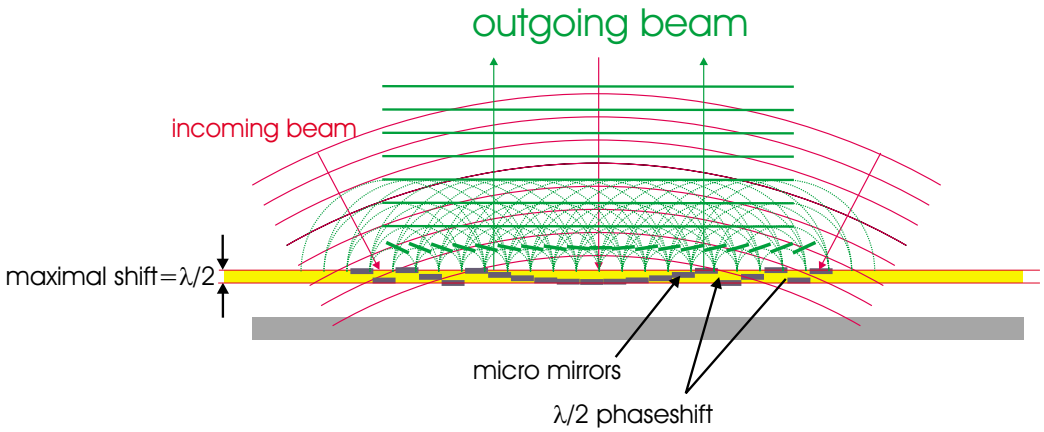

Figure 4.6: Functionality of the micromirror

4.5 The Active Mirror

An active matrix mirror (Aktive Senk-Spiegel Matrix, AKSM) is used in the device (see fig. 4.5). It is an array of 200 x 240 micromirrors ((40 μm x 40 μm each). Each one of the mirrors can be lowered up to 400 μm independently. The mirrors can only be lowered without the facility of tilting. With this technique wavefronts can be corrected up to the double height of deflection - more than one wavelength. By using the 2-π method (fig. 4.6) the range of the wavefront deformations to be corrected can be enlarged by far.
The 2-π method makes use of the phase properties of light. A sag of 2-π between two neighboring mirrors has no effect on the direction of the light and can be subtracted without any effect on the wavefront. So the range of movement needed for the correction of any wavefront-deformation can be reduced to $\lambda/2$. In fact the use of the mirror is limited to light of one wavelength when using the 2-π method.

4.6 The Measurement Unit

This section gives a description of the main components of the process of wavefront measuring.

4.6.1 Light Source

As light source for the sample beam we use an infrared laser diode. It is optimized to operate close to the lasing threshold. So compared to a standard laser the coherence level is lower, the quality of the wavefront of the beam staying high. The high coherence level leads to a speckle-effect described below. A polarizer in front of the laser supplies a polarization ratio greater than 99 %.
The light of the diode has a wavelength of 780 nm at a power of 60 μW. The power arriving at the eye is reduced to less than 50 μW by the polarizer and as well as by several mirrors and lenses in the beam path.

4.6.2 Hartmann-Shack Sensor

The Hartmann-Shack Sensor consists of a microlens array and a ccd-camera. The microlens array is made of gradient index lenses. Each of the lenses has a diameter of 400 μm and a focal length of 30 mm at a wavelength of 780 nm. The camera has a 2/3“ ccd-chip positioned in the focal plane of the microlenses. It has 737(H) x 575(V) pixel with a size of 11.6 μm(H) x 11.2 μm(V) ($\Rightarrow$ total size: 6.5 mm x 8.6 mm). The signal to noise (S/N) ratio of the camera is very low (59 dB), the sensitivity is very high (min. illumination: 0.05 lx).

4.7 Software

This section is about the use of the software, the Graphical User Interface (GUI) and the options for data export and data analysis.
The software bases on routines developed at the Institut für Angewandte Physik by Michael Schottner, Frank Müller and Stefan Wühl. The version actually used was designed by Frank Müller and Stefan Wühl at 20/10 Perfect Vision.
Fig. 4.7 shows the GUI of “WavePrint“, the software predominantly used. At the top left the Patients Data Input is shown. By pressing “GO“ a second window opens (fig. 4.8) giving the examiner the Hartmann-Shack pattern.

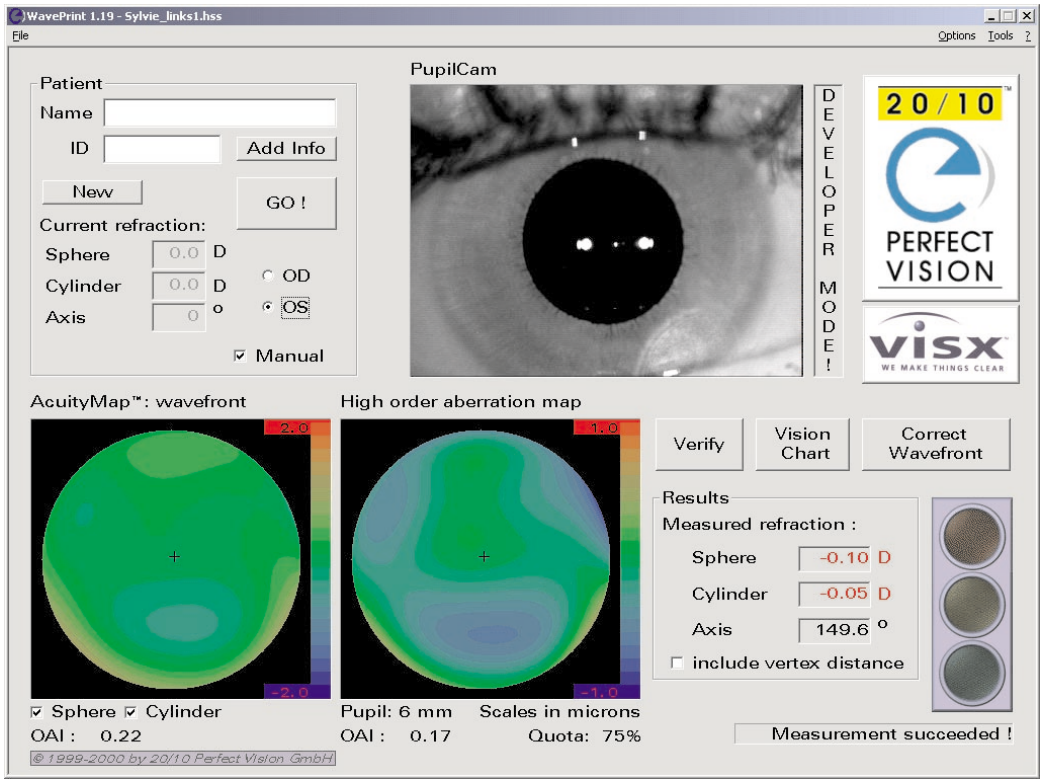

Figure 4.7: The Graphical User Interface

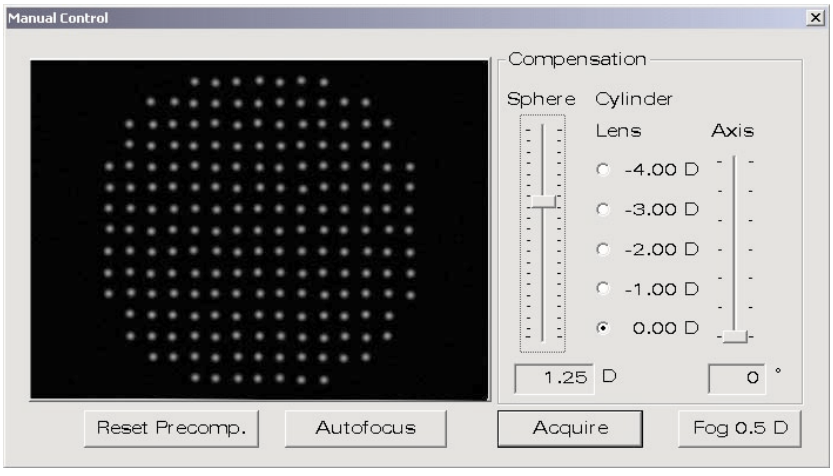

Figure 4.8: The manual control during the measurement

This window enables the user either to start the autofocus for the precompensation of sphere, cylinder and axis or to choose a setting manually.
The "Fog" button starts the fogging of the target. This shifts the target 1.5 D to the hyperope and prevents the patient from accommodation.
As soon as the picture of the iris in the PupilCam and the picture of the Hartmann-Shack array are both sharp the measurement can be started. This is done by pressing the "Acquire" button.
The results are shown in the bottom part of the window. On the left you see the total wavefront map. Next to it on the right you see the higher order aberration map. It shows the wavefront formed by third to sixth order of Zernike polynomials. At the bottom right the refraction data like sphere, astigmatism and axis are given. By checking the vertex distance box the values will be converted to the plane 16 mm in front of the cornea - the plane where glasses would be positioned. This makes them comparable to the manifest refraction normally used by ophthalmologists. The vertex distance is calculated the same way as the failure in the sphere, by the determination of the axial position of the eye.
The programm allows the export of sphere, cylinder, axis, pupil size and the first 27 Zernike coefficients, as well as the total RMS from second to 6th order. This export function opens a way to further investigations.

4.8 Precompensation of Lower Order Aberrations

The principle of the Hartmann-Shack Sensor gives restrictions to the measuring-range. On the one hand the range is restricted by the optical properties of the eye - especially if the higher order aberrations are very large - on the other hand it is restricted by the setup of the WaveScan in multiple ways.
The task of the precompensation unit is not restricted to the compensation of the beam coming out of the eye for the lower orders. It also has to supply a good light-source for the sensor beam by keeping the focus-spot on the retina very small. The larger the light source, the poorer the results at the HSS-measurement will be. Every point of the HSS-pattern is a convolution

of the point-lightsource on the retina, with the PSF of the particular part of the total optics passed (eye plus WaveScan). The sphere and the cylinder are corrected (sphere from -12 D to +12Ḋ, cylinder from (-6 D to 6 D)). Only higher order terms can restrict the measurement range.
The restrictions in the measuring range are twofold. One is caused by the aperture of the second telescope, the other one by the principle of the HSS itself.
The first lens in our telescope works as a Fourier-Transformer. It causes a Fourier-Transformation of the incoming beam on the focal plane. An aperture placed in this plane works as a high-frequency filter for the beam. The smaller the aperture gets the lower the frequencies filtered out are.
Moreover the active range is limited by the spot distance on the HSS-camera as described in chapter 3.

4.8.1 Pre-Correction of Sphere

The Precompensation of the sphere is done by a Badal system. It consists of two similar lenses. The distance between them can be varied by the use of a mirror system.
The eye is positioned in the focal plane of the first lens. The HSS is fixed in the focal plain of the second lens. These positions do not depend on the distance between the lenses. The Badal system images the wavefront of the eye-plane to the HSS-plane, modifying the sphere by changing the distance between the lenses. For thin lenses the relation between the distance of the lenses and the sphere is given by

$$\Delta Sphere = \frac{2}{f} - \frac{d}{f^2} \tag{4.3}$$

For d=2f the change in sphere is zero. The relation between the correction and the distance of the lenses is linear. The compensation becomes far more complicated if the eye has not just sphere, but also astigmatism and higher order aberrations.

4.8.2 Pre-Correction of Astigmatism

To precompensate the cylinder of the eye there are different setups. Most widely-used in autorefractometer is a system with two crossing cylinder lenses. All setups of this kind have two main problems in common:

a) The distance between the cylinder-lenses is small, but not zero. So the correction is not perfect. Higher order aberrations occur, as well as a beam distortion.

b) The cylinder-lenses commercially available normally induce a sphere. So you cannot simply take two identical lenses. You can either take cylinder-lenses different in sign or add a spherical lens close to the cylinder-unit.

4.8.3 Calculating Sphero-Cylindrical Lenses

A short introduction into a mathematical formalism for sphero-cylindrical lenses will be given. It is based on an article by Thibos, Wheeler and Horner [Th94].
Thibos formalism uses a vector method. The main advantage - compared to the convention used in Ophthalmology - lies in the fact that the vector components are independent. So lenses can be added and the effect of a lens on a wavefront can be determined simply by a vector addition. The length of the vector is connected to the size of the blur on the retina. The RMS can also be taken directly from the vector. So the relation between the vector and the Visual Acuity is very close. Thibos supposes that the length of the vector is an even better characteristic of the Visual Acuity than the RMS.
The optical power of a refracting surface is defined by:

$$P = \kappa(n' - n) \tag{4.4}$$

with $\kappa = curvature$ and n' and n the refractive indices of the media in front of and behind the media separated by the surface.

$$\kappa(\theta) = \kappa_x \cos^2(\theta - \alpha) + \kappa_y \sin^2(\theta - \alpha) \tag{4.5}$$

$$= \kappa_x + (\kappa_x - \kappa_y) \cos^2(\theta - \alpha) \tag{4.6}$$

If you substitute

$$S = \kappa_x(n - n') \tag{4.7}$$

$$C = (\kappa_x - \kappa_y)(n - n') \tag{4.8}$$

you get

$$P(\theta) = S + C\cos^2(\theta - \alpha) \tag{4.9}$$

$$= S + \frac{C}{2} + \frac{C}{2}\cos(2(\theta - \alpha)) \tag{4.10}$$

The last equation shows how the "refracting power" of an arbitrary surface changes with the meridian. The definition of "refracting power" used here is slightly different from the definition technically used, but it is very convenient as approximation.
Starting with this equation a Fourier approach can be used. $M = S + \frac{C}{2}$ form the constant term and $J * \cos(2(\theta - \alpha))$, with $J = \frac{C}{2}$ the harmonic term. This leads directly to

$$P(\theta) = M + J\cos(2(\theta - \alpha)) \tag{4.11}$$

This equation can be converted from polar into rectangular form. This results in:

$$P(\theta) = M + J_0\cos(2\theta) + J_{45}\sin(2\theta) \tag{4.12}$$

After this transformation any sphero-cylindrical lens can be represented by the 3 independent values M, J_0, J_{45}. Combined they can be written as a power vector. In this convention lenses can be handled as vectors which makes all calculations very simple.

4.8.4 The Use of Power Vectors

The optometric convention for describing sphero-cylindrical lenses are in polar form:

$$\text{Refraction} = \text{Sphere (in D) Cylinder (in D)} \times \text{axis (in}^\circ\text{)} \tag{4.13}$$

This notation is very useful for an optometrist as it tells him how to design a lens.

However there are various disadvantages as well. Higher sphere may even improve vision in cases where the sign of the cylinder is opposite. So problems arise in connecting the Visual Acuity to the refraction data and in calculating the effect of several cylinder lenses lined up. Doing statistics with the values used by optometrists brings further problems.
The power vector method gives an answer to just these problems. A spherocylindrical lens is represented by a triple of values, the mean sphere, a cross-cylinder at 0 degree, and a cross cylinder at 45 degree. These values can be interpreted as coordinates of a vector representation. You can add two lenses by simply adding the two vectors. The conversion from medical notation to vector notation is given by:

$$M = S + \frac{C}{2} \tag{4.14}$$

$$J_0 = \frac{C}{2}\cos(2\beta) \tag{4.15}$$

$$J_{45} = \frac{C}{2}\sin(2\beta) \tag{4.16}$$

The transformation back is given by:

$$S = M - \sqrt{J_0^2 + J_{45}^2} \tag{4.17}$$

$$C = 2\sqrt{J_0^2 + J_{45}^2} \tag{4.18}$$

$$\beta = \frac{1}{2\tan(\frac{J_{45}}{J_0})} \tag{4.19}$$

4.9 Speckles

If the light is collimated the spots seem to have steady granular patterns. These patterns are called speckles. Speckles always occur if coherent light is scattered from a stationary rough surface. The phase of the light field is shifted in space randomly.
The size of the speckles can be estimated as shown in fig. 4.9. There is no detailed information about the surface, so it is not possible to know where an interference will occur. If we know a place with maximum interference we can estimate the distance to the place of minimum interference from the

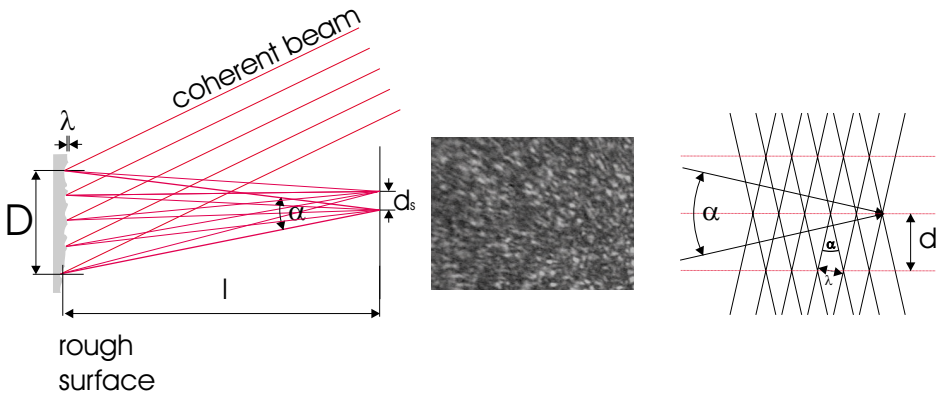

Figure 4.9: Development of speckles

opening angle α and the wavelength λ. The smallest Speckle diameter d_s is given by the maximum angle:

$$d_s = \frac{\lambda}{2\sin(\alpha/2)} \cong \lambda\frac{l}{D} \tag{4.20}$$

with $\lambda = wavelength$, $\alpha = apex\ angle$, $l = length$ and $D = diameter\ of\ the\ scattering\ surface$. For smaller angles the distance rises. The roughness of the surface does not have any influence on the size of the speckles, but it has an effect on their contrast.

In our setup there are two locations which have an effect on the size of speckles: Firstly the eye with the size of the light-spot as dimension of the scattering surface (objective speckles) and secondly the HSS with the microlens diameter as dominating size (subjective speckles). So the speckle sizes differ with kind, the first effect leading to up to about 800 μm, the second one to 60 μm. While the first kind of speckles will shade an area of some focal points, the second kind destroys the structure of a single focal point.

For handling the speckles - reduction or elimination - there are various methods. Having the coherence length of the laser far below the roughness of the object reduces the intensity of the speckles. In a different approach the phases are changed very rapidly. Though speckles occur, they do not affect the measurement: Since their locations shift rapidly a time integrated picture is free of any speckles.

A third possibility is be to reduce the speckles to a size that does not affect

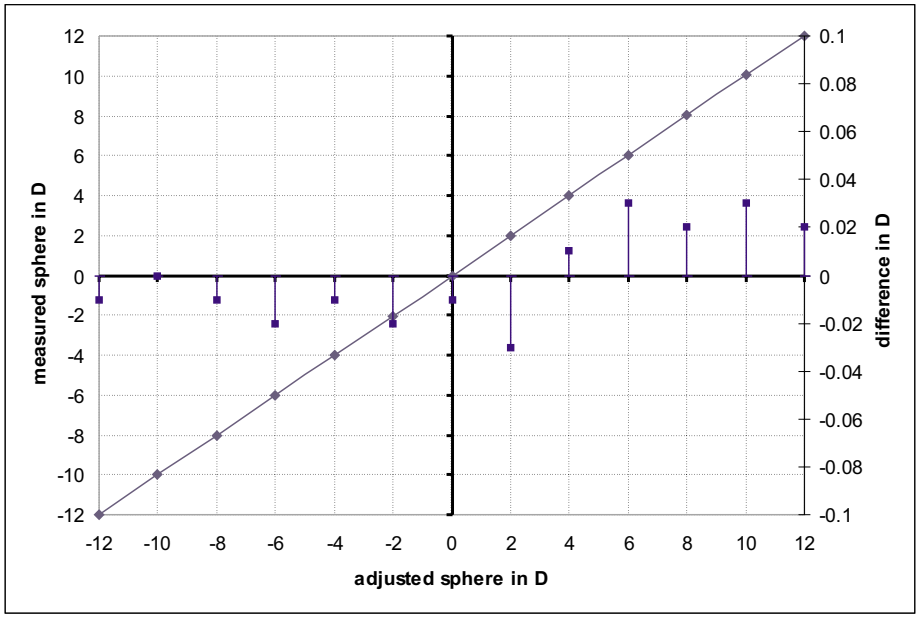

Figure 4.10: Measurement of best corrected sphere: Difference between ZEMAX results and measured results

our measurement.
In our device we use a laser with a small coherence length and a time integration of about 25 ms to reduce speckles.

4.10 Test Measurements on Artificial Eyes

The precision of the device has been tested for different kinds of the performance. Various artificial eyes were designed for this purpose.

4.10.1 Testing Sphero-Cylindrical Measurements

The artificial eye designed for testing sphere is very simple. The optic consists of a single lens with a reflector behind. By shifting the distance between lens and retina the sphere can be adjusted. The correlation between sphere and distance was simulated with ZEMAX. As retina a SPECTRALON plate which has a high diffuse reflection is used.

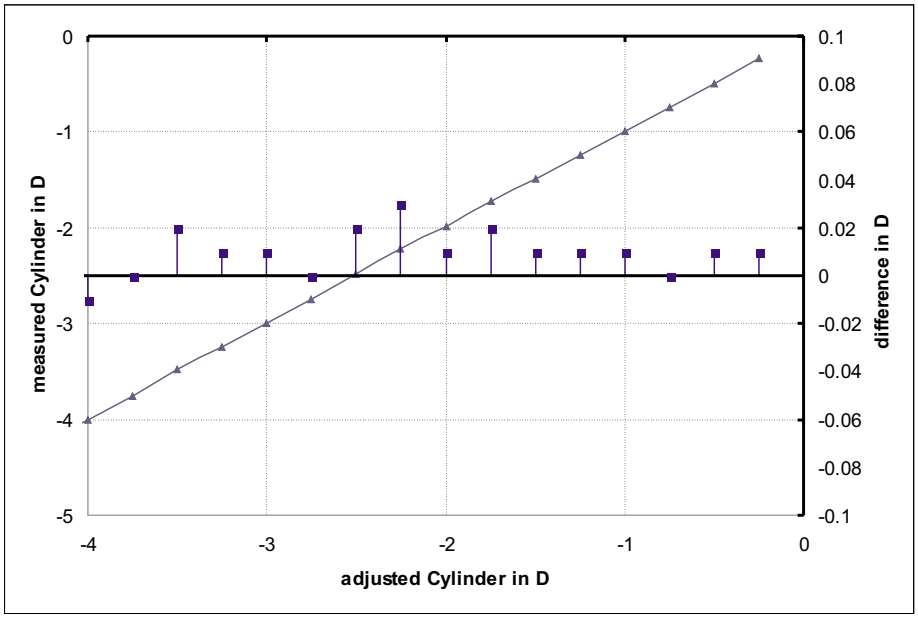

Figure 4.11: Measurement of best corrected cylinder: Difference between simulated results (ZEMAX) and measured results

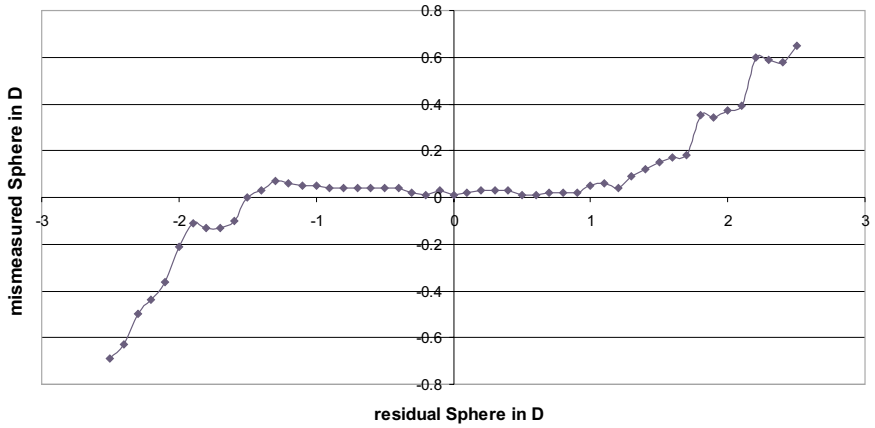

Figure 4.12: Measurement of sphere without precompensation: Difference between ZEMAX results and measured results

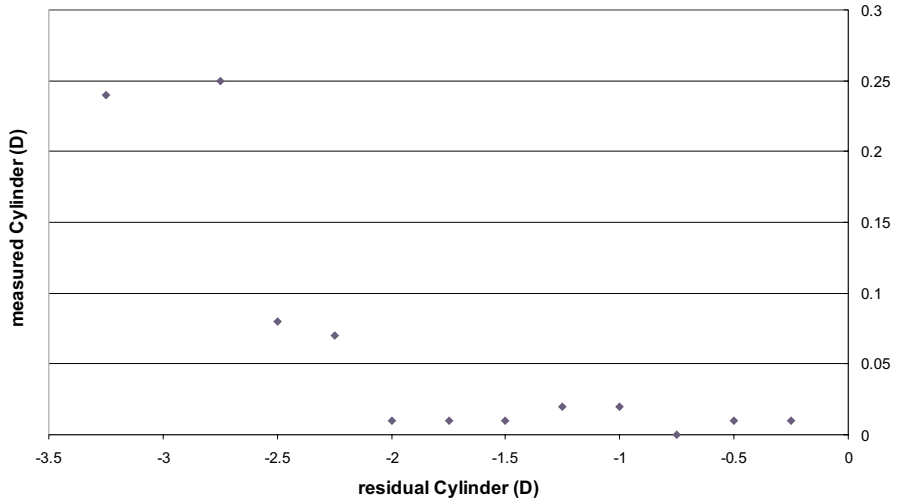

Figure 4.13: Measurement of cylinder without precompensation: Difference between ZEMAX results and measured results

In a first test the device measures the sphere with an optimal precompensation. The information given by this test is more about the acuity of the precompensation than about the Hartmann-Shack Sensor itself.
The test for cylinder is quite similar. The artificial eye in this case consists of an achromatic lens and a second cylindrical lens in front of a reflector. The distance between the achromatic lens and the reflector is kept constant. The cylinder can be changed by moving the cylindrical lens.
The results are shown in fig. 4.10 and fig. 4.11. For both sphere and cylinder the accuracy is higher than 0.04 D throughout measuring range.
The Hartmann-Shack Sensor itself was object of the second test. The eyes used were the same. The sphere slider and the cylinder precompensation were not moved at all. This is also a measurement for the active range of the device.
The precision of the measurement of sphere is very high (difference $\leq 0.05\,\mathrm{D}$) for an active range up to $\pm 1\,\mathrm{D}$ and the precision is acceptable (difference $\leq 0.1\,\mathrm{D}$) for an active range up to 1.5 D (fig. 4.12). Outside this range the failure rises rapidly. This is due to the pinhole in the second telescope which

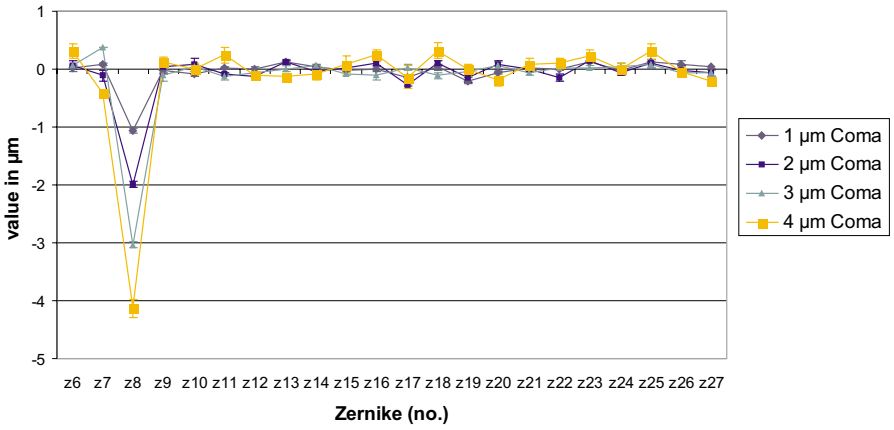

Figure 4.14: Measurement of different Coma plates: Each Graph shows mean values from 4 measurements.

prevents light with higher angles from arriving at the sensor.
These failures can be avoided by disregard HSS-values larger than a set limit. The result at high cylinder is close to this (fig. 4.13). The cylinder precompensation was not used. Half of the sphere was corrected by the sphere slider, so the cross-cylinder was isolated for measurement. The result was very much the same as at the sphere measurement. In a range up to 2 D of cylinder the precision was very high (difference ≤ 0.03 D). Up to a range of 2.5 D the result was acceptable (difference ≤ 0.1 D). Outside this range the result was poor due to the same effect of a wavefront tilt at the pinhole.

4.10.2 Testing Higher Order Aberration Measurements

For the performance of the equipment at higher order aberrations a special kind of artificial eye was produced: PMMA discs were taken and treated with a STAR S3 laser from VISX, an excimer laser system for refractive eye surgery, described below. Its variable spot scanning system permits removing any quantity of material wanted and altering the anterior profile of the plastic discs.

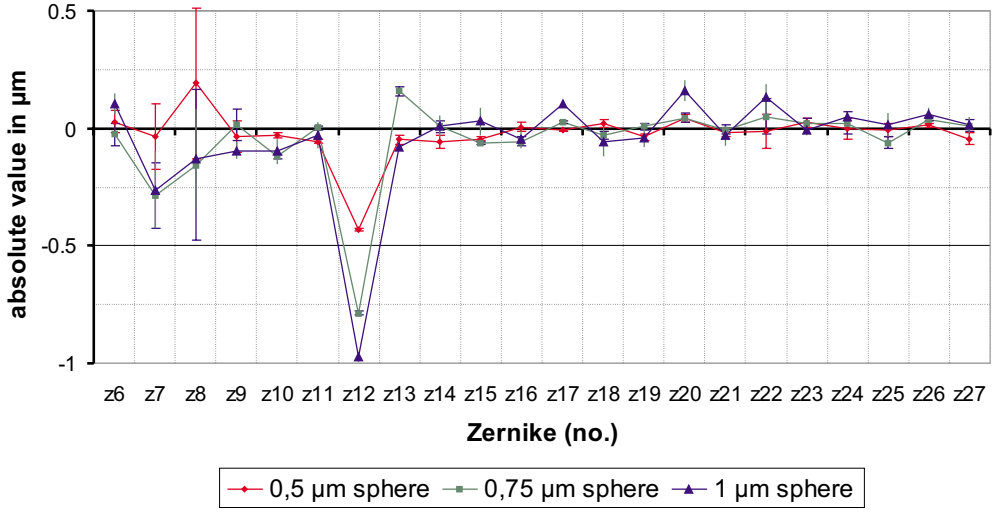

Figure 4.15: Measurement of different plates with 3rd order spherical aberration: Each Graph shows mean values from 4 measurements.

Seven discs of this kind were produced: Three discs with a coma-like shape for generating coma of an amount of $2\,\mu$m to $6\,\mu$m peak to valley (PTV) in steps of $2\,\mu$m, three discs with third order spherical aberration ($0.5\,\mu$m to $1\,\mu$m PTV in steps of $0.5\,\mu$m) and one disc with the aberrations of an average left eye.

These discs were placed in the measurement plane of the sensor having the SPECTRALON-plate as reflector in a definite position behind them. In the test setup there are no other lenses which could cause additional higher order aberrations.

In fig. 4.14 the results for the the coma plates are shown. The plates were introduced in such a way that the coma is orientated along y-axis (Z 8). The Zernike terms are all below $0.3\,\mu$m except the Z 7-term. The existence of a higher coefficient of Z 7 can be attributed to a failure in the alignment of the plate. Fig. 4.16 shows the attempt to simulate the aberrations of a normal eye with a plastic disc. You can see that the centering of the ablation could be a problem.

In fig. 4.15 the results of the higher order spherical plates are shown. Here

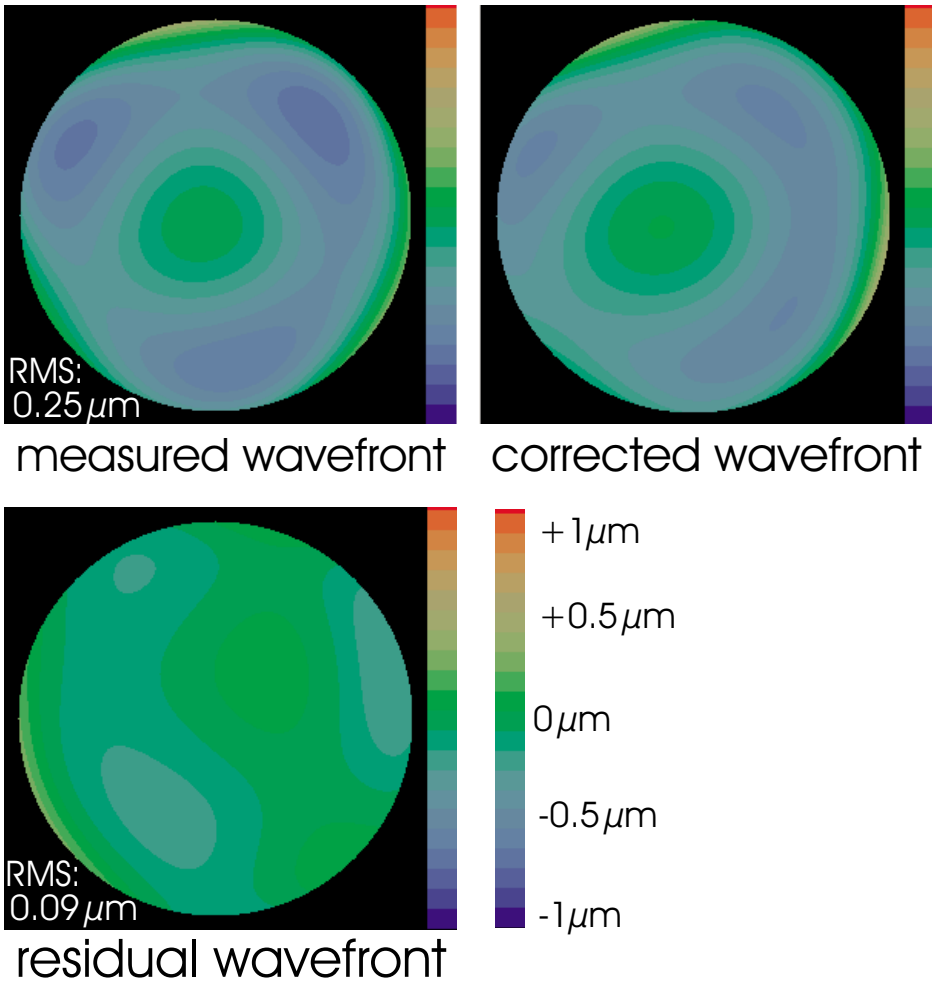

Figure 4.16: Wavefront of an average eye (average of 140 measurements of left eyes): The picture top left shows the average eye, the picture top right shows the measured result of the plate and bottom left shows the difference.

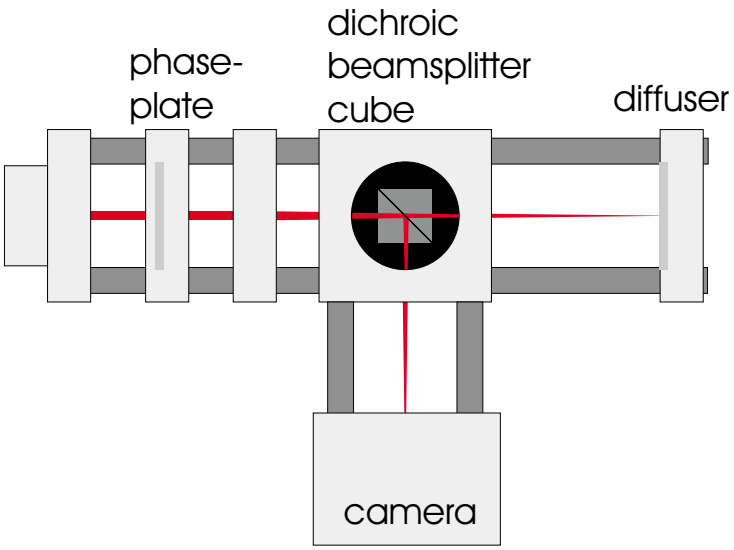

Figure 4.17: Test device for the active mirror: Light entering from the left through the phase plate is divided by the dichroic beamsplitter cube. The aberrations get measured in the right arm. The bottom arm is used to record an image of the target.

are larger effects to the coma terms Z 7 and Z 8 which may be evoked by a non-central ablation. While the results for the two plates with the larger ablations were precise, those for the third plate proved to be to small.
Fig. 4.16 shows the attempt to simulate the aberrations of a normal eye with a plastic disc. On top left the average wavefront of a left eye is shown. Top right can be seen the measurement of the plate manufactured with these data. On the bottom the difference between these two aberrations is shown. It can be seen that the rotation of the ablation was not done precisely.

4.10.3 Performance Test of the Active Mirror

For an objective test of the active mirror a test device was constructed (fig. 4.17). This device enables us to measure a phase-plate and look through it into the machine at the same time. By the camera at the test device we get an image of the target. For the measurements presented here, a target was used with 1‘ apex angle corresponding to a VA of 1.0.

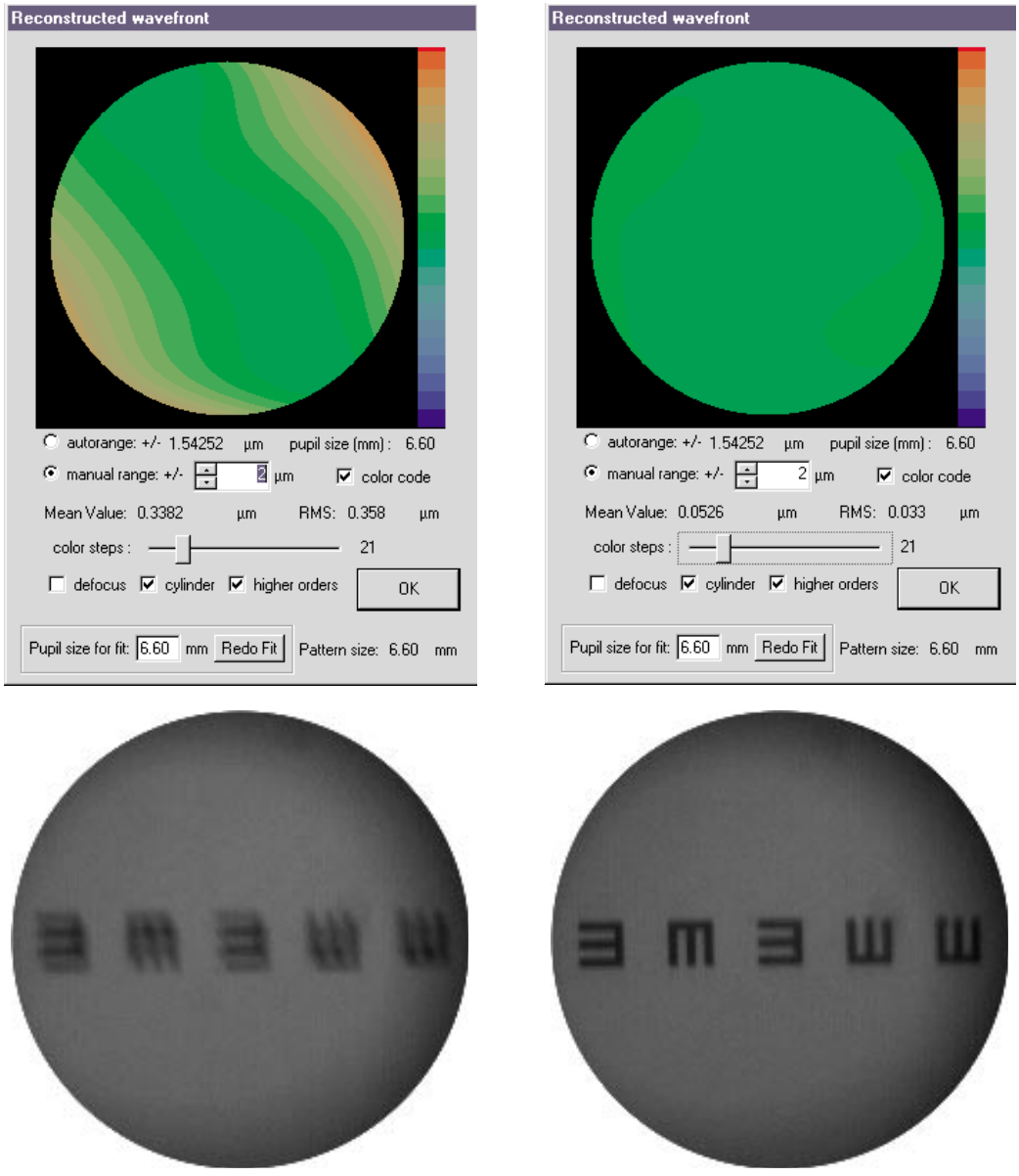

Figure 4.18: Active mirror correcting cylinder

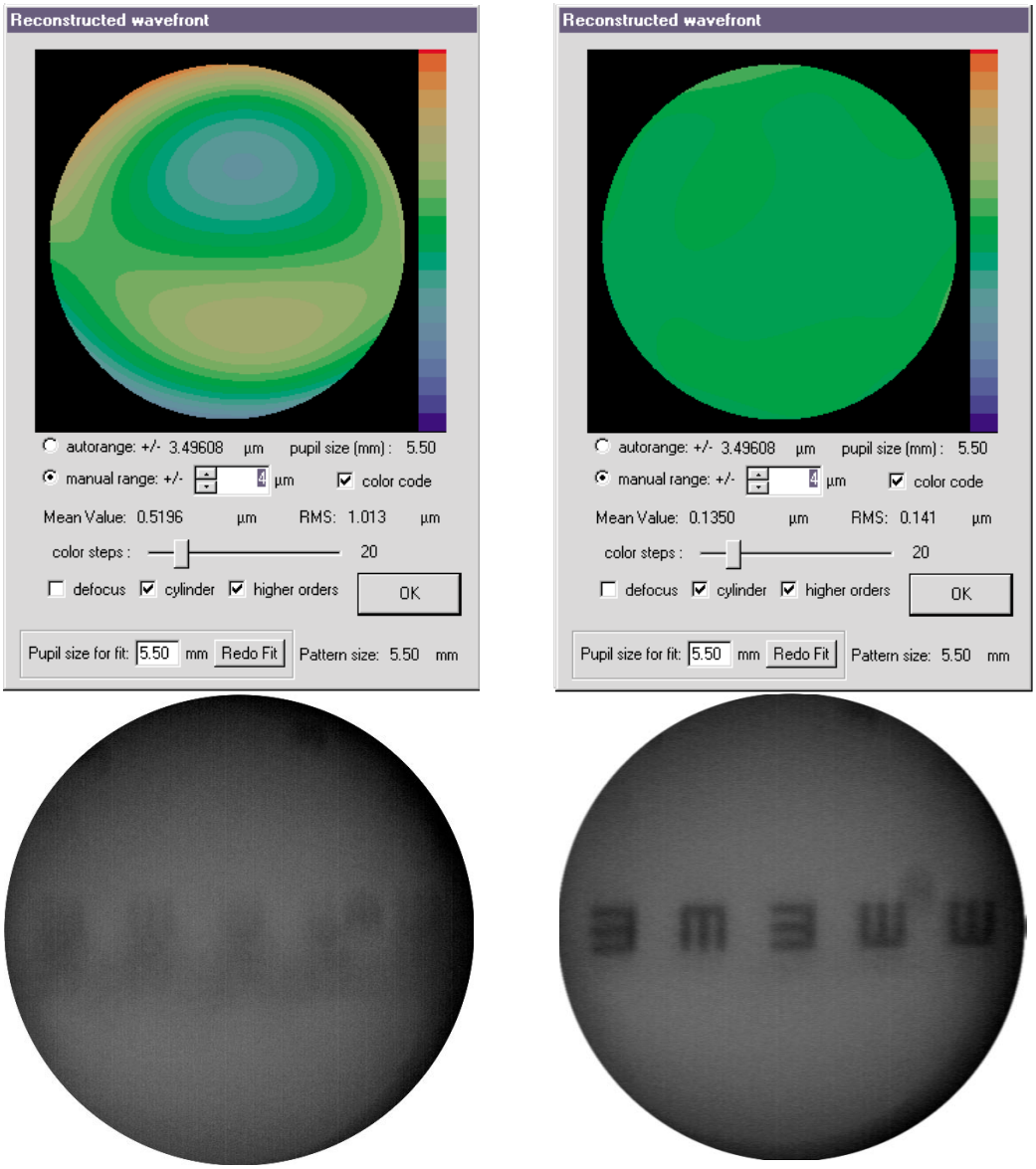

Figure 4.19: Active mirror correcting coma

Fig. 4.18 shows the correction of a small cylinder of about 0.3 D. In the top left can be seen the wavefront without using the active mirror, below that picture the image of the vision chart received by the camera. Activating the mirror leads to a large enhancement of both, wavefront and image. The wavefront error can be minimized to 0.033 μm, which is less than a tenth of the earlier error. Also the image gets much sharper. While the left is on the border of the detectable, the right image looks quite sharp.
In fig. 4.19 can be seen the effect on a strong coma. Without using the mirror the RMS is larger than 1 μm and the image of the VA-chart is not detectable.
By activating the mirror the wavefront error can be minimized to about 0.15 μm, which is about a seventh of the uncorrected wavefront error. Since the PTV change in the wavefront is close to 7000 nm and the wavelength of the vision chart is close to 550 nm more than 10 2-π jumps were used for correcting this wavefront. This shows how well the principle of this mirror works.

Chapter 5

The Hartmann-Shack Sensor at the Human Eye

Different measurements at human eyes were made. First the capability of measuring the refraction of the eye was tested. Then typical patterns and changes of higher order aberrations were studied.
At the end of this chapter two studies will be presented.
The first study was about perfect vision. 70 eyes were measured in order to compare the higher order aberrations with their Best Spherical Corrected Visual Acuity (BSCVA). The assumption was that some special wavefront shape is connected to high visual acuity. A small wavefront error should be better than a larger one.
In the second study the device was tested for use in ophthalmology, in special for planning LASIK or PRK treatment in the human eye. For 38 patients the eyes were measured before operation. In every patient one eye was treated the classical way, the other one wavefront guided. The results were compared. Furthermore one device was installed in the Praxisaugenklinik in Heidelberg to take values for comparing the results.

5.1 Measurements at the Human Eye

In the last chapter the accuracy in measuring test eyes was analyzed and it proved to be very high. But there is a big difference between measuring a

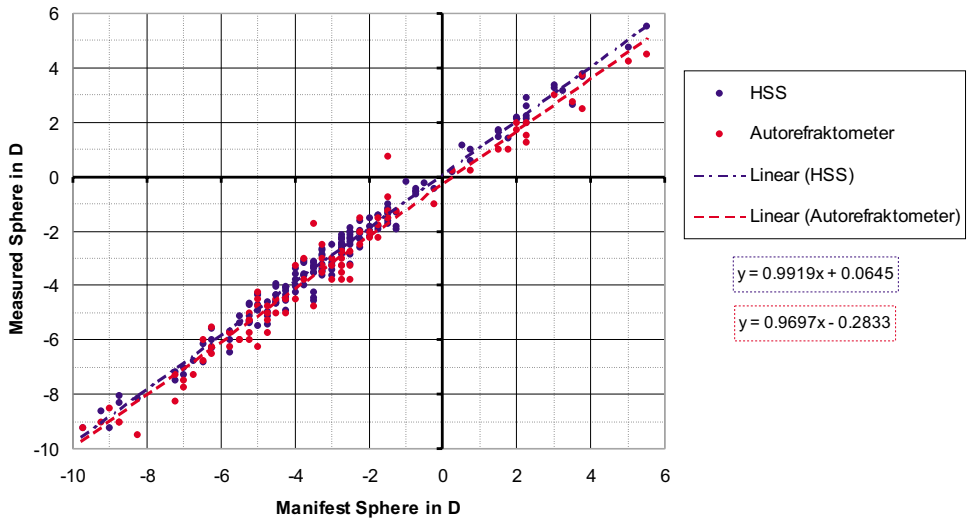

Figure 5.1: Comparison of a manifest measurement of sphere with an autorefractor and by wavefront method.

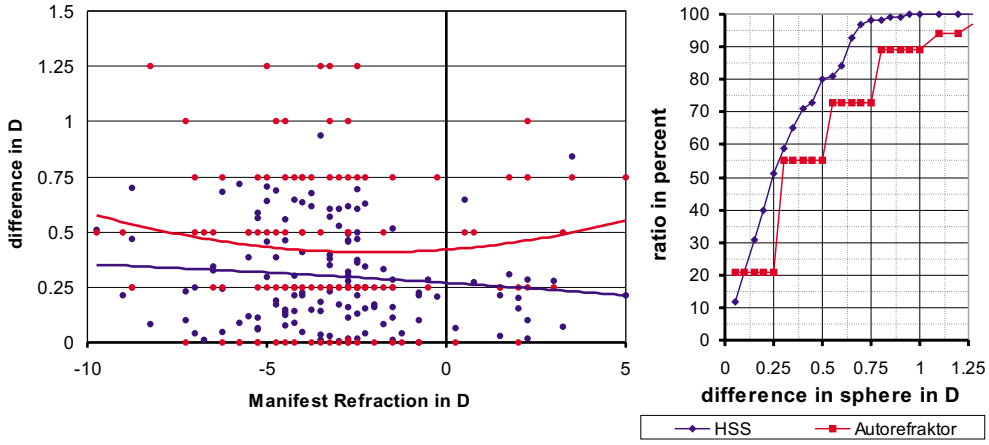

Figure 5.2: HSS vs. Autorefractometer: Sphere
Left: Absolute error vs. sphere
Right: Deviation of objective to subjective measurement

fixed unmoveable artificial eye and a real human eye.
The main problems in measuring a real eye are caused by accommodation, movement and rotation of the eye and the fact, that the variety of interferences in the optics is much wider in a natural eye.
Moreover there is the fact that what we measure is not really the classical refraction: a mean value for the radius of curvature of the wavefront for just one pupil size. On our results we can calculate the average refraction for different pupil sizes, but these sizes may be different from the size used for the subjective refraction.

5.1.1 Comparing the Sphero-Cylindrical Refraction

A first requirement for the sensor is that its refraction values (sphere, cylinder and axis) stay in close agreement with the values measured by an ophthalmologist. Common autorefractometers aim at having more than 80 % of the results within 0.5 D of the manifest refraction. As a first test we compared the wavefront refraction to the manifest refraction. In cooperation with the Praxis-Augenklinik in Heidelberg we took measurements on 132 eyes with the wavefront system. Parallel to this an ophthalmologist determined the manifest refraction and furthermore to this measured the refraction with an autorefractometer. These results were used to test the capability in measuring eyes of untrained people in a typical environment.
In measuring the manifest refraction the ophthalmologist puts a lens in the visual axis in front of a patients eye and asks him if his visual performance rises or falls. By repeating this with other lenses in steps of quarter diopters the best correction lens is found. The procedure is the same with cylinder lenses. This method depends strongly on the patient‘s help, so it is very subjective.
Fig. 5.1 shows the results. The x-axis gives the manifest refraction, the y-axis the objective refraction. The manifest refraction and the autorefractometer refraction are given in quarter diopter steps, the HSS values in steps of a hundredth of a diopter.
The blue dots show the results of the HSS measurement, the red dots those of the autorefractometer. The black dotted line gives the ± 0.5 D tolerance of

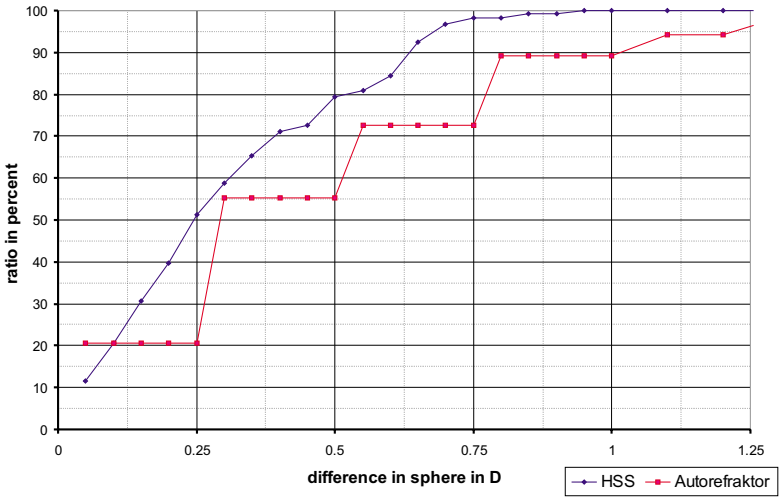

Figure 5.3: Comparison of measuring the cylinder with a wavefront system and in a subjective way.

the manifest refraction. The correlation of the HSS-refraction measurement - 0.993 - is far better than that of the autorefractometer (AR) (0.982): The spreading of the results is much smaller. Furthermore the regression of the HSS is much closer with a regression coefficient of 0.99 (AR: 0.97) and an axis interception of 0.06 (AR: -0.28).

As can be seen in the right diagram in fig. 5.2 more than 50 % of the results are closer than 0.25 D to the manifest refraction and about 80 % are within a range of 0.5 D. No measurement was more than 1 D off. The agreement of the results does not depend strongly on the total sphere, as can be seen on the left. So the z-positioning works well. Fig. 5.3 shows the results of the quality in measuring cylinder. In this examination the lengths of the power vectors were used. Their values - given in this figure - correspond to the amount of the cylinder lens that would correct the aberration.

Accommodation has no strong effect on measuring the cylinder. So it can be expected to match even better. Here only 40 % of the results are closer than 0.25 D, more than 85 % of the results lie within a range of 0.5 D of the manifest refraction. The results show: For the specified task the setup is

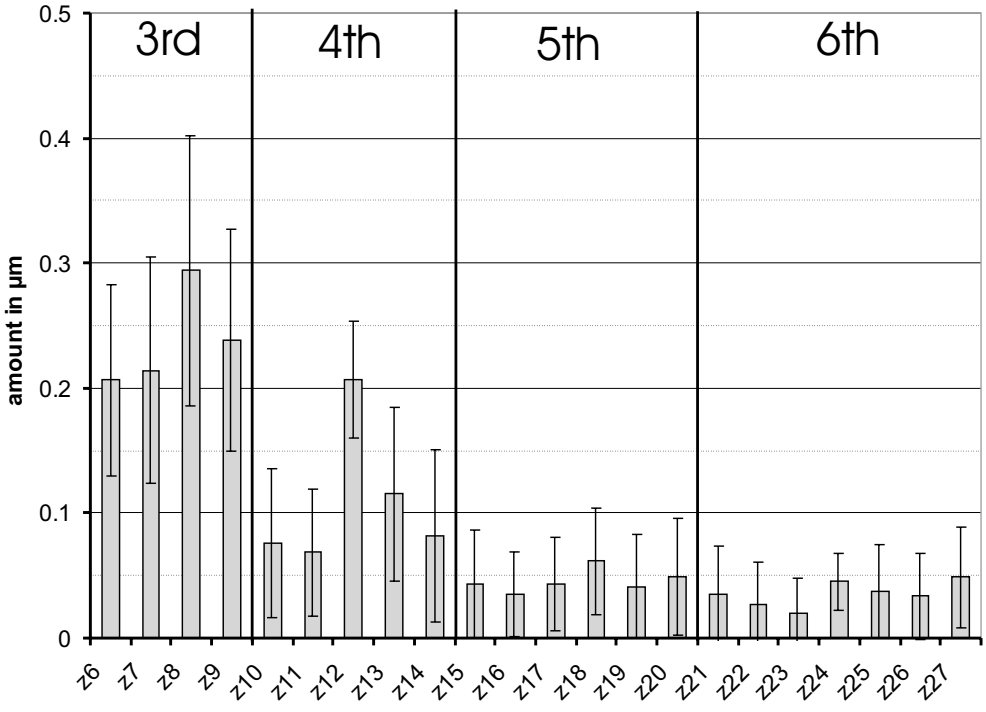

Figure 5.4: Reproducibility of 10 measurements: Zernike polynomials

very well suited.
At cylinder, too the result of the HSS is more reliable than that of the autorefractometer. This is, what the result of the autorefractometer tells us.

5.1.2 Reproducibility of the Results

For checking the reproducibility of the measurements on 84 eyes measurements were repeated 10 consecutive times. In fig. 5.4 you see the average amount of Zernike coefficients in μm, the error beams give the mean standard deviation. In third and 4th order the error beams are smaller than the amount, in 5th and 6th order they are larger in most cases. This is not necessarily due to changes in the eye. It may as well be ascribed to failures in the centering of the pupil with a strong impact on the higher order aberrations. The reproducibility of the RMS is shown in fig. 5.5. The standard deviation of the total higher order RMS is about $\pm 0.03\,\mu$m at a total amount of

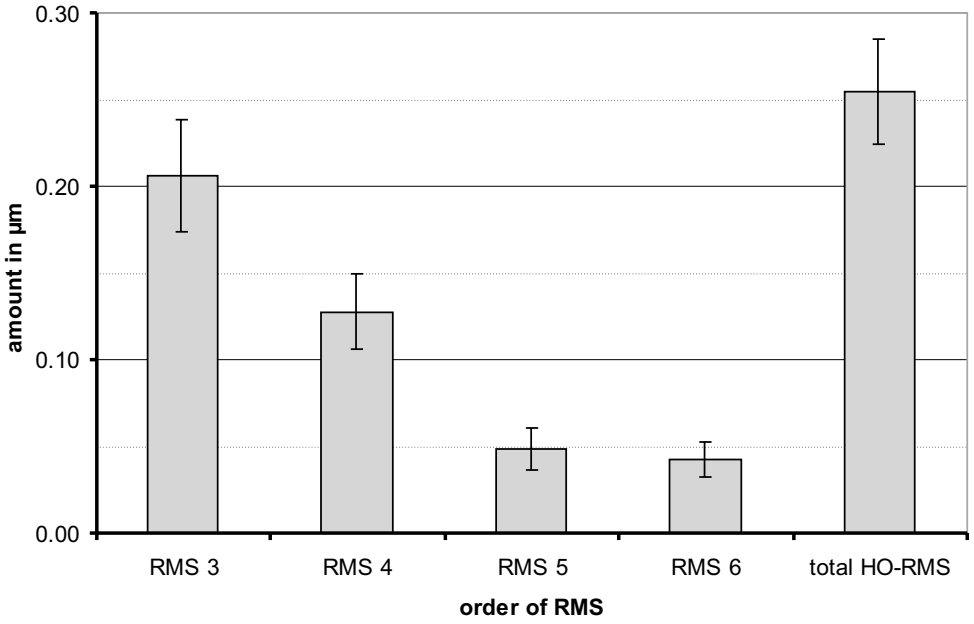

Figure 5.5: Reproducibility of 10 measurements: RMS

0.25 μm. It is remarkable that the mean standard deviation of the 3rd order RMS exceeds that of the total RMS.

5.2 Standard Deviation of Sphere and Cylinder

Fig. 5.6 shows the reproducibility of the measurements of sphere and cylinder. Sphere can be measured with a reproducibility below 0.13 D, cylinder with less than 0.1 D. As shown on the left the axis can be measured with a reproducibility of 3 degrees for cylinders larger than 0.5 D. Unfortunately there are no measurements for the autorefractometer to compare.

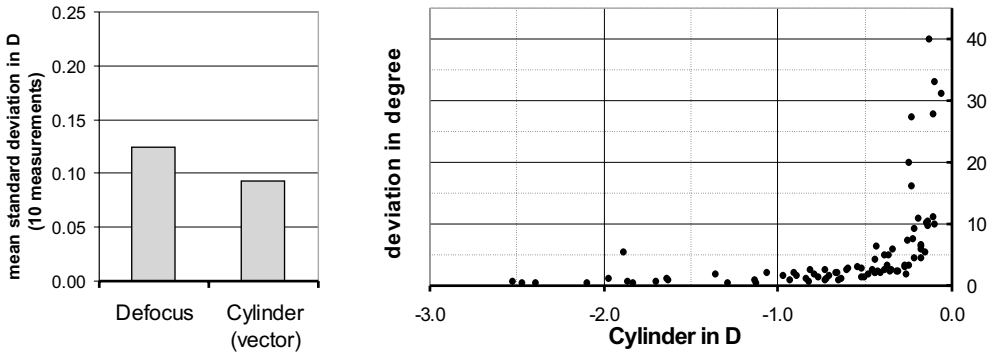

Figure 5.6: Reproducibility of values: RMS

5.3 Change of Higher Order Aberration

As to the use of the wavefront sensor for planning refractive surgery it is important to know how much the wavefront error of the eye - for different reasons - changes. The change of the lens due to accommodation and the growth in life-time will have large influence. The change of the shape of the cornea during the day should be taken into account too.

5.3.1 Age

Long-time measurements on the same eye were not possible. So changes in the mean wavefront errors with age in a set of different eyes were analyzed instead. With respect to a single eye this procedure can only give an idea of the changes with age, probably leading to an underestimation of the real effect.

The results are shown in fig. 5.7. In particular the mean third order spherical aberration shows a strong change with age. From age 20 to 70 the mean value of spherical aberration shifts about $0.5\,\mu$m. The changes of the coefficients of Z 9 and Z 12 seem to be a physiological effect that can be attributed to the growth of the lens.

With a RMS of $0.28\,\mu$m the amount of the change is about the same order as the total wavefront error.

The other aberrations will change with age too, but their mean values do not

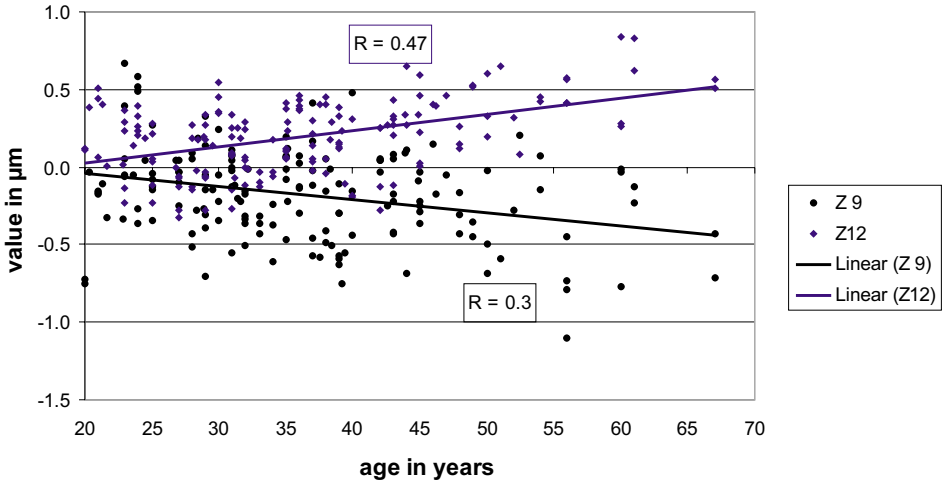

Figure 5.7: Change of the HOA with age

change that much.

5.3.2 Accommodation

Modifying the shape of the lens - for accommodation of the eye - is a major invasion in the optical properties. An influence of the state of accommodation on the HOA is presumed.
The wavefront device is highly qualified for measuring just this. Without using the fogging-feature the eye accommodates with the sphere precompensation. By shifting the sphere-slider from infinity to the near point of the eye the wavefront error for the whole accommodation range can be measured.
One minor problem is that the pupil size has changed with accommodation, so that the analysis had to be done with a pupil size of only 5 mm.
The results of this measurement can be seen in fig. 5.8. The dependence between accommodation and Z 12 is strong for all four eyes. Other Zernike coefficients changed too, especially the coma term which is involved in the age related change of the wavefront already.

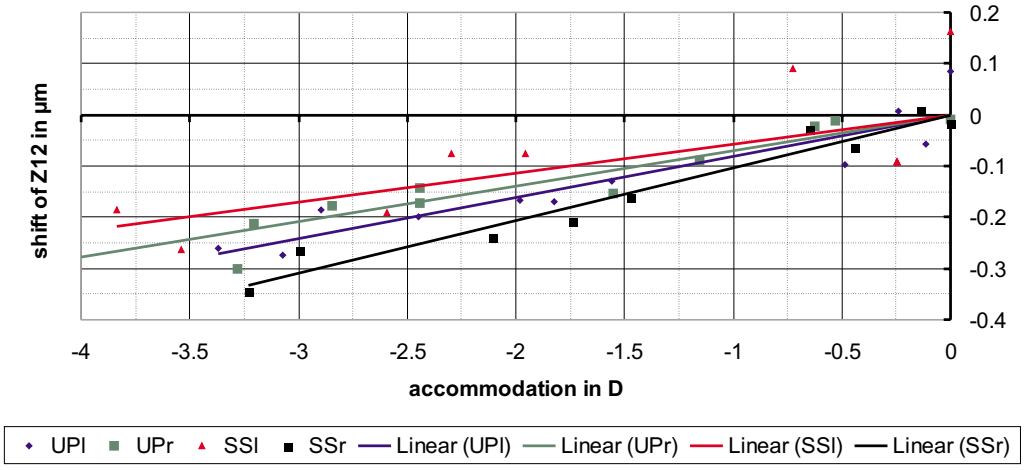

Figure 5.8: Change of the HOA with accomodation on 4 eyes

5.3.3 Daily Fluctuations

The refraction of the eye varies - as pointed out in many articles - during the day up to 0.5 D. For the cylinder values alter due to the pressure of the eyelid on the cornea during night. The change of cylinder suggests that the HOA of the eye differs during daytime too.
To verify this assumption, four eyes were measured in intervals of 2 hours during the day. The wavefront maps are shown in fig. 5.9. No larger changes occur and - above all - there is no time trend to be seen.
The same is true for the RMS (fig. 5.10). There are small fluctuations but there is no general trend. The same applies for coma and spherical aberration terms which had the largest fluctuations in the other measurements. For sphere and cylinder the variation stayed behind expectation.
The change of the shape may possibly be due to temporary effects in the morning.

5.4 Perfect Vision Study

There are many factors influencing the visual acuity. In the next chapter the influences of the single steps - from optical image-forming to image pro-

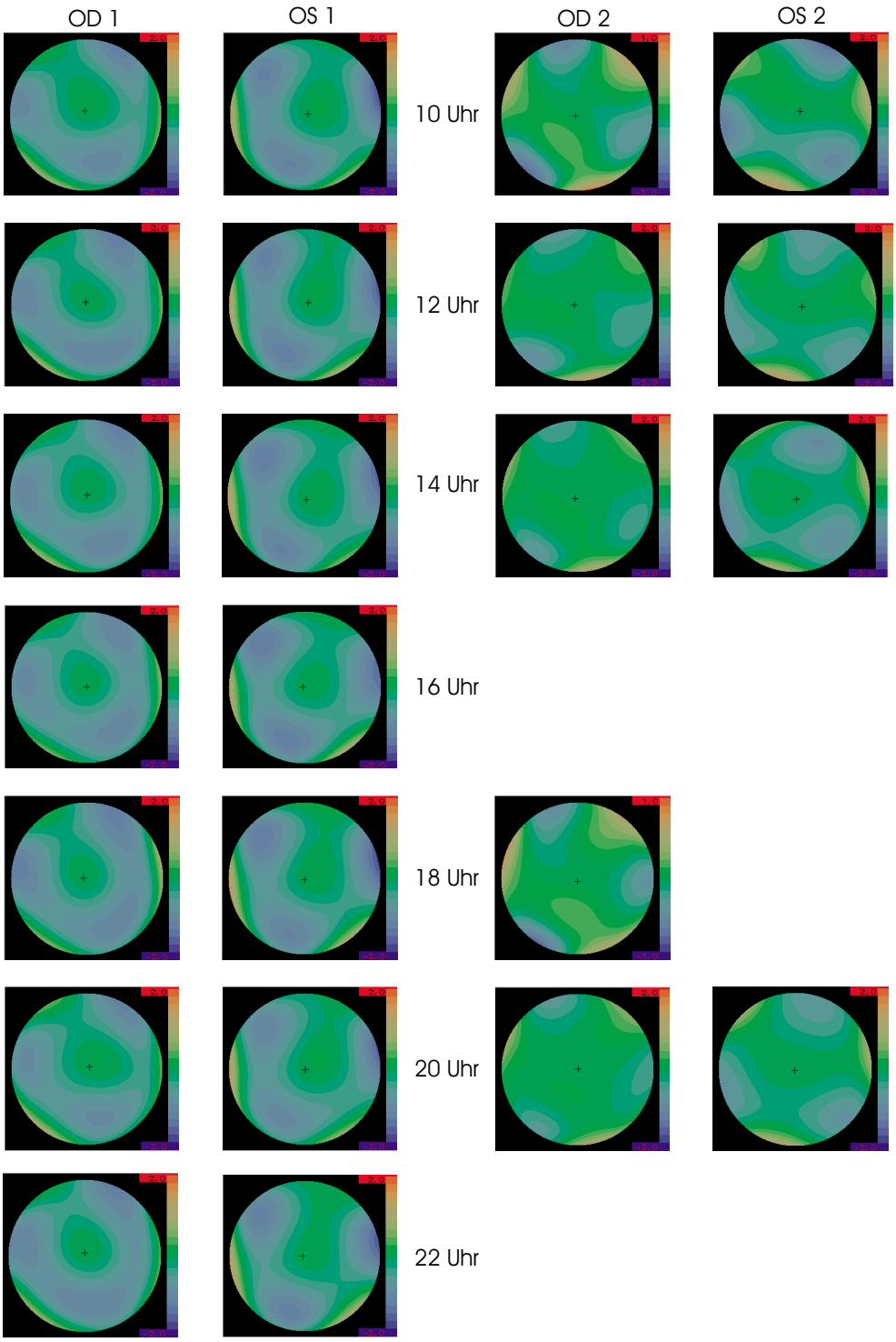

Figure 5.9: Daily fluctuations on 4 eyes: Higher Order Aberration Wavefront Maps

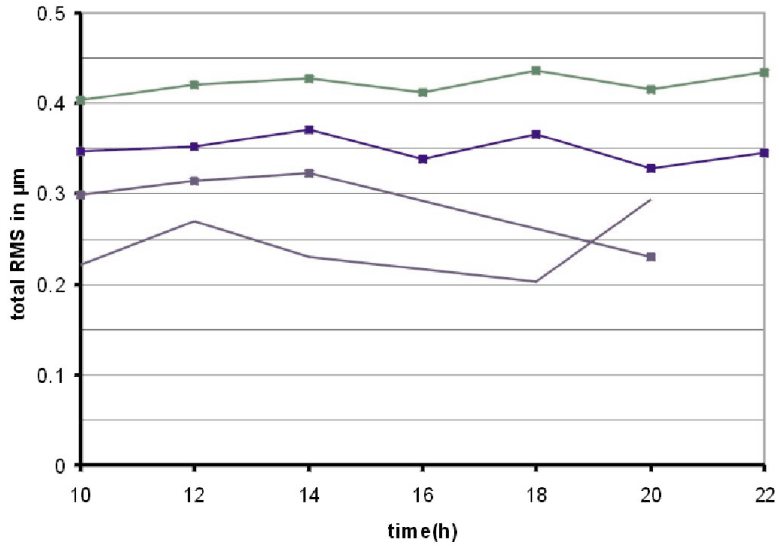

Figure 5.10: Daily fluctuation of the total HOA-RMS on 4 eyes

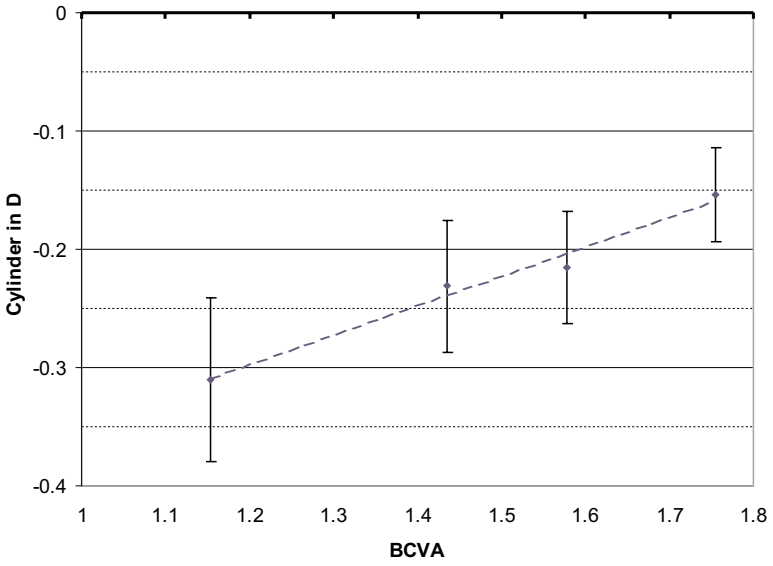

Figure 5.11: Influence of small lower order aberrations on the BCVA

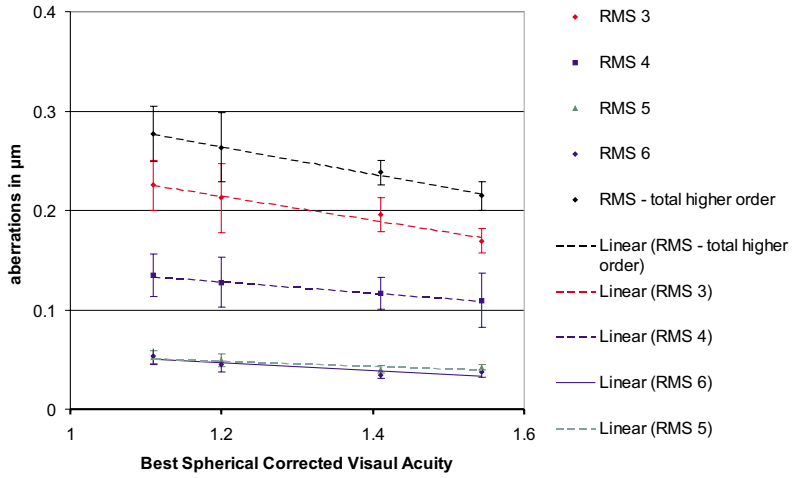

Figure 5.12: Influence of higher order aberrations on the BCVA

cessing in the brain - will be discussed. The Hartmann-Shack Sensor gives us a chance to examine the first of these steps - the image forming - very precisely.

In this section the dependence of visual acuity on higher order aberration will be studied.

The Best Corrected Visual Acuity (BCVA) was measured for 80 eyes, the result was compared to their higher order aberrations.

The BCVA specifies the Visual Acuity of an eye with the best possible correction of sphere and cylinder. Ophthalmologists measure the spherocylindrical correction parameters in steps of quarter diopters only. So the BCVA is affected by residual lower order aberrations, too. The influence of the sphere is less important as it can be compensated by accommodation. Provided the ophthalmologist is absolutely perfect only cylinder up to 0.125 D remains. This cylinder corresponds to a RMS of about 0.18 μm. In fact this value will be even larger. An eighth diopter of sphere would lead to a RMS of 0.25 μm. Fig. 5.11 shows the influence of cylinder on the BCVA. Each single point stands for the mean of about 18 eyes. The error bars give the 95% confidence intervals for the values.

Only cylinder values below 0.5 D were considered as larger cylinder had prob-

ably been corrected. An explicit dependence of the BCVA on the cylinder can be seen. In average eyes with a visual acuity of 1.75 the cylinder value is only half compared to eyes with a BCVA of 1.15. However, no interdependence between sphere and BCVA could be made out.
The influence of higher order aberrations is shown in fig. 5.12. For the BCVA a dependence occurs, but it stays small. An increase in the BCVA from 1.1 to 1.55 is associated with a decrease of the total higher order aberrations by about $0.05\,\mu$m. This relatively small decrease can be ascribed to the strong influence of the cylinder.
It would be of great interest to have a closer correlation between higher order aberration and Visual Acuity. The connection can be studied with the lately integrated cylinder correction unit. As described in the last chapter this unit can correct cylinder to less than a twentieth of a diopter. With the implemented vision chart unit it would be possible to correct the lower order aberrations much better than up to now.
The active mirror enables us to perform a real BCVA test with all kinds of aberrations removed.

5.5 Excimer Study

The object of our study was: Is there any difference in the result if in the planning of the laser-ablation pattern higher order aberrations are taken into account? 42 patients took part in the study. 37 were treated with LASIK and 5 with PRK.
What we wanted to show is: The results that excimer-laser refractive surgery with wavefront-derived ablation targets yield in the treatment of refractive error and higher order aberrations are clinically acceptable.
Treatment of the wavefront error of the eye should improve - not worsen - the patients Uncorrected Visual Acuity (UCVA), in particular the Best Spherical Corrected Visual Acuity (BSCVA).
One eye of the patient was treated with a wavefront-derived pattern, the other one - serving as control - in the conventional manner. The study is prospective, single-center, non-randomized and unmasked.

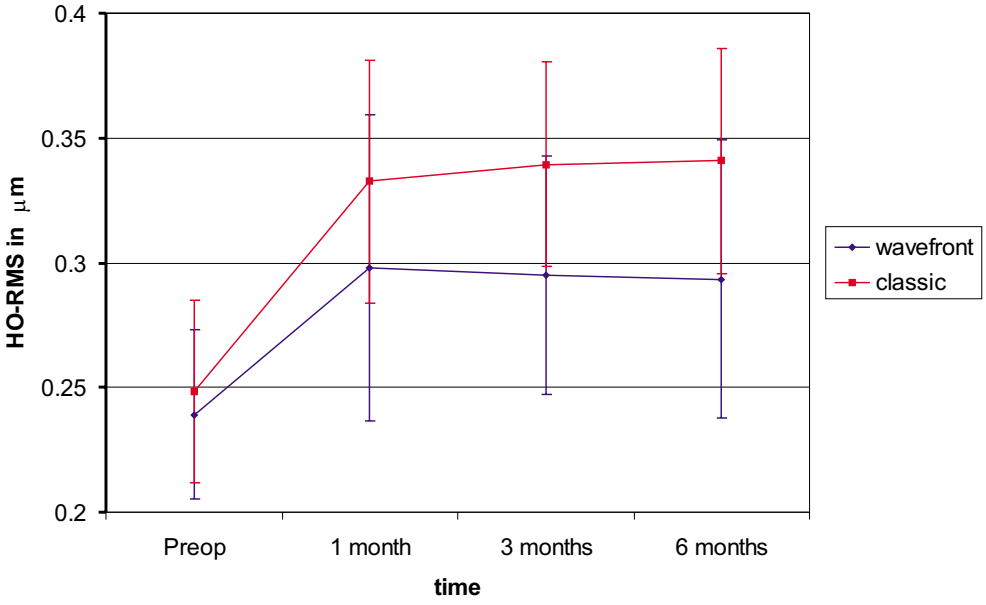

Figure 5.13: Excimer Laser Study: time trend of total higher order RMS

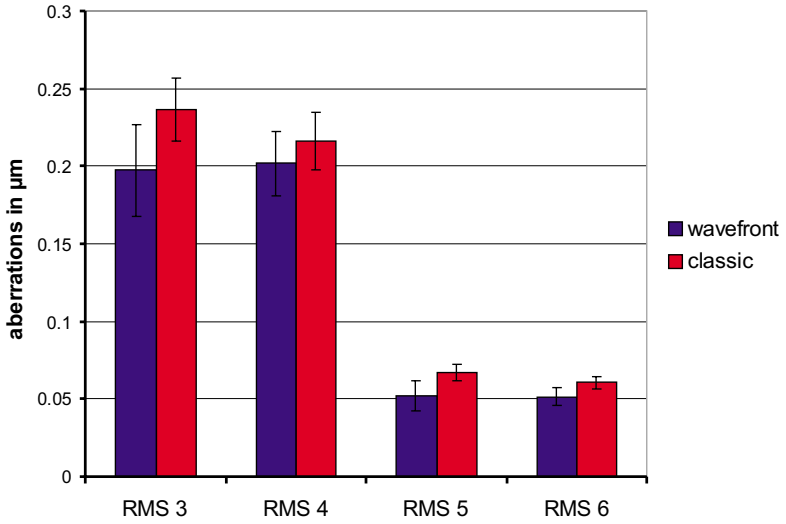

Figure 5.14: Excimer Laser Study: Distribution of RMS 6 m postop

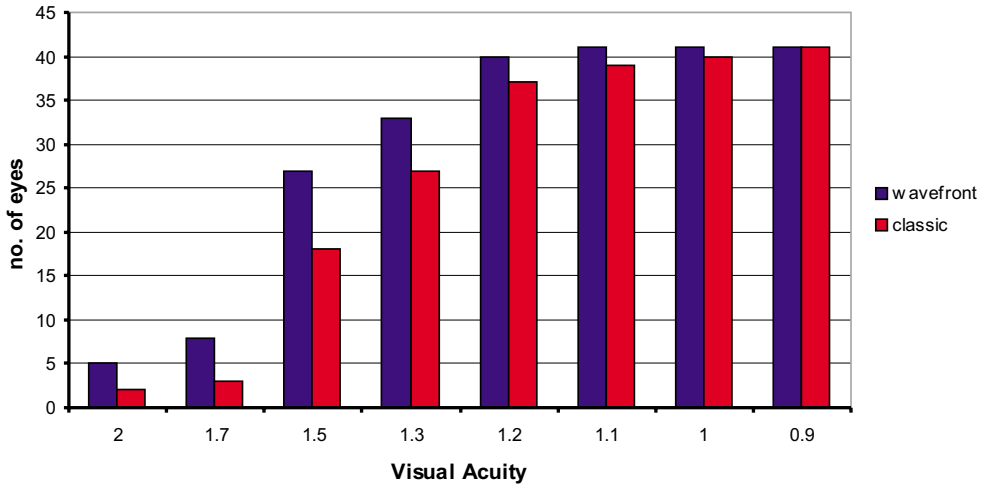

Figure 5.15: Excimer Laser Study: Best Spherical Corrected Visual Acuity (BSCVA)

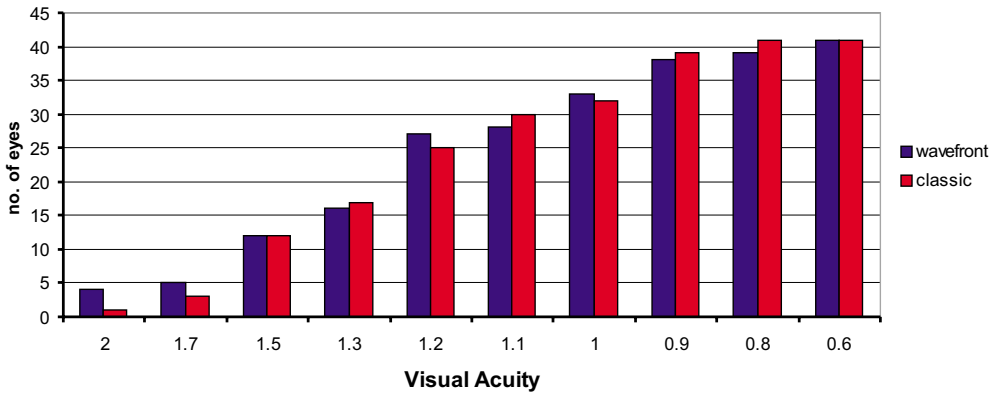

Figure 5.16: Excimer Laser Study: Un-Corrected Visual Acuity (UCVA)

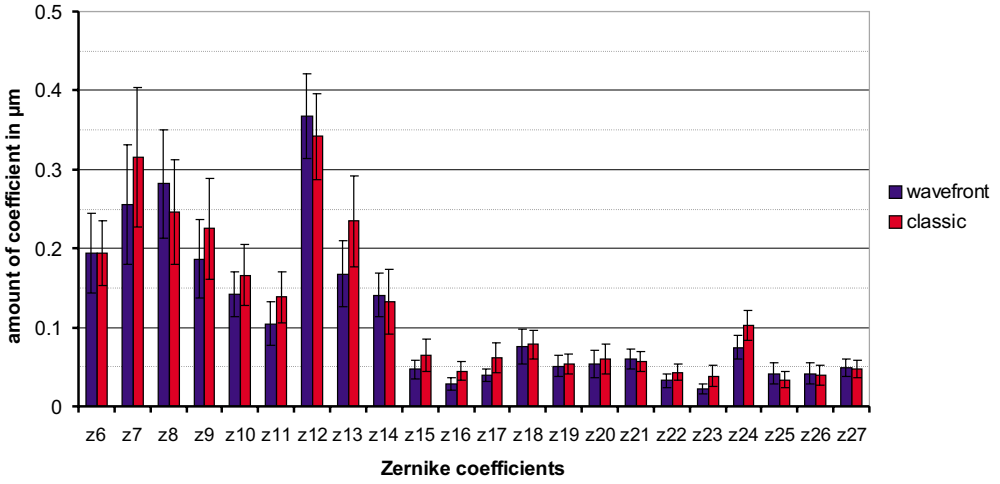

Figure 5.17: Excimer Laser Study: Comparison of the single Zernike coefficients

5.5.1 The Excimer Laser System

For doing the reshaping of the cornea, a Star S3 Laser System from VISX was used. This is a 193 nm argon-fluoride excimer laser system with a repetition rate of 10 Hz. Compared to common excimer laser systems two features are new: An eye-tracker and the Variable Spot Scanning (VSS).
The eye-tracker has 2 infrared cameras using the natural pupil as a landmark to monitor the x-, y-, and z- movements of the eye at 60 Hz. It serves as a user control for the alignment of the eye.
The VSS permits the STAR laser to ablate complex non symmetric shapes and - in this way - to correct higher order aberrations. The spot size varies: During the wavefront treatments it is between 0.65 mm to 6.5 mm in diameter.
The data files of the wavefront device were transferred to a VISX researcher for conversion to an ablation plan. The individual treatment tables contain the necessary information for the treatment, as there are the position of every pulse, the size of the spot and the dwell.

5.5.2 Refractive Surgery Methods

For refractive laser surgery there are two methods most widely in use today: Photorefractive Keratectomy (PRK) and Laser Assisted In-Situ Keratomileusis (LASIK).
In PRK the excimer procedure is applied directly at the surface of the cornea. For the laser procedure only the epithelium has to be removed. It needs about 3 days for healing. This healing process may be non uniform and provoke new aberrations.
LASIK is much more popular. The eye surgeon creates a thin surface flap of the cornea using a microkeratome. This flap will be opened, so the deeper layers can be exposed to the Excimer Laser. The invasion into the eye is more extensive.
Still the eye can be used very soon after closing the flap. This is a great advantage over the PRK. The problem here lies in the fact that if the repositioning of the flap is not perfect, strong higher order aberrations occur.
So both methods bear a risk of provoking further aberrations.

5.5.3 Study Group

42 patients - ages ranging from 21 to 52 - were tested for their aptitude first. The conditions were: Cylinder less than 2 D, wavefront error less than 4 μm PTV, maximum sphere 4 D. The difference between manifest and wavefront refraction had to be smaller than 0.5 D. Contact lens wearers had to remove their soft lenses at least one week prior to measurements (two weeks for rigid lenses).
10 measurements were taken of each eye with the Hartmann-Shack Sensor.
All eyes were treated with the VISX STAR S3. At one eye the treatment was based on the results of the wavefront sensor, at the other it relied on preoperative manifest refraction. The eyetracker and VSS were used throughout.

5.5.4 Results

Follow-up examinations took place at 1 month, 3 months and 6 months after treatment. The examinations consisted of 5 wavefront measurements, manifest refraction and a determination of UCVA and BSCVA.

Fig. 5.13 shows the time trend of the total higher order RMS before and after the intervention, separated for the classic method and the one using the higher order aberrations. The error beams show the 95 % confidence interval. We should assume that in wavefront treated eyes the aberrations are smaller. For definite results the sample-size obviously is too small.

Fig. 5.14 shows that the differences are spread over all orders of Zernike coefficients. Obviously the results are better not only in the treatment of spherical and coma aberration, the advantages cover the more complex kinds of aberrations as well. Here again the number of measurements and the differences in effect are too small to obtain assured results.

Fig. 5.17 shows the mean absolute values for both methods. The differences in the single coefficients stay small, the values for the classic method being larger in most cases.

These results are promising. Nobody is interested in reducing the wavefront error however, it is the actual visual acuity that we are all interested in. In fact the visual acuity seems to profit as well, especially at the higher end of the visual acuity chart.

The difference should be largest at the BSCVA. Here in wavefront treatment 8 eyes reached a visual acuity of 1.7 and better compared to 3 eyes with classical treatment.

A similar success was achieved at the UCVA. In this case the advantage disappears for a visual acuity of 1.5 or worse, while at the BSCVA the wavefront treatment is superior on the whole range. An explanation could lie in the fact that lower order aberrations are more or less the same for both methods.

Chapter 6

Visual Acuity

Visual Acuity is the ability to resolve a spatial pattern separated by a visual angle. A Visual Acuity of 1 corresponds to a resolution of one minute of arc. For measurements there are eye charts with optotypes (fig. 6.1).
Resolving a pattern works in two steps (fig. 6.4). First the optic of the eye images the object on the retina. In the second step the neuronal system of the retina converts the retinal image into a neuronal image in the brain.
This chapter gives some information about the procedure of measuring visual acuity. From the point of physiology for the Visual Acuity achievable there is a limit. An estimation will be given.

6.1 Vision Charts

The optotypes implemented in the device are Snellen-type. The shape is that one of the letter "E" with height and width identical, the width of the lines being the same as the distance between. The types are arranged on a chart in lines of 6 with different scales. The chart is put up at a distance of about two meters. An apex angle of 0.86' corresponds to a Visual Acuity of 1.0 (European notation). Exact values are given below.
The relation between VA and the size of the optotypes is linear. A VA of 1.0 is testified if a person is able to determine the open sides for all 1.0 optotypes but fails with the smaller ones in the next line. The standard of 1.0 is accustomed to the average VA of a young person. The American notation

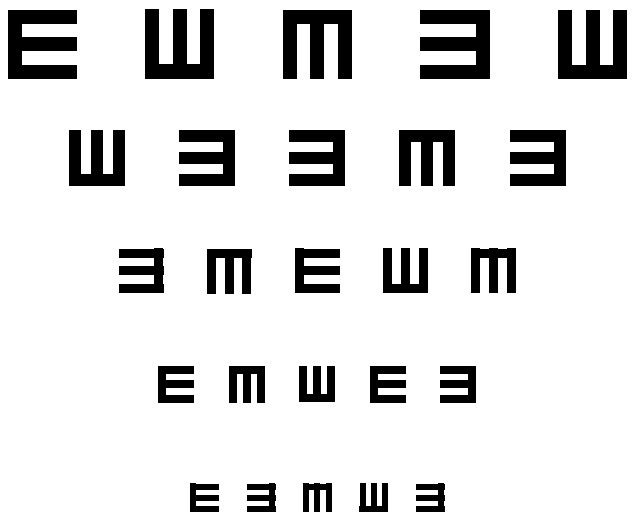

Figure 6.1: Snellen Optotypes

Decimal	20 feet	6 meters	logMAR	apex angle
2,0	20/10	6/3	-0,3	0.43
1,6	20/12.5	6/3.75	-0,2	0.537
1,25	20/16	6/5	-0.1	0.688
1	20/20	6/6	0	0.86
0,8	20/25	6/7.5	0.10	1.075
0,63	20/32	6/10	0.20	1.43

Table 6.1: Different Notations of the Visual Acuity (Snellen)

for VA simply gives the distance at which a normal person can read the same sign. A vision of 20/10 means that the distance at which a sign can be read is double that of a normal person. The reference distance is always 20 foot (about 6 m) The notations are compared in tabular 6.1. The difference in notation does not imply any difference in the technique of measurement.

6.1.1 Conditions For Visual Acuity Measurements

For performing a Visual Acuity test there are very precise regulations. In Germany this is given by DIN 58220. The most important rules are listed

below. The concern is visual acuity in the distance.

- The eye chart should have a minimum distance of 4 m. The optimal distance is about 6 m ($\approx$ 20 foot).
- The size of the test field should be at least 4° ($\pm$ 10 %).
- The luminescence of the eye chart must lie between 160 cd/m^2 and 320 cd/m^2.
- The luminescence outside the test field must lie between 10 % and 25 % of the luminescence inside.
- The contrast of the optotypes must be more than 85 %.
- The distance between the optotypes must be larger than the optotype itself.
- Every line of optotypes must have at least 5 optotypes.
- A degree of acuity is achieved if at least 60 % of the optotypes are identified correctly.

6.2 Fundamental Limits to Visual Performance

For the Visual Acuity man can achieve there are limitations of two kinds. One limitation is set by the optics of the eye, the other by the neuronal structure of the retina and the image processing. The first limitation can be calculated without problems, for the second there are some questions still open.

6.2.1 Optical Limits

The optical limits are given in two ways:
By the size of the pupil (diffraction limited) and by aberrations of the optical system.
The refraction limited resolution is given by the Rayleigh criterion:

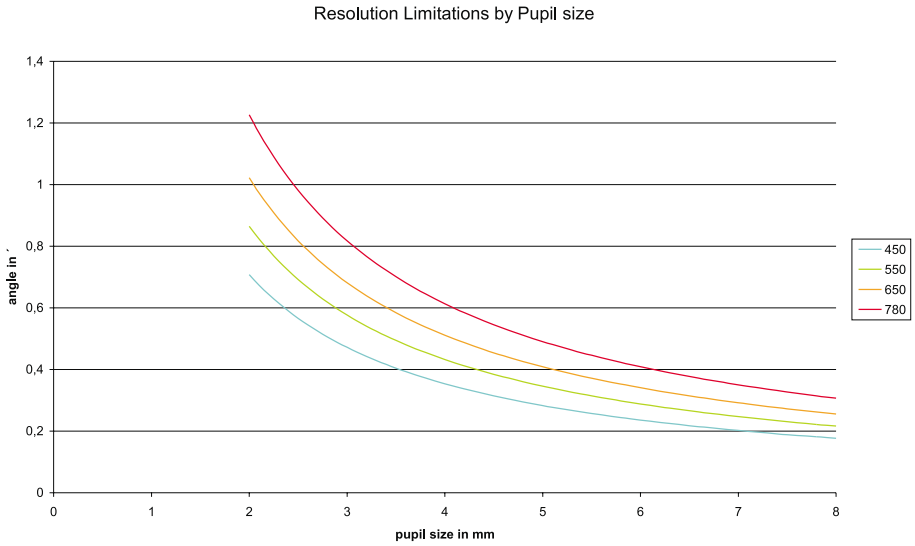

Figure 6.2: Diffraction limited resolution as function of pupil size and wavelength

The coincidence of the zero order diffraction maximum of one object with the first order diffraction minimum of another object gives the minimum-condition for separate perception of two objects. This case is given by:

$$\sin \delta \geq 1,22 \frac{\lambda}{b} \tag{6.1}$$

with $\delta = apex\ angle$, $\lambda = wavelength$ and $b = size\ of\ aperture$. The refraction index in the eye is about 1.33, so the wavelength in the eye is smaller by the factor $\frac{3}{4}$.
As fig. 6.2 shows the diffraction limited resolution depends on the pupil size and the wavelength to a higher degree. Resolution increases with pupil size. This would make vision better at twilight.
To get a vision of 20/10 at 650 nm - with the assumption of a perfect optic - you need at least a 4 mm pupil as shown in fig. 6.2
The effect in real optics is opposite: With the pupil size the aberrations of the eye increase, especially spherical aberrations and cylinder.
Fig. 6.3 compares the diffraction limited MTF‘s to the MTF‘s for an average

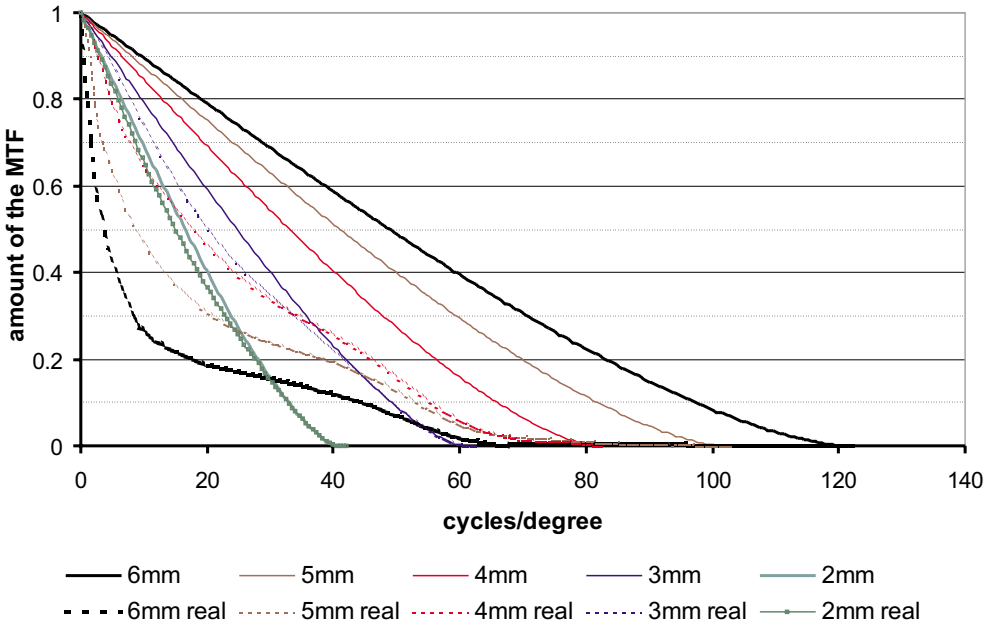

Figure 6.3: Dependence of the MTF on pupil size at a diffraction limited eye and at a real eye (at 550 nm)

eye. The model of an average eye bases on measurements taken from 90 eyes. To obtain aberrations of higher order the mean absolute values of the Zernike coefficients were used with the sign of their mean values. The x-axis gives the frequency in cycles/degree, the y-axis the contrast of the image. The graph results from a simulation with ZEMAX, an optic design programme. The MTF of the diffraction limited eye increases with pupil size. In contrast the mean real MTF has its minimum for the largest pupil, it increases with pupils size going down. The maximum lies at about 3 mm pupil size. For the 2 mm pupil the real MTF is very close to the diffraction limited MTF.
Compared to Visual Acuity a spatial frequency of 30 cycles/degree corresponds to a Visual Acuity of 1.0 (=20/20).

6.2.2 Retinal Limits

There is a fundamental retinal limitation to visual performance too: The ability of the photoreceptors to sample the retinal image is restricted. The sample is always a discrete array.
In a very simple model the condition for two points to be separated by the foveola is, that their images are recognized by two neurons with a third neuron in between without a signal (Helmholtz 1867). With a neuron distance of about 2 μm the minimum for the visual angle can be calculated by

$$\sin\delta \geq \frac{2d}{l} \tag{6.2}$$

with $d = distance\ between\ two\ cones$ (about 2.5 μm) and $l = length\ of\ the\ eye$. The length of the eye has to be corrected by the refraction index of the eye (n=1,3). This allows a resolution of about 0.4‘, corresponding to a visual acuity of about 2.5 (20/8) at the smallest cones in the fovea. Further improvement of the optics will not improve acuity any more, it only increases contrast, in particular for larger pupil sizes.
A more precise model takes into account the image processing of the retina and the more complex configuration of the cones. This - in fact - could increase the visual performance.
These considerations show that the retinal limitations are close to the 2.0 vision. For all developments in refractive surgery this is the target.

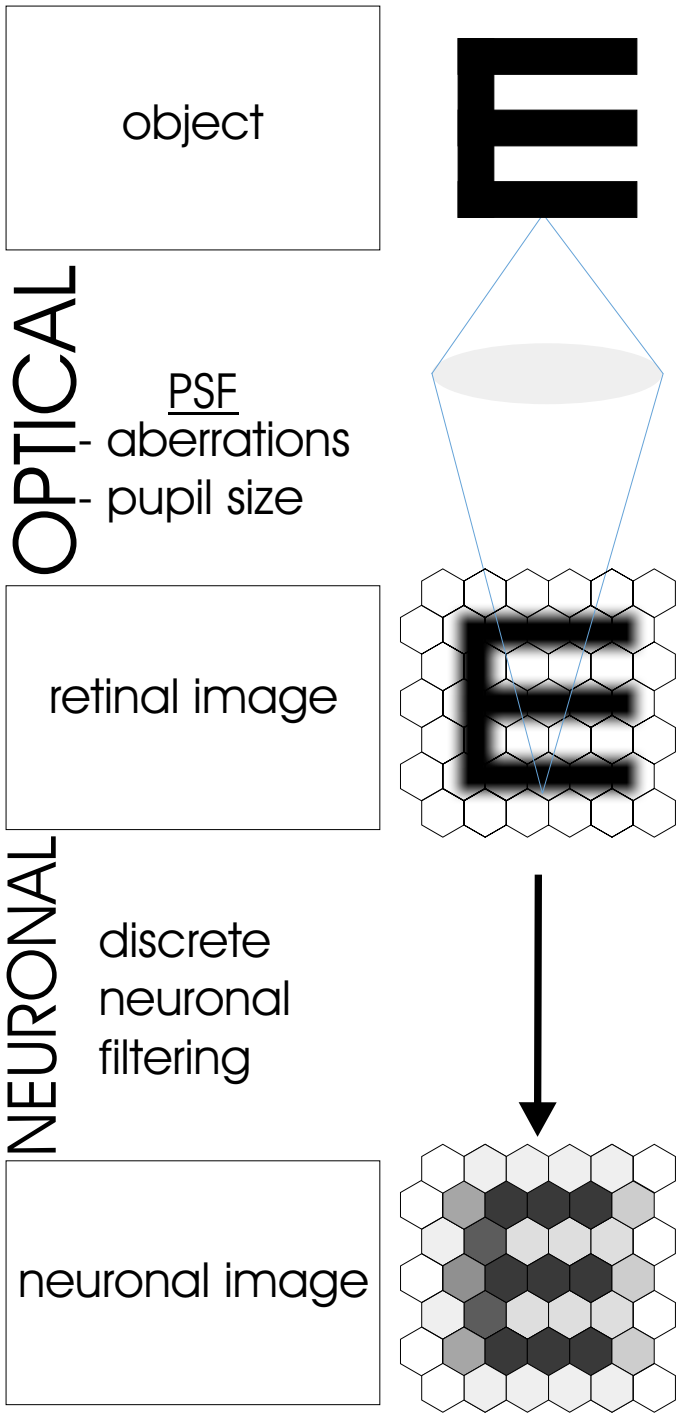

Figure 6.4: Origin of the Retinal Image

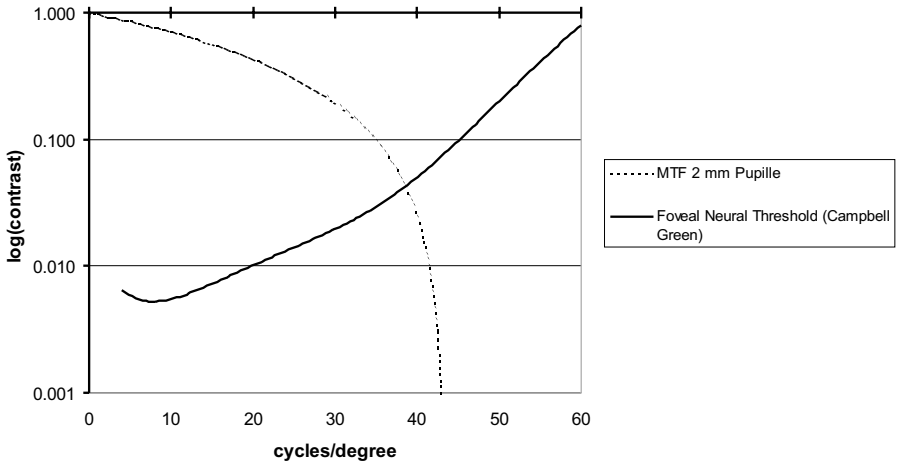

Figure 6.5: Foveal neural threshold

6.3 Predicting Visual Performance

The Visual Performance can be predicted by comparing the MTF of the eye with the Foveal Neural Threshold, the AIM of the retina. The MTF gives the remaining contrast of the retinal image at any spatial frequency. The Foveal Neural Threshold is the contrast necessary for the fovea to record a signal as function of spatial frequency: If the MTF lies above this threshold a structure can be detected otherwise the information gets lost. The MTF decreases with spatial frequency, the foveal neural threshold increases. To determine the neural threshold of a single eye is a major problem. Fig. 6.5 shows the aberration free MTF for a 2 mm pupil and a mean foveal neural threshold identified by Campbell and Green (1965). For different eyes this curve varies considerably.

Opticians and medical doctors are not familiar with the MTF. So a characteristic more suitable is to be found. Comparing the blur caused by higher order aberrations with the defocus blur gives a value apt to easy interpretation. The effect of higher order aberrations would be accessible in D as well as in Visual Acuity. A straight way would be using the RMS get for the blur of defocus and compare it to the RMS received from higher order aberrations. This value of course makes a gross simplification: A function

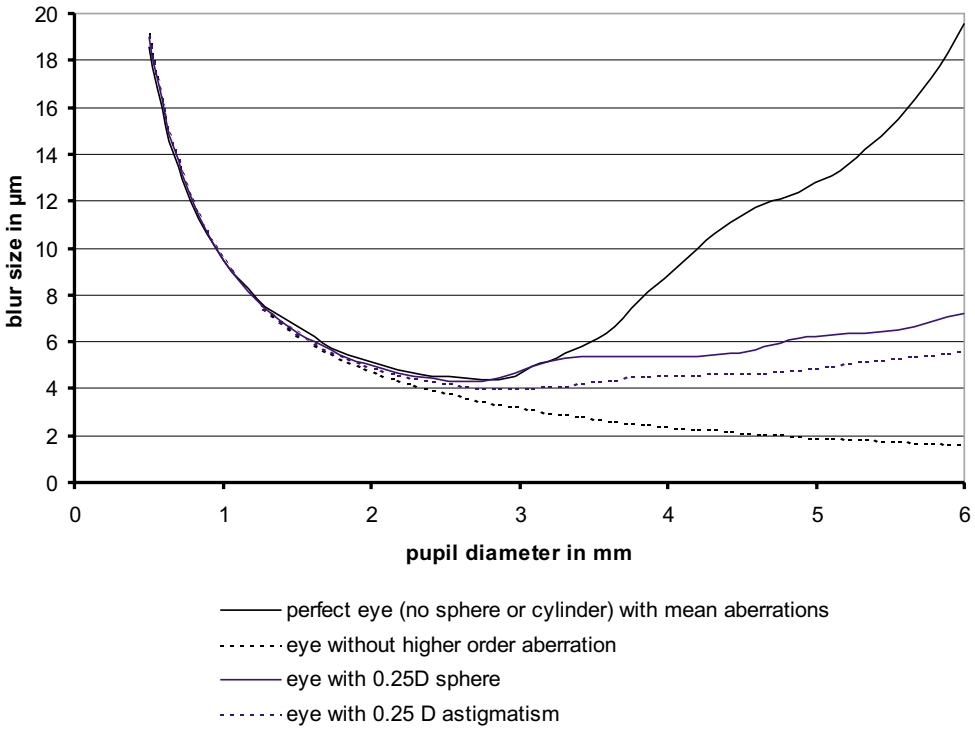

Figure 6.6: Sizes of blur circles for different kinds of aberrations

describing the contrast sensitivity for every spatial frequency is replaced by a single figure. However the figure is much easier to handle.
Fig. 6.6 shows blur sizes for different kinds of aberrations. The blur size here is defined as the diameter encircling 70 % of the energy. For a pupil size below 2.5 mm the blur size is dominated by diffraction as can be seen. For larger pupils the importance of the aberrations grows. For a 6 mm pupil the blur is less than the cone size in the fovea. The blur caused by higher order aberrations is much larger than the blur of a quarter D of astigmatism or even of sphere.

Chapter 7

Conclusion and Outlook

The precise measurement of the total aberrations of the human eye is the basis for obtaining good results in refractive surgery. The high potential of the wavefront device in measuring wavefront errors is demonstrated on test optics. In application to human eyes the device shows to be good for results needed in surgery. The precision of the device exceeds the standard set by the temporary fluctuations of the aberrations.
The visual acuity study gives evidence for the importance of high precision in measuring sphere and astigmatism: In most eyes the higher order aberrations lie below the range of the residual 2nd order aberrations sphere and astigmatism, not detected due to the resolution in quarter diopter steps.
Some wavefront errors occur in one state of accommodation or just for a short period in life. As to the importance of detecting and correcting these errors there is some doubt. Measurements in relation to accommodation and to age suggest: The correction of very small higher order aberrations of eyes without any other deficiency may be not reasonable. Finding limits is of great interest here.
The excimer laser study is encouraging in whole. For a precise documentation of the advantage of wavefront guided to the traditional procedure further studies are needed. Improving the interface between wavefront sensor and excimer laser will be of great importance here. A major improvement would lie in using the observation image of the iris for finding the pupil center and for detecting any rotation of the eye.

It would be ideal to have this information directly in the eyetracker of the excimer laser.

Transferring the application to a further laser technology for refractive surgery could be an important step: With intrastromal femtosecond lasers the cornea could be reshaped without having the unpredictable effects in the healing-process. In case the higher order aberrations have changed in time there could be repetition in the reshaping.
The most recent implemented improvements - the continuously adjustable cylinder compensation and the adaptive optics - open the gate for real Best Corrected Visual Acuity tests. The effects of higher order aberrations on the visual ability and in special on the maximum in the visual acuity achievable can be studied now.

First in interest is the further development of the wavefront device itself:
Enlarging the diameter of the ccd-camera gives the option for measuring bigger pupil sizes. Correcting the higher order aberrations of the illumination beam provides a new line of improvement. In addition to an increase in the precision the effective range for strongly aberrated eyes would be enlarged.

List of Figures

Bibliography

[Ap01] R. Applegate, L. Thibos, G. Hilmantel
Optics of aberroscopy and super vision
Journal of Cataract and Refractive Surgery
Vol 27, No.7 pp. 1093-1107 (2001)

[Ar95] P. Artal, S. Marcos, R. Navarro, D. Williams
Odd aberrations and double pass measurements of retinal image quality
JOSA A Vol. 12, pp. 195-201 (1995)

[Ar00] P. Artal
Understanding Aberrations by Using Double-Pass Techniques
Journal of Refractive Surgery, Vol. 16, Sep./Oct. 2000

[At00] D. Atchison, G. Smith
Optics of the Human Eye
Oxford, Ma: Butterworth and Henemann, 2000

[Ax92] Axenfeld, Pau
Lehrbuch der Augenheilkunde
Stuttgart - Jena - New York: Gustav Fischer Verlag, 1992

[Ca65] F. Campbell, D. Green
Optical and retinal factors affecting visual resolution
J. Physiol.,Vol. 181, pp. 576-593 (1965)

[Ca66] F. Campbell, R. Gubisch
Optical Quality of the Human Eye
J. Physiol., Vol. 186, pp. 579-595 (1966)

[Ca95] E. Carterette, M.Friedmann (Ed.)
Cognitive Ecology (Handbook of Perception and Cognition (2nd Ed))
Academic Press, 1995

[Di00] L. Diaz-Santana, J. Dainty
Effects of retinal scattering in the ocular double-pass process
JOSA A, Vol. 18, No. 7, pp. 1437-1444, July 2001

[Fo94] C.W.Fowler and T.N. Dave
Review of past and present techniques of measuring corneal topography
Ophthal. Physiol. Opt., Vol. 14, pp. 49-53, 1994

[Fr85] H. Freyler
Augenheilkunde
Wien: Springer, 1985

[Ge95] J. Geary
Introduction to wavefront sensors
Washington: SPIE-The International Society for Optical Engineering, 1995

[Ge97] H. Vogel
Gerthsen Physik 19. Auflage
Berlin, Heidelberg, New-York: Springer, 1997

[Go95] J.Goodman
Introduction to Fourier Optics
New York: Mc-Graw-Hill, 1995

[Ho86] A. Howarth, A. Bradley
The longitudinal chromatic aberration of the human eye, and its correction
Vis. Research, Vol. 26, No. 2, pp. 361-366, 1986

[Kl98] S. Klein
Optimal Corneal Ablation for eyes with arbitrary Hartmann-Shack

aberrations
JOSA A, Vol. 15, no. 9, Sep 1998

[Kl00] S. Klyce
Corneal Topography and the New Wave
Cornea, Vol 19, No. 5, pp. 723-729, 2000

[La99] B. Lachenmayr, D. Friedburg, E. Hartmann
Auge - Brille - Refraktion: Begleitheft zum "Schober-Kurs"
Stuttgart: Enke 1999

[Li91] J. Liang
A new method to precisely measure the Wave Aberrations of the Human Eye with a Hartmann-Shack Sensor
Dissertation, Ruprecht-Karls-Universität, Heidelberg 1991

[Li90] H. Lippert
Lehrbuch Anatomie
München, Wien, Baltimore: Urban und Schwarzenberg, 1990

[Li97] H. Liou, N. Brennan
Anatomically accurate, finite model eye for optical modeling
JOSA A, Vol. 14, No. 8, pp. 1684-1695, 1997

[Ma98] V. Mahajan
Optical Imaging and Aberrations
Washington, USA: SPIE-The International Society for Optical Engineering, 1998

[Ma92] D. Malacara
Optical Shop Testing (second edition)
New York: John Wiley & sons, 1992

[Me96] D. Methling
Bestimmen von Sehhilfen
Stuttgart: Enke, 1996

[Mu01] F. Müller
Konzeption und Entwicklung eines adaptiv-optisch korrigierten Laser-Scanning Retina-Tomographen
Heidelberg: Dissertation, Ruprecht-Karls-Universität Heidelberg, 2001

[Mr01] M. Mrochen, T. Seiler
Grundlagen der Wellenfrontgeführten refraktiven Hornhautchirurgie
Der Ophthalmologe, Vol. 98, pp. 703-714, 2001

[Na98] R. Navarro, E. Moreno et al.
Monochromatic aberrations and point-spread functions of the human eye across the visual field
JOSA A, Vol. 15, no. 9, September 1998

[Pe96] J. Ph. Perez
Optik
Heidelberg: Spektrum Akademischer Verlag, 1996

[Pl71] B. Platt, R. Shack
Lenticuloar Hartmann Screen
Optical Science Center Newsletter, Vol 5, no. 1 (3/71)
University of Arizona

[Ry98] M. Rynders, R. Navarro, M. Losada
Objective Measurement of the Off-Axis Longitudinal Chromatic Aberration in the Human Eye
Vision Research, Vol. 38 No. 4 pp. 513-522, 1998

[Sc98] G. Schroeder
Technische Optik: Grundlagen und Anwendungen
Würzburg: Vogel Fachbuch (Kamprath Reihe), 1998

[Sc97] M. Schottner
Aufbau eines kompakten Hartmann-Shack Wellenfrontsensors für den Einsatz in der Ophthalmologie
Heidelberg: Diplomarbeit, Institut für Angewandte Physik, 1997

[Sc00] J. Schwiegerling
Theoretical Limits to Visual Performance
Survey Ophthalm, Vol. 45 (2), pp. 139-146, September-October 2000

[Se00] T. Seiler (Hrsg.)
Refraktive Chirurgie der Hornhaut
Stuttgart: Thieme, 2000

[Si00] T. Seiler, M. Mrochen, M. Kaemmerer
Operative Correction of Ocular Aberrations to Improve Visual Acuity
Journal of Refractive Surgery, Vol. 16, Sep./Oct. 2000

[Sm00] W. Smith
Modern Optical Engineering 3rd edition
New York: Mc Graw-Hill , 2000

[Th90] L. Thibos
New Methodologies for Discriminationg Neural and Optical Losses of Vision
Hirsch Memorial Lecture, AAO Meeting 1990

[Th94] L. Thibos, W. Wheeler, D. Horner
A vector method for the analysis of astigmatic refractive errors
Vision Science and Its Applications, Vol. 2, pp. 14-17, 1994

[Th97] L. Thibos
Acuity Perimetry and the Sampling Theory of Visual Resolution
The 1997 Glen Fry Award Lecture, Indiana University, USA

[Th99] L. Thibos, A. Bradley
Visual Instrumentation: Modelling the Refractive and Neuro-Sensor Systems of the Eye
New York: McGraw-Hill, 1999

[Tu74] J. Tucker
The chromatic aberrations of the eye between wavelengths 200 nm and 2000 nm: Some theoretical considerations
1974

[Tu00] A. Tuerpitz
Entwicklung eines adaptiv-optischen Closed Loop System zur Kompensation der Aberration des menschlichen Auges
Heidelberg: Dissertation, Kirchhoff Institut für Physik, 2000

Acknowledgement

My thanks go to ...

- Prof. Dr. Josef Bille who gave me the chance to work on such a challenging project in the field of ophtomological optics.
- Prof. Dr. Brenner for his interest in my work and his willingness to take on the second referees.
- 20/10 Perfect Vision: for making this project possible and for giving me their support.
- Dr. med. Volz, Dr. med. Gleibs and Mrs. Pankrath for their cooperation and help in the clinical studies.
- Peter Brockhaus who helped me getting started with my dissertation.
- Tobias Kuhn, Stefan Wühl, Bernhard Gress, Michael Schumacher and my other colleagues for the excellent atmosphere at work.
- Frank Müller, Joana Costa, Michael Schottner, Karaneh Razavi, Nina Korablinova and the other group members for critical discussions and support.
- Sylvia for the wonderful time we spent together when not working on this project.
- my parents who encouraged me. Without their support throughout my entire study all this would not have been possible.